THE PERFORMANCE OF AN ACTIVE OPTICAL IMAGING RADAR IN THE TURBULENT ATMOSPHERE

by

John Glenn Himes

S.B., Massachusetts Institute of Technology
(1970)
M.S., Massachusetts Institute of Technology
(1970)

SUBMITTED IN PARTIAL FULFILLMENT OF THE
REQUIREMENTS FOR THE DEGREE OF
DOCTOR OF PHILOSOPHY

at the

MASSACHUSETTS INSTITUTE OF TECHNOLOGY
February, 1975

Signature of Author.....
Department of Electrical Engineering, January 1, 1975

Certified by.....
Thesis Supervisor

Accepted by.....
Chairman, Departmental Committee on Graduate Students

THE PERFORMANCE OF AN ACTIVE OPTICAL IMAGING RADAR IN THE TURBULENT ATMOSPHERE

by

John Glenn Himes

Sumitted to the Department of Electrical Engineering on January in partial fulfillment of the requirements for the Degree of Doctor of Philosophy

ABSTRACT

This research investigates the performance of an active optical imaging radar system which is viewing a diffusely reflecting rough surface through the turbulent atmosphere. The mathematical formulation of this problem is not amenable to standard statistical techniques so that we examine a collection of related simplifications in order to evaluate the performance of this system. The results thus obtained indicate that appropriate utilization of the active aspect of the radar system can significantly improve the attainable performance. Returning to the original formulation, we discuss several suboptimal imaging techniques which are adapted from techniques employed in simpler contexts and which partially circumvent image degradations due to turbulence. Finally, we describe certain practical applications for this system.

THESIS SUPERVISOR: E. V. Hoversten
TITLE: Associate Professor of Electrical Engineering

TABLE OF CONTENTS

CHAPTER 1

There is considerable interest in imaging or otherwise identifying objects which may be present in the atmosphere. For imaging such objects, optical systems in principle offer significant improvement (more detailed resolution) over their microwave counterparts. This potential advantage has not been fully realized, however, because atmospheric turbulence severely limits the quality of images formed by optical systems. While this restriction is most familiar in the context of passive systems which view naturally illuminated or self-luminous objects, it also applies to active systems wherein the transmitter illuminates the entire object. In undertaking this research, we thus sought to determine whether the active aspect of the transmitter could be utilized to circumvent turbulent limitations on imaging.

In pursuit of this objective, the available literature concerning wave propagation in turbulence and scattering from rough surfaces was employed to develop a formulation which correctly described these relevant physical phenomena. This model was not amenable to standard statistical techniques so various simplifications of the original formulation were examined in order to obtain a quantitative

measure for the performance of such a system. The results derived in these simplified models were then used to generate some imaging methods that were applicable in the general formulation.

In each of these analyses, the proper utilization of the active transmitter provides a meaningful improvement in the performance of the radar system. For example, in those contexts where the target is completely characterized by its coherent cross section, transmitter diversity can be employed to significantly reduce the amount of temporal diversity (*i.e.*, length of time) required to obtain a satisfactory measurement of this parameter. An additional example occurs in the general formulation where transmitter diversity provides the basis for scanning techniques that adequately image certain classes of targets which cannot be handled by other available methods.

This report is organized in the following manner. The general formulation and a hierarchy of related simplifications are developed in Chapter 2. Certain of these specializations involving isoplanatic scattering surfaces are examined in Chapter 3 while other specializations relating to more complicated surfaces are considered in Chapter 4.

The results obtained in these chapters are the basis fo the imaging techniques (applicable to the general formulation) discussed in Chapter 5. Some applications of this material are described in Chapter 6 and a brief summary is given in Chapter 7.

CHAPTER 2

In this chapter, we formulate a problem model to serve as the basis for future analysis. Because the relevant literature appears in less general contexts, we employ a three-step procedure to incorporate these results into our model. First, in Section 2.1, we collect useful results concerning the propagation of (optical) electromagnetic waves over a line-of-sight path between two apertures through the clear turbulent atmosphere. Next, in Section 2.2, we gather the appropriate material dealing with the scattering of electromagnetic waves from rough surfaces. These results are then merged in Section 2.3 to obtain the desired formulation, henceforth termed the radar model.

2.1 Wave Propagation in the Clear Turbulent Atmosphere

There exists an extensive literature on this topic which has been summarized from both physical [1,2] and communication theoretical [3,4] viewpoints. We therefore draw freely on established results and refer those concerned about this issue *per se* to the preceding references. To our knowledge, no updated summary is available despite the continuing appearance of related material.

2.1.1 Channel Model

The geometry for line-of-sight propagation through the turbulent atmosphere is established in Figure 2.1. Here A_1 and A_2 are parallel, planar apertures which are centered on a common perpendicular (length L) connecting the input and output planes. For analytical convenience, we consider only scalar fields since their use entails no loss of generality for this channel [1,3]. We may exploit the linearity of Maxwell's equations to write the received field, $E_0(r,t)$, in terms of the transmitted field, $E_i(\hat{r},\hat{t})$, by means of the channel impulse response $h_{21}(r,\hat{r},t,\hat{t})$

$$E_0(r,t) = \int_{A_1} d\hat{r} \int_{T_1} d\hat{t}\; E_i(\hat{r},t-\hat{t}) h_{21}(r,\hat{r},t,\hat{t}),$$

$$r \in A_2,\ t \in T_2. \qquad (2.1)$$

Provided these fields are temporally narrowband about the optical carrier frequency, f_0, we may employ complex envelope representation to obtain the

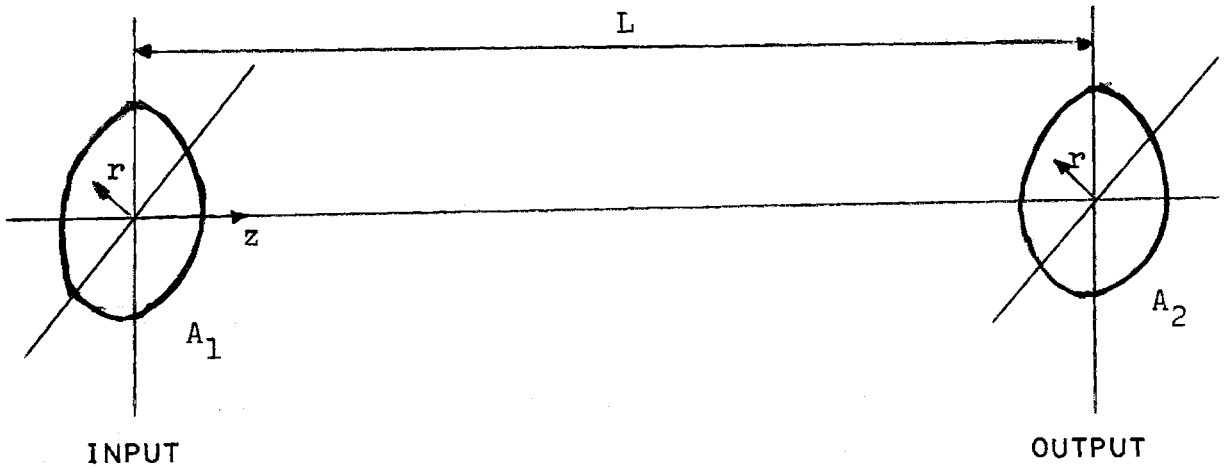

FIGURE 2.1: GEOMETRY FOR A LINE-OF-SIGHT PATH

following input-output relationship for this channel

$$E_0(r,t) = \int_{A_1} d\hat{r}\, E_i(\hat{r},t - \tfrac{L}{c})h_{21}(r,\hat{r},t),$$

$$r \in A_2,\ t \in T_2 \qquad (2.2a)$$

where T_2 becomes a time-shifted (by L/c) version of T_1. In this expression $E_0(r,t)$ and $E_i(\hat{r},\hat{t})$ are the respective complex envelopes

$$E_0(r,t) = \mathrm{Re}[E_0(r,t)\exp(j2\pi f_0 t)],$$

$$r \in A_2,\ t \in T_2, \qquad (2.2b)$$

$$E_i(\hat{r},\hat{t}) = \mathrm{Re}[E_i(\hat{r},\hat{t})\exp(j2\pi f_0 \hat{t})],$$

$$\hat{r} \in A_1,\ \hat{t} \in T_1 \qquad (2.2c)$$

while $h_{21}(r,\hat{r},t)$ is defined by the following

$$h_{21}(r,\hat{r},t) = \int_0^\infty d\hat{t}\, h_{21}(r,\hat{r},t,\hat{t})\exp(-j2\pi f_0 \hat{t}),$$

$$\hat{r} \in A_1,\ r \in A_2,\ t \in T_2, \qquad (2.2d)$$

which exploits the large temporal coherence bandwidth [1,3] of the turbulent channel relative to these fields. There exists a useful representa-

tion [5] for the impulse response

$$h_{21}(r,\hat{r},t) = h_0(r-\hat{r})\exp[\chi_{21}(r,\hat{r},t)+j\phi_{21}(r,\hat{r},t)],$$

$$r \in A_2,\ t \in T_2,\ \hat{r} \in A_1, \qquad (2.3)$$

where $h_0(r-\hat{r})$ is the free space impulse response for this channel and where $\chi_{21}(r,\hat{r},t)$ and $\phi_{21}(r,\hat{r},t)$ are the turbulence-induced perturbations of a spherical wave source. For transmitted envelopes that are less than a temporal coherence length in extent and that possess no temporal modulation, we obtain the simplified input-output relationship

$$E_0(r) = \int_{A_1} d\hat{r}\, E_i(\hat{r})h_{21}(r,\hat{r}), \qquad r \in A_2, \qquad (2.4)$$

by suppressing all temporal dependences as well as the channel delay time.

2.1.2 Impulse Response Statistics

Complete statistics for the impulse response are provided by the complete statistics for the perturbation terms, $\chi(r,\hat{r},t)$ and $\phi(r,\hat{r},t)$. The latter statistics may be obtained, for suitably restricted pathlengths, by extending the spherical wave propagation theory based upon the Rytov approximation. Within a temporal coherence interval, the specification of the perturbation statistics is time-independent. Here,

$\chi(r,\hat{r},t)$ and $\phi(r,\hat{r},t)$ are jointly Gaussian random fields that are completely characterized by their means and covariance functions which are available elsewhere [21,47]. We typically assume that their cross-covariance is zero despite evidence that this assumption is not well justified physically [2]. Furthermore, we often employ the statistics corresponding to a statistically homogeneous and isotropic channel although those for a locally homogeneous and isotropic channel are more accurate. The statistics which are most relevant to our analysis include the mean values

$$\langle \chi_{21}(r,\hat{r},t)\rangle = -\sigma^2, \tag{2.5a}$$

$$\langle \phi_{21}(r,\hat{r},t)\rangle = 0; \tag{2.5b}$$

the variances

$$\langle \chi_{21}^2(r,\hat{r},t)\rangle - \langle \chi_{21}(r,\hat{r},t)\rangle^2 = \sigma^2, \tag{2.5c}$$

$$\langle \phi_{21}^2(r,\hat{r},t)\rangle = \sigma_\phi^2; \tag{2.5d}$$

and the structure functions [11]

$$D_\chi(r-\rho,\hat{r}-\hat{\rho}) = \langle\{\chi_{21}(r,\hat{r},t)-\chi_{21}(\rho,\hat{\rho},t)\}^2\rangle, \tag{2.5e}$$

$$D_{\phi}(r-\rho,\hat{r}-\hat{\rho}) = \langle\{\phi_{21}(r,\hat{r},t)-\phi_{21}(\rho,\hat{\rho},t)\}^2\rangle. \tag{2.5f}$$

We also utilize the wave structure function which is defined to be the sum of the preceding (log-amplitude and phase) structure functions

$$D(r-\rho,\hat{r}-\hat{\rho}) = D_{\chi}(r-\rho,\hat{r}-\hat{\rho}) + D_{\phi}(r-\rho,\hat{r}-\hat{\rho}). \tag{2.5g}$$

For lengthier temporal intervals, the statistics of the impulse response exhibit temporal dependence and an additional assumption is required to evaluate their behavior. Taylor's hypothesis asserts that this dependence is due solely to a deterministic wind blowing a fixed spatial configuration of refractive index fluctuations perpendicularly to the propagation path. A discussion of this assumption and its effects is contained in Lawrence and Strohbehn [1]. The frozen atmosphere hypothesis models the atmosphere as undergoing a succession of fixed states each of which endures for a temporal coherence interval. This assumption, its statistics and the restrictions on its use are examined by Brookner [4].

The received field is accompanied by the appropriate polarization component of the background radiation. This complex noise envelope is usually modeled as a zero mean complex Gaussian random process that is white with independent quadrature components that are stationary in time and homogeneous in space [7]. The characterization of the noise coupled with the impulse response statistics completes the specification of the model of the channel.

2.1.3 Normal Made Decomposition

In this section, we examine some results obtained by Shapiro [8] who has applied the normal-mode decomposition associated with linear systems to the line-of-sight propagation model just described. In particular, for the input-output relationship of Equation 2.4 the decomposition consists of a set of input eigenfunctions $\{\Phi_{in}(\hat{r}): 1 \leq n < \infty, \hat{r} \in A_1\}$, a set of output eigenfunctions $\{\Phi_{On}(r): 1 \leq n < \infty, r \in A_2\}$ and a set of eigenvalues $\{\eta_n: 1 \leq n < \infty\}$. The input eigenfunctions form a complete orthonormal (CON) set on A_1 and, with the eigenvalues, are solutions of the integral equation

$$\int_{A_1} d\hat{r}_2 \{ \int_{A_2} dr\, h_{21}^*(r,\hat{r}_1) h_{21}(r,\hat{r}_2) \} \Phi_{in}(\hat{r}_2) = \eta_n \Phi_{in}(\hat{r}_1),$$

$$\hat{r}_1 \in A_1. \qquad (2.6a)$$

The output eigenfunctions form a CON set on A_2 and are obtained from the input eigenfunctions by means of Equation 2.4:

$$\eta_n \Phi_{On}(r) = \int_{A_1} d\hat{r}\, \Phi_{in}(\hat{r}) h_{21}(r,\hat{r}), \quad r \in A_2. \qquad (2.6b)$$

Because the channel is random, it follows that the eigenvalues and both sets of eigenfunctions are also random so that they must be characterized statistically. The input-output relationship for the corresponding free space channel permits a similar normal mode decomposition

$\{\Phi_{in,0}(\hat{\mathbf{r}}),\Phi_{On,0}(r),\eta_{n,0}: \ 1 \leq n < \infty, \ \hat{\mathbf{r}} \in A_1, r \in A_2\}$ wherein the input and output eigenfunctions as well as the eigenvalues are deterministic.

The behavior of the eigenvalue statistics is intimately connected with the parameter

$$D_f = \int_{A_1} d\hat{\mathbf{r}} \int_{A_2} dr \, |h_{21}(r,\hat{\mathbf{r}})|^2 = \sum_{n=1}^{\infty} \eta_n \tag{2.7}$$

which functions as an effective Fresnel number. For $\langle D_f \rangle << 1$ (the far field), the maximum eigenvalue is approximately equal to D_f; all other eigenvalues are insignificant relative to D_f. For $\langle D_f \rangle >> 1$ (the near field), there are D_f near unity eigenvalues; all other eigenvalues are approximately zero. Thus, for the turbulent atmosphere, we are able to define near-field and far-field regions solely in terms of eigenvalue behavior. This behavior is analogous to that of the corresponding free space channel with Fresnel number D_{f0}.

Furthermore, under certain conditions, the eigenfunctions associated with the turbulent channel are similar to those for the free space channel. Specifically, in the far field, the two channels have the same input eigenfunction whenever the diameter of the aperture A_1 is less than the spherical-wave phase coherence length; they have the same output eigenfunction whenever the diameter of the aperture A_2 is similarly restricted. For the near field, so long as aperture A_1 is not larger than aperture A_2, the input eigenfunctions with near unity eigenvalues are identical for the free space and turbulent channels.

2.1.4 Approximations for the Impulse Response

The behavior of the atmospheric impulse response is complicated due principally to its dependence on the spherical wave perturbation term as indicated by the following simplification of Equation 2.3.

$$h_{21}(r,\hat{r}) = h_0(r-\hat{r})\exp[\chi_{21}(r,\hat{r})+j\phi_{21}(r,\hat{r})],$$

$$r \in A_2,\ \hat{r} \in A_1. \qquad (2.8)$$

We herein examine some approximations for the perturbation term which, in turn, simplify the behavior of the atmospheric impulse response. Most available research has assumed the validity of one such approximation (isoplanatism) although this topic is currently undergoing re-examination [9,10].

A trivial simplification occurs when the perturbation term exhibits no spatial variation over the relevant apertures so that the random process is well-modeled as a random variable. Quantitatively, we require that the mean-square difference between any two pairs of input and output aperture points satisfy the following

$$\sup_{\substack{r,\rho \\ \hat{r},\hat{\rho}}} <\left|\{\chi_{21}(r,\hat{r})+j\phi_{21}(r,\hat{r})\}-\{\chi_{21}(\rho,\hat{\rho})+j\phi_{21}(\rho,\hat{\rho})\}\right|^2> \leq 1,$$

$$r,\rho \in A_2,\ \hat{r},\hat{\rho} \in A_1. \qquad (2.9)$$

For a statistically homogeneous and isotropic path, this requirement involves only the structure function for the turbulence

$$\sup_{\substack{r,\rho \\ \hat{r},\hat{\rho}}} \{D(r-\rho, r-\rho)\} \leq 1,$$

$$r,\rho \in A_2,\ \hat{r},\hat{\rho} \in A_1, \tag{2.10}$$

which, in turn, leads to the conditions

$$\text{diam } A_2 \triangleq \sup_{r,\rho \in A_2} \{|r-\rho|\} \leq \rho_{PW}, \tag{2.11a}$$

$$\text{diam } A_1 \triangleq \sup_{\hat{r},\hat{\rho} \in A_1} \{|\hat{r}-\hat{\rho}|\} \leq \rho_{PW}, \tag{2.11b}$$

where ρ_{PW} is the plane wave coherence distance. Although the computational merits of this approximation are substantial, its usefulness is limited by the extremely short pathlengths over which energy can be effectively transferred between apertures satisfying Equation 2.11. Typical pathlengths (cf., Table 2.1) for which this approximation is valid are obtained by recalling that [11]

$$\rho_{PW} = (2.92\ k^2 C_n^2 L)^{-3/5} \tag{2.12}$$

and requiring that $\langle D_f \rangle$ be nearly unity to ensure the energy transfer. Here $\langle D_f \rangle$ equals D_{f_0}, the free space Fresnel number

TABLE 2.1

C_n^2 \ λ	$6.28 \cdot 10^{-6}$	$6.28 \cdot 10^{-7}$
$3 \cdot 10^{-14}$	$1.87 \cdot 10^{2}$	$3.39 \cdot 10^{1}$
$3 \cdot 10^{-15}$	$5.13 \cdot 10^{2}$	$1.18 \cdot 10^{2}$
$3 \cdot 10^{-16}$	$1.78 \cdot 10^{3}$	$4.08 \cdot 10^{2}$

These entries are the longest pathlengths over which energy can be efficiently transferred between two apertures that satisfy the restrictions imposed by the random variable approximation. Their values (in meters) are displayed as functions of the carrier wavelength (in meters) and the turbulence strength parameter (in centimeters to the inverse two-thirds power).

$$\langle D_f \rangle = D_{f_0} = \left| \frac{\pi \rho_{PW}^2}{4\lambda L} \right|^2 . \qquad (2.13)$$

Interestingly, the maximum pathlengths which permit the random variable approximation are about one-sixth of the corresponding minimum saturation pathlengths.

A hierarchy of related approximations can be developed by the use of successively more general spatial variations in the representation of the perturbation term. This approach has been employed by Fried [12] in the context of plane wave transmission. These approximations, especially higher order ones, are not particularly useful to the ensuing analysis so we relegate further analysis to Appendix 2A.

Other useful simplifications follow from approximating the perturbation term, a double-argument random process, with single argument random processes. The best known of these approximations is the (strict) isoplanatic approximation (cf. [9] and [10] for less restrictive forms of this approximation) which requires that $\{\chi_{21}(r,\hat{r})+j\phi_{21}(r,\hat{r})\}$ be well modeled by $\{\chi_{21}(r-\hat{r},0)+j\phi_{21}(r-\hat{r},0)\}$. The mean square difference criterion supplies the following requirement

$$\sup_{r,\hat{r}} \langle |\{\chi_{21}(r,\hat{r})+j\phi_{21}(r,\hat{r})\}-\{\chi_{21}(r-\hat{r},0)+j\phi_{21}(r-\hat{r},0)\}|^2 \rangle \ll 1,$$

$$r \in A_2,\ \hat{r} \in A_1. \qquad (2.14)$$

Assuming statistical homogeneity and isotropy, this becomes

$$\sup_{\hat{\mathbf{r}}}\{D(\hat{\mathbf{r}},\hat{\mathbf{r}})\} << 1, \qquad \hat{\mathbf{r}} \in A_1 \tag{2.15}$$

which leads to the requirement

$$\text{diam } A_1 \lesssim \rho_{PW}. \tag{2.16}$$

When the aperture A_1 satisfies this condition, the approximation is valid for all pathlengths including those in the saturation regime [8] in contrast to the limited validity of the random variable approximation.

A related simplification, called the unilateral coherence approximation, is obtained by requiring that $\{\chi_{21}(\mathbf{r},\hat{\mathbf{r}})+j\phi_{21}(\mathbf{r},\hat{\mathbf{r}})\}$ be well modeled by $\{\chi_{21}(\mathbf{r},0)+j\phi_{21}(\mathbf{r},0)\}$. Here the mean-square difference criterion yields the following

$$\sup_{\mathbf{r},\hat{\mathbf{r}}}\langle|\{\chi_{21}(\mathbf{r},\hat{\mathbf{r}})+j\phi_{21}(\mathbf{r},\hat{\mathbf{r}})\}-\{\chi_{21}(\mathbf{r},0)+j\phi_{21}(\mathbf{r},0)\}|^2\rangle << 1, \qquad \mathbf{r} \in A_2,\ \hat{\mathbf{r}} \in A_1, \tag{2.17}$$

which, for the usual assumptions, becomes

$$\sup_{\hat{\mathbf{r}}}\{D(0,\hat{\mathbf{r}})\} << 1, \qquad \hat{\mathbf{r}} \in A_1, \tag{2.18}$$

thus establishing the condition

$$\text{diam } A_1 \tilde{<} \rho_{SW} \tag{2.19}$$

where ρ_{SW} is the spherical wave coherence distance. Again, whenever A_1 satisfies this condition, the approximation is valid for all path-lengths. Because this criterion involves the spherical wave, rather than the plane wave, coherence distance, it is valid whenever the isoplanatic approximation is valid. A more rigorous development of this result is included in Appendix 2B. The derivation therein parallels exactly Shapiro's [10] derivation for the isoplanatic approximation.

The utility of these approximations is evident from the ensuing form of the impulse response. For isoplanatism, Equation 2.8 becomes

$$h_{21}(r,\hat{r}) = h_0(r-\hat{r})\exp[x_{21}(r-\hat{r},0)+j\phi_{21}(r-\hat{r},0)] \triangleq h_{21}(r-\hat{r}),$$
$$r \in A_2,\ \hat{r} \in A_1, \tag{2.20}$$

whereas, for unilateral coherence, it reduces to the following

$$h_{21}(r,\hat{r}) = h_0(r-\hat{r})\exp[x_{21}(r,0)+j\phi_{21}(r,0)] \triangleq$$
$$h_0(r-\hat{r})\exp[x_{21}(r)+j\phi_{21}(r)],$$
$$r \in A_2,\ \hat{r} \in A_1. \tag{2.21}$$

For the random variable approximation, the input-output relationship is simply

$$h_{21}(r,\hat{r}) = h_0(r-\hat{r})\exp[x_{21}(0,0)+j\phi_{21}(0,0)] \triangleq h_0(r-\hat{r})\exp[x_{21}+j\phi_{21}],$$

$$r \in A_2,\ \hat{r} \in A_1. \qquad (2.22)$$

While other simplifications are possible, these three are adequate for our purposes.

2.2 Scattering of Electromagnetic Waves from Rough Surfaces

This subject possesses a long established, vast literature that has been summarized by Beckmann and Spizzichino [13]. It consists of very specialized models developed in response to the prohibitive complexity of the general formulation. Herein, we describe the derivation of two distinct models in the free space environment and subsequently extend them to the turbulent atmosphere.

2.2.1 Scattering Model

The scattering geometry is indicated in Figure 2.2. There A_1 and A_2 are parallel apertures contained in planes located at distances L_1 and L_2, respectively, from the parallel plane which contains the origin of the coordinate system attached to the rough surface S. These distances are much larger than the planar dimensions and center offsets of the apertures as well as the planar dimensions and the height (z') variations of the surface. This surface possesses a fixed shape, described by the function z'(r'), and maintains a fixed orientation with respect to the apertures.

Again, we restrict attention to scalar fields thereby compromising the generality of the analysis since many surfaces depolarize incident radiation. Maxwell's equations apply to the formulation so that we may define a (scattering) impulse response, $h_{2S1}(r,\hat{r},t,\hat{t})$, which relates the transmitted field, $E_i(\hat{r},\hat{t})$, and the received field, $E_0(r,t)$, obtained via reflection from the surface S

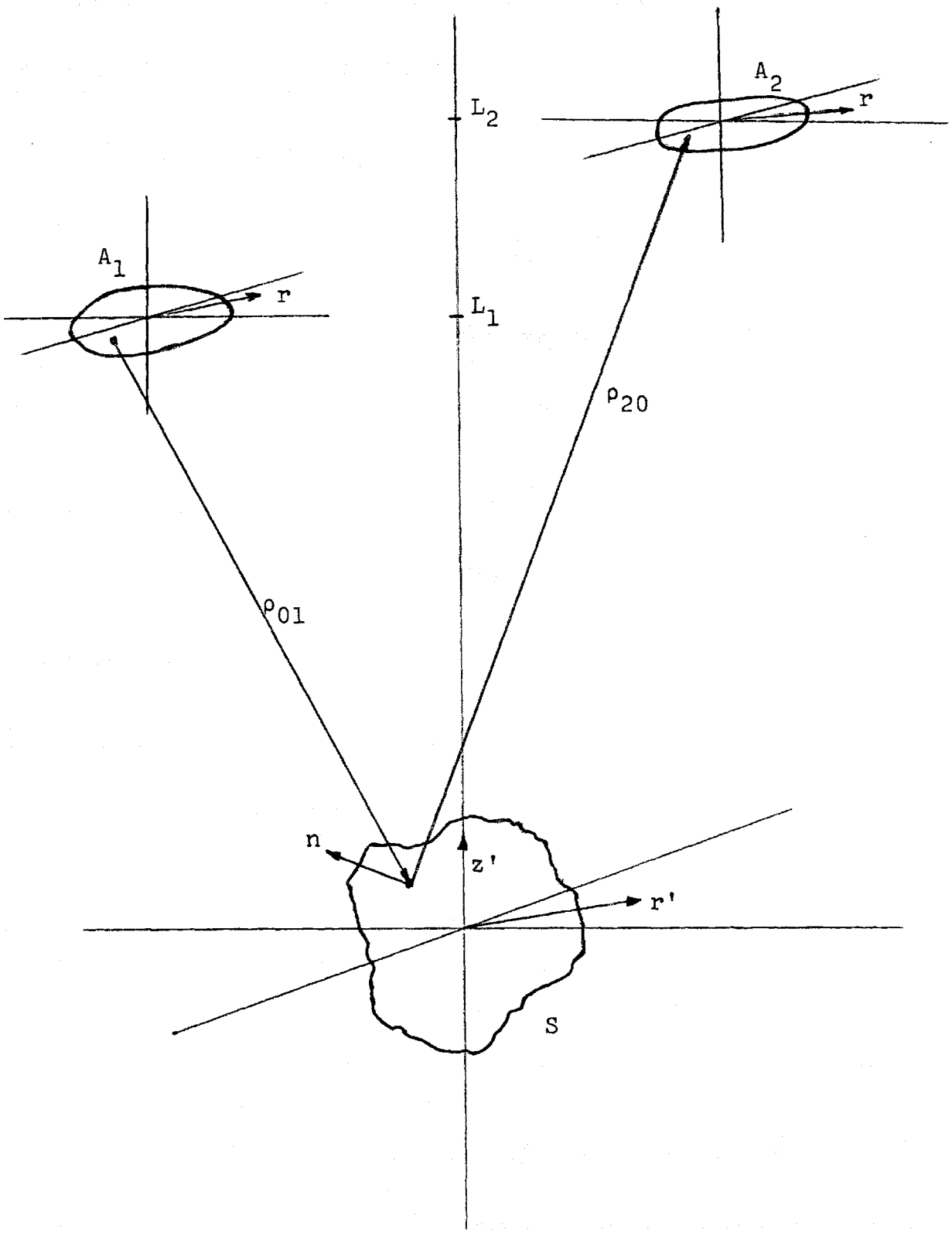

FIGURE 2.2: GEOMETRY UTILIZED IN FORMULATING THE SCATTERING MODEL AND THE RADAR MODEL

$$E_0(r,t) = \int_{A_1} d\hat{r} \int_{T_1} d\hat{t}\; E_i(\hat{r},t-\hat{t})\; h_{2S1}(r,\hat{r},t,\hat{t}),$$

$$r \in A_2,\ t \in T_2. \qquad (2.23)$$

Because the field incident on the surface, $E_{is}(r',t')$, may be calculated from the transmitted field via the Huygens-Fresnel principle [14] and since the field reflected from the surface, $E_{0s}(r',t')$, may be used to calculate the received field by means of the Kirchhoff-Helmholtz integral theorem [15], evaluation of this impulse response requires, in principle, only the development of a relationship between the incident field and the reflected field. Determination of the necessary relationship and its subsequent use in the integral theorem remains a difficult diffraction-theory problem which has been rigorously solved only for very specialized surfaces [15]. In the ensuing subsections, we examine two approximate methods for accomplishing this task.

Once a mathematical relationship between $E_{is}(r',t')$ and $E_{0s}(r',t')$ has been developed, there is still significant difficulty in deducing the physical properties of the corresponding surface. We avoid these issues which are discussed elsewhere [16] as, for our purposes, the relationship itself is a satisfactory specification of the surface.

2.2.2 Point Scatterer

Sufficiently rough surfaces [13] scatter incident, nongrazing radiation diffusely, *i.e.*, with negligible specular component. For these

surfaces, a simple yet accurate model [17, 18, 19] is obtained when the surface is approximated by a collection of point scatterers each of which is characterized by its location (r_n', z_n') and strength $\alpha_n' \delta r_n'$. When the field $E_{is}(r', z', t')$ is incident upon this collection, the reflected field, $E_{0s}(r', z', t')$ may be modeled in the following manner

$$E_{0s}(r', z', t') = \sum_n E_{is}(r_n', z_n', t_n')\alpha'(r_n')\delta r_n' \; u_0(r' - r_n'),$$

$$r'z' \in S, \; t' \in T_0 \qquad (2.24)$$

provided this relationship is not used to calculate scattered fields near to (within one-half the planar diameter of) the rough surface [20].

For a temporally narrowband field, the complex envelopes are similarly related

$$E_{0s}(r', z', t') = \sum_n E_{is}(r_n', z_n', t_n')\alpha'(r_n') \; \delta r_n' \; u_0(r' - r_n'),$$

$$r', z' \in S, \; t' \in T_0. \qquad (2.25)$$

The principal advantage of this approximation is that the Huygens-Fresnel principle may be used to interject both the received and the transmitted envelopes into this expression

$$E_0(r,t) = \sum_n \int_{A_1} d\hat{r}\, E_i\left(\hat{r}, t - \frac{\hat{d}_n}{c} - \frac{d_n}{c}\right) \frac{e^{jk\hat{d}_n}}{j\lambda\hat{d}_n}\, \alpha'(r_n')\, \delta r_n' \frac{e^{jkd_n}}{j\lambda d_n},$$

$$r \in A_2,\ t \in T_2. \qquad (2.26)$$

Here, T_2 is a time-shifted (by $[L_1+L_2]c^{-1}$) version of T_1 and the distances d_n and d_n are given by the following modifications of the usual paraxial approximation [14]

$$\hat{d}_n = (L_1-z_n')^2 + |\hat{r}-r_n'|^2 \tilde{=} L_1 + \frac{|\hat{r}-r_n'|^2}{2L_1} - z_n' \triangleq \hat{s}_n - z_n', \qquad (2.27a)$$

$$d_n = (L_2-z_n')^2 + |r-r_n'|^2 \tilde{=} L_2 + \frac{|r-r_n'|^2}{2L_2} - z_n' \triangleq s_n - z_n', \qquad (2.27b)$$

where the approximations also utilize the assumptions of the previous section. We rewrite Equation 2.26 in terms of the distance parameters s_n and s_n simultaneously exploiting the narrow bandwidth of the transmitted envelope to disregard the z' terms in $E_i(\cdot)$

$$E_0(r,t) = \sum_n \int_{A_1} d\hat{r}\, E_i\left(\hat{r}, t - \frac{\hat{s}_n}{c} - \frac{s_n}{c}\right)\left(\frac{e^{jk\hat{s}_n}}{j\lambda\hat{s}_n}\right)\left(\frac{e^{jks_n}}{j\lambda s_n}\right) \alpha'(r_n')\, \delta r_n' \exp[-2jkz'(r_n')],$$

$$t \in T_2,\ r \in A_2,\ r_n' \in P. \qquad (2.28)$$

where P is the projection of S onto the plane $\{z' = 0\}$. Thus, the surface is being represented as a co-planar collection of point scatterers with individual strength

$$b(r_n') = \alpha'(r_n')\ \delta r_n'\ \exp[-2jkz'(r_n')], \qquad r_n' \in P. \tag{2.29a}$$

In the limit as the scatterers become infinitely dense, the surface is represented by the function

$$b(r') = \alpha'(r')\ \exp[-2jkz'(r')], \quad r' \in P, \tag{2.29b}$$

and the scattering impulse response for complex envelopes is the following

$$h_{2S1}(r,\hat{r},t,\hat{t}) = \int_P dr'\ b(r')h_0(r,r')h_0(r',\hat{r})u_0(t-\hat{t}-\frac{\hat{s}}{c}-\frac{s}{c}), \qquad t \in T_2,\ \hat{t} \in T_1,\ r \in A_2,\ \hat{r} \in A_1, \tag{2.30}$$

where the previous definitions are used for $\hat{s}$ and s.

2.2.3 Tangent Plane Approximation

In this section, we examine a physically oriented approach [13] that is based on the assumption that the radius of curvature of any irregularity on the surface S is large in comparison with the carrier wavelength, λ_0.

This assumption implies that, for an incident plane wave, the reflected field at any point on the surface is equal to the field that would be present on the tangent plane at that point, *i.e.*, that the reflected field and its normal derivative (the dot product of its gradient and the unit normal to the surface) are specified as follows

$$E_{0s}(r',z',t') = [1 + R(r')]\, E_{is}(r',z',t'),$$

$$r',z' \in S,\ t' \in T_0, \qquad (2.31a)$$

$$\frac{\partial E_{0s}(r',z',t')}{\partial n} = [1 - R(r')]\, \frac{\partial E_{is}(r',z',t')}{\partial n},$$

$$r',z' \in S,\ t' \in T_0 \qquad (2.31b)$$

where $\vec{n}$ is the unit normal to the surface, R is the reflection coefficient, and $E_{is}(r',z',t')$ is required to be a plane wave. Again, the complex envelopes satisfy similar relationships

$$E_{0s}(r',z',t') = [1 + R(r')]\, E_{is}(r',z',t'),$$

$$r',z' \in S,\ t' \in T_0, \qquad (2.32a)$$

$$\frac{\partial E_{0s}(r',z',t')}{\partial n} = [1 - R(r')]\, \frac{\partial E_{is}(r',z',t')}{\partial n},$$

$$r',z' \in S,\ t' \in T_0, \qquad (2.32b)$$

when $E_{is}(r',z',t')$ is the complex envelope of a plane wave.

To handle more general incident envelopes, we decompose them into Fourier components over the plane $\{z' = 0\}$

$$F_{is}(K',t') = \int_P dr' \exp[-j(K'\cdot r')] E_{is}(r',0,t'),$$

$$t' \in T_0. \qquad (2.33)$$

The reflected envelope is determined by the following equations

$$E_{0s}(r',z',t') = E_{is}(r',z',t') +$$

$$\exp[-jkz'(r')]\{\int dK\exp[+j(K\cdot r')] \int dK'R(r',K,K')F_{is}(K',t')\},$$

$$t' \in T_0,\ r',z' \in S, \quad (2.34a)$$

$$[\partial E_{os}(r',z',t')/\partial n] = [\partial E_{is}(r',z',t')/\partial n] - \exp[-jkz'(r')]\int dK$$

$$\exp[j(K\cdot r')]\{\int dK'R(r',K,K')[u_{z'}\cdot\vec{n}(r')]F_{is}(K',t')\},$$

$$t' \in T_0,\ r',z' \in S, \qquad (2.34b)$$

where $\vec{u}_{z'}$ is a unit vector in the z' direction. To obtain Equation 2.34b, we have further assumed that the surface is perfectly conducting (cf.,

Beckmann [13]). Substituting these forms into the Kirchoff-Helmholtz integral theorem, we determine the received complex envelope

$$E_0(r,t) = \int_P dr' \exp[-2jkz'(r')]\, h_0(r,r')$$

$$[\int dK \exp[j(K\cdot r')] \int dK' R(r',K,K') F_{is}(K',t-[s/c])],$$

$$r \in A_2,\ t \in T_2. \qquad (2.35)$$

The presence of the free space impulse response in Equation 2.35 permits the definition of an effective reflected envelope, $E_{0s}'(r',0,t')$, *i.e.*, one which propagates from P to A_2 according to the Huygens-Fresnel principle,

$$E_{0s}'(r',0,t') = \exp[-2jkz'(r')] \int dK \exp[j(K\cdot r')]$$

$$\int dK' R(r',K,K') \int_P dr'' E_{is}(r'',0,t') \exp[-j(K'\cdot r'')],$$

$$r' \in P,\ t' \in T_0. \qquad (2.36)$$

For this derivation, the scattering impulse response for complex envelopes is given by the ensuing expression

$$h_{2S1}(r,\hat{r},t,\hat{t}) = \int_P dr' \exp[-2jkz'(r')]h_0(r,r') \int dK \exp[(j(K\cdot r')]$$

$$\int dK' R(r',K,K') \int dr'' \exp[-j(K'\cdot r'')]h_0(r'',\hat{r})u_0(t-\hat{t}-[s/c]-[s/c]),$$

$$r \in A_2,\ r \in A_1,\ t \in T_2,\ t \in T_1. \quad (2.37)$$

Although the equation (2.36) has limited utility due to its complicated form, an interesting specialization results when the reflection coefficient satisfies the following

$$R(r',K,K') = R_0(r')\ F(K-K'),$$

$$r' \in P, \quad (2.38)$$

where $R_0(r')$ controls the local reflection strength and $F(K-K')$ represents the scattering pattern for the surface. Equation 2.38 leads to the relationship

$$E_{0s}'(r',0,t') = \exp[-2jkz'(r')]R_0(r')\delta(r')E_{is}(r',0,t'),$$

$$r' \in P,\ t' \in T_0, \quad (2.39)$$

where $\delta(r')$ is the inverse Fourier transform of $F(K)$. In accord with previous results (cf., Equation 2.29b), the surface is again represented by a multiplicative operator.

2.2.4 Turbulent Scattering Model

The analogous scattering impulse response for complex envelopes in a turbulent environment follows from the observation that the interrelationship between the reflected and incident envelopes (either (2.28) or (2.35)) does not involve the medium itself. In both derivations, the Huygens-Fresnel principle is used to introduce both the transmitted and received envelopes into the scattering impulse responses ((2.30) and (2.37)). Consequently, for the turbulent medium, we may use the extended Huygens-Fresnel principle [21] to form the scattering impulse response from the relationship between the reflected and incident envelopes. For the point scatterer approximation, we thus obtain

$$h_{2S1}(r,\hat{r},t,\hat{t}) = \int_P dr'\ b(r')h_{2P}(r,r',t)h_{P1}(r',\hat{r},t-[s/c])$$

$$u_0(t-\hat{t}-[\hat{s}/c]-[s/c]),$$

$$t \in T_2,\ \hat{t} \in T_1,\ r \in A_2,\ \hat{r} \in A_1, \quad (2.40)$$

where the turbulent impulse response has been defined in (2.2). The more complicated result for the tangent plane approximation is given by the following expression

$$h_{2S1}(r,\hat{r},t,\hat{t}) = \int_P dr' \exp[-2jkz'(r')]h_{2P}(r,r',t) \int dK \exp[j(K\cdot r')]$$

$$\int dK' R(r',K,K') \int dr'' \exp[-j(K'\cdot r'')]h_{P1}(r'',\hat{r},t-[s/c])$$

$$\cdot u_0(t-\hat{t}-[\hat{s}/c]-[s/c]),$$

$$r \in A_2,\ \hat{r} \in A_1,\ t \in T_2,\ \hat{t} \in T_1. \quad (2.41)$$

Henceforth, we shall employ the point scatterer model as specified by Equation 2.29b andEquation 2.40 since it combines analytical simplicity with an accurate description of physical phenomena. Some of its applications are discussed in the recent literature [22, 23].

2.3 An Optical Radar in the Clear Turbulent Atmosphere

Previous treatments [*e.g.*, 24-27] of optical radar systems concerned themselves primarily with specific applications and concentrated on the temporal aspects of this subject. By combining the material in the preceding sections, we obtain a model which includes the spatial behavior of these systems. The complexity of this model then necessitates the development of a hierarchy of related specializations.

2.3.1 Radar Model

The relevant geometry has been established in Figure 2.2 and the specification of this system was developed in Section 2.2.4 (Equations 2.29 and 2.40). The characterization of this model is completed by specification of the joint statistics of the pair of turbulent channel impulse responses involved in Equation 2.40. To avoid analytical complications, we shall assume that these terms are statistically independent. Although it is not always physically justifiable, this assumption becomes more accurate as the pathlengths or the aperture offsets are increased. Each of these terms is specified according to the method of Section 2.1.2 and can be subjected to the decomposition and approximations of the succeeding sections.

To complete the description of the model, we must include the relevant polarization component of the complex envelope of the additive background noise which has also been specified in Section 2.1.2. The received envelope is now given by the following expression

$$E_0(r,t) = \int_P dr'\ h_0(r,r')\exp[x_{2p}(r,r',t)+j\phi_{2p}(r,r',t)]b(r')$$

$$+ \{\int_{A_1} d\hat{r}\ E_i(\hat{r}\text{-}t\text{-}[s/c]\text{-}[\hat{s}/c])h_0(r',r)\exp[x_{p1}(r',\hat{r},t\text{-}[\hat{s}/c])+j\phi_{p1}(r',\hat{r},t\text{-}[\hat{s}/c])]$$

$$n(r,t), \qquad r \in A_2,\ t \in T_2, \tag{2.42}$$

where $n(r,t)$ represents the background noise. If the transmission interval is less than a temporal coherence length, then we may employ the simplified relationship

$$E_0(r,t) = \int_P dr'\ h_0(r,r')\exp[x_{2p}(r,r')+j\phi_{2p}(r,r')]\ b(r')$$

$$\{\int_{A_1} d\hat{r}\ E_i(\hat{r},t)h_0(r',\hat{r})\exp[x_{p1}(r',\hat{r})+j\phi_{p1}(r',\hat{r})]\} + n(r,t),$$

$$r \in A_2,\ t \in T_2, \tag{2.43}$$

where we ignore the channel delay times.

In order to account for quantum effects which are important at optical frequencies, we employ the structured approach [3] with emphasis on heterodyne receivers. For our purposes, it is sufficient to describe the statistics of the receiver output in terms of the field which serves as the input to the receiver. In the heterodyne receiver the local oscillator field with complex envelope

$$E_h(r,t) = E_h(r)\exp[j2\pi f_h t], \qquad r \in A_2,\ t \in T_2, \tag{2.44}$$

is purposely added to the received field. The resulting field is then incident on an array of photodetectors where the i-*th* such detector occupies the area $A_{2,i}$. The complex envelope of the normalized output from the i-*th* detector, conditioned on knowledge of $E_0(r,t)$, may be modeled as

$$y_i(t) = \{\int_{A_{2,i}} E_0(r,t)E_h^*(r,t)/[\int_{A_{2,i}} dr|E_h(r)|^2]^{1/2}\} + w_i(t),$$

$$t \in T_2,\ i \in 1,2,\ldots,N_{DET}, \tag{2.45}$$

where N_{DET} is the number of photodetectors. The signal-independent noise process $\{w_i(t)\}$ are independent, zero-mean white complex Gaussian random processes which possess independent real and imaginary parts with identical correlation functions. The spectral height of each complex process is given by

$$N_0 = N_{0b} + [hf_0/\eta_{eff}], \tag{2.46}$$

where N_{0b} is the spectral height of the component of the background noise (cf., Section 2.1.2) extracted by heterodyning [82], h is Planck's constant and η_{eff} is the quantum efficiency of the photodetector.

During the development of this model, we have utilized certain assumptions as a matter of convenience. Included in this group are these:

(0) transmitted envelopes are temporally narrowband;

(1) surface depolarization effects are unimportant;

(2) the perturbation statistics for a statistically homogeneous and isotropic channel are employed;

(3) the cross-covariance of the log-amplitude and the phase of the perturbation term is zero;

(4) the background radiation is temporally and spatially white;

(5) the viewing angle between the transmitter and the receiver is small;

(6) the height variations of the surface are much smaller than either pathlength which is involved;

(7) the surface has a fixed shape;

(8) the surface maintains a fixed orientation with respect to the system apertures;

(9) the surface scatters incident radiation diffusely;

(10) the statistics of the two perturbation terms are independent.

For contexts wherein an assumption (collection of assumptions) contained in this list is not valid, it (they) may be removed from the development of the radar model with a concomitant increase in the complexity of the resulting formulation. For our analysis, the model originally derived is satisfactory.

2.3.2 Estimation Formulation

Using the radar model, we consider the problem of estimating the nonrandom function, $b(r')$, which describes the rough surface. Estimators are formed by processing the received signal and their quality is judged by a minimum-mean-square-error criterion. The maximum likelihood technique [28] generates useful estimators under these circumstances and the Cramer-Rao bound [28] indicates indirectly the quality of an arbitrary estimator. Application of these techniques here is intractable because a suitable representation for the received field cannot be found. To gain insight into this model, we therefore develop a hierarchy of related, albeit simpler, estimation problems based on the results given in Section 2.1.

In particular, we dichotomize the apertures and the effective surface P in accordance with the number of turbulent coherence areas (one or more than one) that each contains and the channels according to the number of turbulent modes (one or more than one) that are supported. Thus the formulation denoted 11mm1 means that A_1 and A_2 each contain a single coherence area; P contains more than one coherence area, one mode propagates from A_1 to P and many modes propagate from P to A_2. Because the number of modes and the number of coherence areas are interrelated, some of the formulations thus obtained do not represent physically realistic situations. Specifically, we disallow any formulation which involves, over either of its channels, many modes propagating between two single-coherence-area apertures or a single mode propagating between two

multi-coherence-area apertures. A discussion of these disregarded cases is given in Appendix 2C. The remaining formulations are collected in related groups in Table 2.2. The estimation problems thus formulated are the basis for further work and the tractable ones will be analyzed in the ensuing chapters.

TABLE 2.2

Coherent Target	Partially Coherent Target
Cross-Section	*Cross-Section*
1-1-1-1-1	1-1-m-1-1
1-1-1-1-m	
m-1-1-1-1	
m-1-1-1-m	
Imaging	*Imaging*
1-1-1-m-m	1-1-m-m-1
m-1-1-m-m	1-1-m-m-m
Scanning	*Scanning*
m-m-1-1-1	1-m-m-1-1
m-m-1-1-m	m-m-m-1-1
Imaging & Scanning	*General Formulation*
m-m-1-m-m	1-m-m-m-1
	1-m-m-m-m
	m-m-m-m-1
	m-m-m-m-m

This is the hierarchy of estimation problems generated by the decomposition technique described in Section 2.3.2.

CHAPTER 3

In this chapter we consider simplified formulations for which the effective surface aperture P is contained within a turbulent coherence area. As discussed in Section 2.1.4, this restriction justifies the use of the (strict) isoplanatic approximation for the reception channel thereby obtaining a formulation which is commonly encountered in the literature, *e.g.*, [10,31,45]. For convenience, we are using its counterpart, the unilateral coherence approximation, in our work. The chapter is divided into sections based on the propagation regimes of the reception channel.

CHAPTER 3

In this chapter we consider simplified formulations for which the effective surface aperture P is contained within a turbulent coherence area. As discussed in Section 2.1.4, this restriction justifies the use of the (strict) isoplanatic approximation which is commonly encountered in the literature, *e.g.*, [10, 31, 45]. The chapter is divided into sections based on the propagation regimes of the reception channel.

3.1 Coherent Cross Section

Here we examine the specific cases which are collected in the coherent cross section group in Table 2.2. They involve far field propagation in both channels as well as a reflecting surface that is contained within the appropriate coherence area so that the surface is completely characterized by its coherent cross section. On account of their length, the required computations are explicitly given only for the simplest formulation; but they follow analogously for more complicated ones. A summary which compares the attainable performance for these cases is also included.

3.1.1 Simple Fading Model (11111)

Here all of the apertures, including the effective surface aperture, are contained within the appropriate coherence areas and the transmission interval is limited to a temporal coherence interval so that both perturbation terms may be approximated by random variables (cf., Equation 2.11). Consequently, the modes for both channels ($\hat{\Phi}_{i1}(\hat{r})$ and $\hat{\Phi}_{01}(r')$ for the transmission channel and $\Phi_{i1}(r')$ and $\Phi_{01}(r)$ for the reception channel) are deterministic and equal to the corresponding free space modes. The most general transmitted envelope with energy $|E_{i1}|^2$ thus has the form

$$E_{i1}(\hat{r},\hat{t}) = E_{i1}\,\Phi_{i1,0}(\hat{r})\,[1/\sqrt{T}],$$

$$\hat{r} \in A_1, \quad \hat{t} \in T_1, \tag{3.1}$$

where T is the length of the transmission interval. This transmission produces the received envelope (obtained from Equation 2.43 by use of Equation 2.6)

$$\gamma(r,t) = E_{02}(r,t) + n(r,t) =$$

$$[1/\sqrt{T}]\exp[x_1+j\phi_1]\exp[x_2+j\phi_2]\alpha_0 b_0 E_{i1}\Phi_{01,0}(r) + n(r,t),$$

$$r \in A_2,\ t \in T_2, \tag{3.2}$$

where T_2 is a time-shifted (by $(L_1+L_2)c^{-1}$) version of T_1. In this expression, we have employed the following definitions:

$$\alpha_0 \triangleq [-\exp[jk(L_1+L_2)]P(A_1A_2)^{1/2} =$$

$$-\exp[jk(L_1+L_2)](n_{1,0}\hat{n}_{1,0})^{1/2}; \tag{3.3a}$$

$$b_0 \triangleq [1/P]\int_P dr'\ b(r')\ \hat{\Phi}_{01,0}(r')\ \Phi_{i1,0}^{*}(r'); \tag{3.3b}$$

$$\exp[x_1+j\phi_1] \triangleq \exp[x_{P1}(0,0)+j\phi_{P1}(0,0)]; \tag{3.3c}$$

$$\exp[x_2+j\phi_2] \triangleq \exp[x_{2P}(0,0)+j\phi_{2P}(0,0)]. \tag{3.3d}$$

In Equation 3.3a $\hat{n}_{1,0}(n_{1,0})$ is the eigenvalue corresponding to the mode $\hat{\Phi}_{i1,0}(\hat{r})$ $(\Phi_{i1,0}(r'))$ which is supported by the free space transmission (reception) channel. The parameter α_0 may be interpreted as a free space propagation parameter for this model and the parameter b_0 represents the coherent cross section of the surface (target).

For this model, the additive noise, n(r,t), consists of background noise and an additional term included to represent quantum noise. Since subsequent processing of the received envelope invariably involves a spatial correlation (*e.g.*, Equation 3.7), the level of this additional noise term is adjusted according to Equation 2.46 so that the correlation corresponds to the operation of a heterodyne receiver (*cf.*, Section 2.3.1). If N_0 denotes the height of the power spectrum for the additive noise, then the likelihood ratio for this formulation is the following expression

$$= \langle \exp\{[-\exp[2x_2]\exp[2x_1]|b_0\alpha_0 E_{i1}|^2/N_0]\}$$

$$\cdot \exp\{[2/\sqrt{T}\, N_0]\mathrm{Re}[\exp x_1 + j\phi_1]\exp[x_2 + j\phi_2]$$

$$\alpha_0 b_0 E_{i1} \int_{T_2} dt \int_{A_2} dr\, \gamma^*(r,t)\Phi_{01,0}(r)]\}\rangle_{\substack{x_1 x_2 \\ \phi_1 \phi_2}} \qquad (3.4)$$

where $\langle\cdot\rangle$ denotes an ensemble average. The received envelope appears in (3.4) only as a correlation, γ_0,

$$\gamma_0 \triangleq \int_{T_2} dt \int_{A_2} dr\ \gamma(r,t)\ \phi_{01,0}^{*}(r)\ [1/\sqrt{T}], \tag{3.5}$$

which is therefore a sufficient statistic [28] so that an equivalent formulation is given by

$$\gamma_0 = \exp[x_1+j\phi_1]\exp[x_2+j\phi_2]\alpha_0 E_{i1} b_0 + n_0, \tag{3.6}$$

where n_0 is defined below

$$n_0 = \int_{T_2} dt \int_{A_2} dr\ n(r,t)\ \phi_{01,0}^{*}(r)\ [1/\sqrt{T}]. \tag{3.7}$$

Prior assumptions imply that the four turbulent random variables in (3.6) are independent (cf., Section 2.1.2 and Section 2.3.1). For typical pathlengths, the further approximation of uniform distributions for ϕ_1 and ϕ_2 is well justified [29]. The likelihood ratio now reduces to the form

$$= Fr([|\alpha_0 b_0 E_{i1}|^2/N_0],[|\gamma_0|/N_0^{1/2}];\sigma_1^2 + \sigma_2^2) \tag{3.8}$$

in which $Fr(\cdot)$ is the frustration function defined and tabulated by Halme [30],

$$Fr(\alpha,\beta;\sigma^2) = \int_0^\infty du(\sqrt{2\pi}\,\sigma u)^{-1} \exp[-(\ell nu+\sigma^2)^2/2\sigma^2]$$

$$I_0(2\beta\sqrt{\alpha}\,u)\exp[-\alpha u^2] \qquad (3.9)$$

σ_1^2 is the variance of x_1, and σ_2^2 is the variance of x_2. The only available information about the surface is contained in the quantity $|b_0|$ that we have interpreted as a radar cross section dependent only on the viewing angle in Figure 2.2. This dependence is introduced into (3.3b) by the eigenfunctions but is unimportant to us since we consider a fixed geometry.

In principle, we may apply standard procedures [28] to Λ to form an estimate of $|b_0|$, a nonrandom parameter. This approach, however, does not provide tractable results, *e.g.*, the equation for the ML estimate

$$[\partial/\partial|b_0|]\{\ell n\, Fr([|\alpha_0 b_0 E_{ij}|^2/N_0],[|\gamma_0/N_0^{1/2}];\sigma_1^2+\sigma_2^2)\} = 0 \qquad (3.10)$$

leads to the following expression

$$\Big\langle \exp\Big[-\,|\alpha_0 b_0 E_{i1}|^2 \exp[2x_1]\exp[2x_2]/N_0\Big]$$

$$\Big\{-\exp[2x_1]\exp[2x_2]|\alpha_0 b_0 E_{i1}|\, I_0\big(2\exp[x_1]\exp[x_2]|\alpha_0 b_0 E_{i1}\gamma_0|/N_0\big)$$

$$+\,|\gamma_0|\exp[x_1]\exp[x_2] I_1\big(2\exp[x_1]\exp[x_2]|\alpha_0 b_0 E_{i1}\gamma_0|/N_0\big)\Big\}\Big\rangle_{x_1, x_2} = 0 \tag{3.11}$$

which cannot be solved for the ML estimate. Attempts to evaluate the CR bound are similarly thwarted by mathematical intractabilities. To circumvent these difficulties, we follow an approach due to Moldon [29] which consists of lower bounding the CR bound and approximating the ML estimator with the objective of determining an approximate estimator which possesses a mean-square error that does not significantly differ from the lower bound. While the selection of an estimator remains a matter of approximation and contrivance within the problem framework, a general technique has been developed for generating lower bounds. For this case only we present a detailed application of this approach (henceforth designated Moldon's technique) to indicate the nature of the necessary computations.

Although a variety of approximations for the ML estimator may be obtained from (3.11), these quantities are useful only when we can evaluate (explicitly or within reasonable limits) their biases and mean-square errors which are related to their first and second moments.

Since these approximate estimators depend only on the magnitude of the received parameter, $|\gamma_0|$, its density [84]

$$p(|\gamma_0| \,\Big|\, |b_0|) = [2|\gamma_0|/N_0]\exp[-|\gamma_0|^2/N_0]$$

$$\mathrm{Fr}([|\alpha_0 b_0 E_{i1}|^2/N_0];[|\gamma_0|/N_0^{1/2}];\sigma_1^2 + \sigma_2^2) \tag{3.12}$$

determines which of them are tractable (*i.e.*, have moments which can be evaluated). The only functions which we can presently average over this density are positive even moments of $|\gamma_0|$, namely

$$<|\gamma_0|^{2n}> = N_0^n\, n! \sum_{m=0}^{n} \binom{n}{m} [1/n!](|\alpha_0 b_0 E_{i1}|^2/N_0)^m$$

$$\exp[2(\sigma_1^2+\sigma_2^2)(m^2-m)],$$

$$n = 1,2,3,\ldots, \tag{3.13}$$

wherein the moment theorem [31] for lognormal random variables has been used. This inability to determine other expectations will limit the selection of estimators.

For the parameter $|b_0|$ itself, approximations to Equation 3.11 yield estimators which involve odd powers of $|\gamma_0|$ and which are

therefore intractable. Consequently, we turn to $|b_0|^2$ for which similar approximations involve even powers of $|\gamma_0|$ and thus lead to tractable estimators. This change of parameter is not a serious modification because $|b_0|$ and $|b_0|^2$ share a one-to-one relationship. The estimator obtained by using large argument approximations [28] for the Bessel functions in the equation that specifies the ML estimate of $|b_0|^2$ is proportional to $|\gamma_0|^2$. We remove the bias from this estimator to obtain

$$|b_0|^2 = \left(|\gamma_0|^2 - N_0\right)\left(|\alpha_0|^2 |E_{i1}|^2\right)^{-1} \tag{3.14}$$

which is tractable with normalized mean-square error

$$\mathrm{Var}(|b_0|^2)/|b_0|^4 = (\exp[4(\sigma_1^2+\sigma_2^2)]-1) +$$

$$2N_0/|\alpha_0 b_0 E_{i1}|^2 + N_0^2/|\alpha_0 b_0 E_{i1}|^4, \tag{3.15a}$$

$$\underline{\Delta}\ (\exp[4\sigma^2]-1) + [2/\Lambda_0] + [1/\Lambda_0^2]. \tag{3.15b}$$

where Λ_0 may be interpreted as a signal-to-noise ratio (SNR). From this expression, we observe that the performance of the preceding estimator is optimized by utilizing the largest permissible transmitting and receiving apertures, namely, the respective coherence areas which are denoted $A_{1,coh}$ and $A_{2,coh}$, respectively. Under these conditions,

the mean-square error is given by

$$\mathrm{Var}(|\hat{b}_0|^2)/|b_0|^4 = (\exp[4\sigma^2]-1) + [2/\Lambda_c] + [1/\Lambda_c^2] \tag{3.16a}$$

where we define the parameters

$$\Lambda_c = |\alpha_c b_0 E_{i1}|^2/N_0 \tag{3.16b}$$

$$\alpha_c = \alpha_0\Big|_{\substack{A_{1,coh} \\ A_{2,coh}}} = -\exp[jk(L_1+L_2)]P(A_{1,coh}A_{2,coh})^{1/2}/\lambda^2 L_1 L_2. \tag{3.16c}$$

The quality of this estimator may be determined by comparison with the lower bound to the CR bound. This bound consists of a collection of bounds developed from the observation (proven and discussed in Appendix 3A) that the usual CR bound satisfies the inequality

$$\mathrm{Var}(\hat{\beta}-\beta) \geq -\langle[\partial^2/\partial\beta^2]\ln p(\gamma|\beta)\rangle_\gamma^{-1} \geq -\langle\langle[\partial^2/\partial\beta^2]\ln p(\gamma|\beta,\Delta)\rangle_{\gamma|\Delta}\rangle_\Delta^{-1} \tag{3.17}$$

where γ is the observation, β is a nonrandom real parameter, $\hat{\beta}$ is an unbiased estimate of β, and Δ is a supplementary random variable. This result can be applied here with supplementary vectors $\{x_1,\phi_1,x_2,\phi_2\}$, $\{n_0\}$, and $\{x_1,x_2\}$ which respectively yield the three members of the normalized lower bound

$$\mathrm{Var}(|\hat{b}_0|^2)/(|b_0|^2)^2 \geq \sup([2/\Lambda_c], 4\sigma^2, \ [2\exp[4\sigma^2]\Lambda_c^2+2\exp[12\sigma^2]\Lambda_c^3+\exp[24\sigma^2]\Lambda_c^4]^{-} \tag{3.18a}$$

Alternative techniques, also discussed in Appendix 3A, enable us to tighten this bound as follows

$$\mathrm{Var}(|\hat{b}_0|^2)/(|b_0|^2)^2 \geq \sup([2/\Lambda_c], 4\sigma^2(1+2\sigma^2), \ [2\Lambda_c^2+\Lambda_c^3]^{-1}). \tag{3.18b}$$

This pair of bounds and the mean-square error are co-plotted in Figure 3.1 for the worst case, *i.e.*, for $\sigma^2 = .5$, the largest (saturation) fading variance which the turbulent channel permits [2]. From this graph, we observe that increases in the SNR, Λ_c, provide significant improvement in performance when this quantity is small ($\Lambda_c << 1$) but virtually no improvement when it is large. The performance of the estimator is thus turbulence-limited when favorable signal-to-noise ratios can be achieved. In Figure 3.2, we plot the ratio of estimator error to lower bound which varies modestly (from 1.6 to 3.6) even in the worst case thereby justifying our subsequent use of this estimator.

When the transmission extends over M temporal coherence intervals, we may argue from the frozen atmosphere hypothesis (*cf.*, Section 2.1.2) that the received envelope is a sequence of M independent parameters $\{\gamma_{0m}\}_{m=1}^{M}$ which are similar to γ_0. By linearly combining the appropriate estimator from each coherence interval,

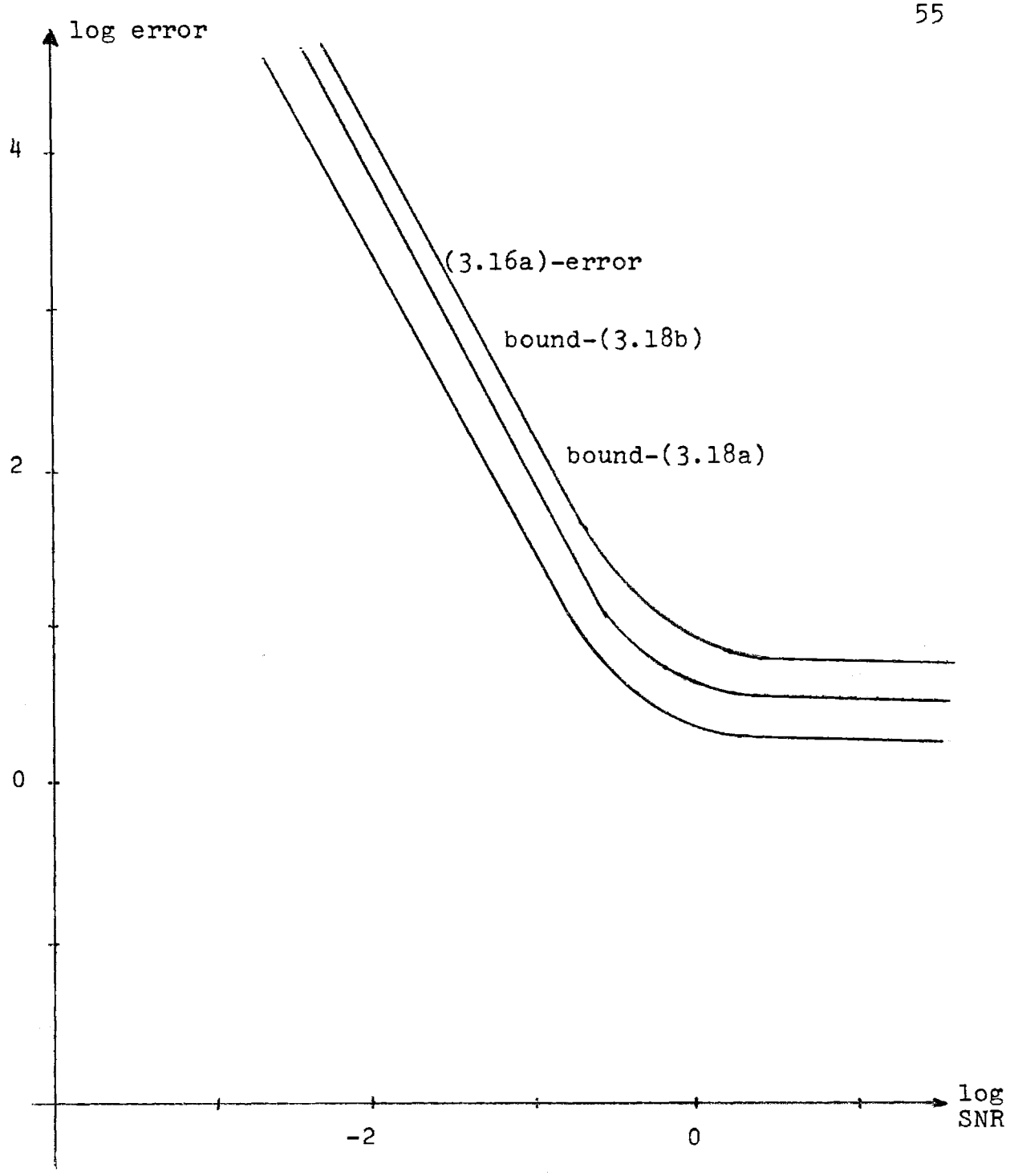

FIGURE 3.1: LOG-LOG PLOT OF NORMALIZED ERROR AND BOUNDS VERSUS SNR, Λ_c, FOR $\sigma^2 = .5$

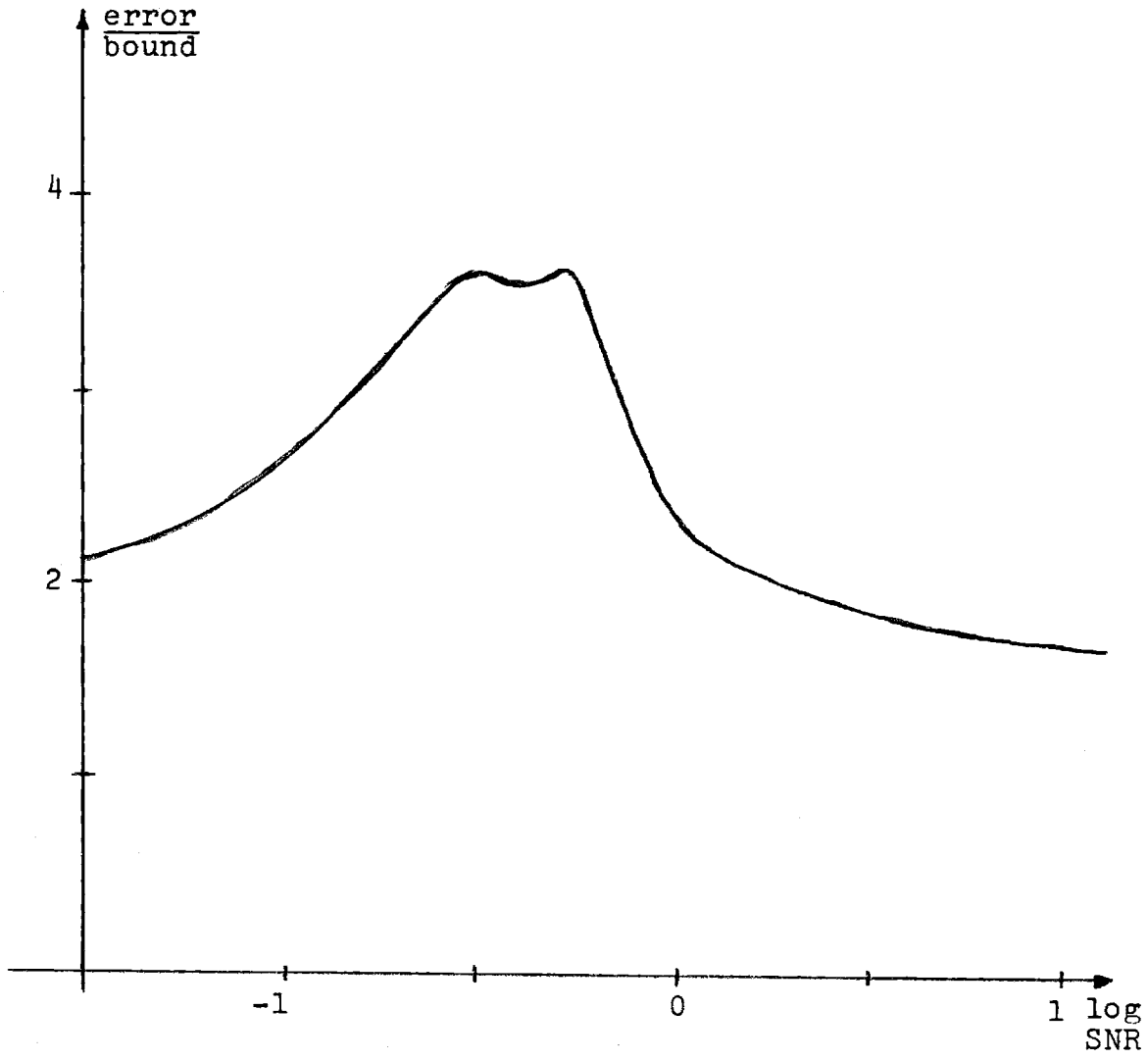

FIGURE 3.2: SEMI-LOG PLOT OF THE RATIO OF ESTIMATOR ERROR (3.16A) TO LOWER BOUND (3.18B) VERSUS SNR, Λ_c, FOR $\sigma^2 = .5$

$$|\hat{b}_0|^2 = [1/M] \sum_{m=1}^{M} [|\gamma_{0m}|^2 - N_0] |\alpha_c E_{i1}|^2 \qquad (3.19)$$

we obtain the usual diversity improvement (M^{-1}) in performance. Since this improvement factor also applies to the lower bound, Figure 3.2 still indicates the relative behavior of the bounds and the error. To ensure the independence of the received parameters, it may be necessary to consider various transmission schemes such as skipping alternate temporal coherence intervals or utilizing only the first half of each interval thereby decreasing the diversity gain.

3.1.2 Receiver Diversity Model (1111m)

In this case, apertures A_1 and P are contained within the appropriate coherence areas, but aperture A_2 is not. Accordingly within a temporal coherence interval, we use the random variable approximation for the perturbation term corresponding to the transmission channel and the unilateral coherence approximation (cf., Equation 2.16) for the perturbation term corresponding to the reception channel. Here, the most general transmitted envelope with energy $|E_{i1}|^2$ is given by

$$E_{i1}(\hat{r},\hat{t}) = E_{i1}\, \hat{\Phi}_{i1,0}(\hat{r})\, [1/\sqrt{T}],$$

$$\hat{r} \in A_1, \hat{t} \in T_1, \qquad (3.20)$$

where T is the length of the transmission interval T_1. This trans-

mission causes the following output

$$\gamma(r,t) = E_{02}(r,t) + n(r,t) =$$

$$[1/\sqrt{T}]\exp[\chi_1+j\phi_1]\exp[\chi_2(r)+j\phi_2(r)]\alpha_0 b_0 E_{i1}\Phi_{01,0}(r) + n(r,t),$$

$$r \in A_2,\ t \in T_2, \tag{3.21}$$

where T_2 is a time-shifted (by $(L_1+L_2)c^{-1}$) version of T_1, where $\exp[\chi_1+j\phi_1]$, α_0, and b_0 were defined in (3.3) and where

$$\exp[\chi_2(r)+j\phi_2(r)] \triangleq \exp[\chi_{2P}(r,0)+j\phi_{2P}(r,0)]. \tag{3.22}$$

If N_0 is the height of the power spectrum for the additive noise, then the likelihood ratio is given by

$$\boldsymbol{\Lambda} = \langle\exp\{[-\exp[2\chi_1]|\alpha_0 b_0 E_{i1}|^2/N_0] \int_{A_2} dr\, \exp[2\chi_2(r)]|\Phi_{01,0}(r)|^2\}\cdot\exp\{[2/\sqrt{T}\,N_0]$$

$$\mathrm{Re}[\exp[\chi_1+j\phi_1]\alpha_0 b_0 E_{i1} \int_{T_2} dt \int_{A_2} dr\, \gamma^*(r,t)\exp[\chi_2(r)+j\phi_2(r)]\Phi_{01,0}(r)] \Big\rangle_{\substack{\chi_1,\phi_2 \\ \chi_2(r),\phi_2(r)}}.$$

(3.23)

To perform the averaging operation with respect to the random process,

$x_2(r) + j\phi_2(r)$, we require a representation for this process. We defer a discussion of this issue to Appendix 3C and arbitrarily employ a method known as the coherence area decomposition technique. This approach partitions the aperture A_2 into N_2 coherence areas, $\{A_{2,\ell}\}_{\ell=1}^{N_2}$ over each of which the perturbation process is modeled as a random variable. We employ this representation in Equation 3.23 to obtain

$$\Lambda = \langle \exp\{[-\exp[2x_1]|\alpha_0 b_0 E_{i1}|^2/N_0] \sum_{\ell=1}^{N_2} \exp[2x_{2,\ell}]\xi_\ell\} \cdot$$

$$\exp\{[2/\sqrt{T}\, N_0]\mathrm{Re}[\exp[x_1+j\phi_1]\alpha_0 b_0 E_{i1} \sum_{\ell=1}^{N_2} \exp[x_{2,\ell}+j\phi_{2,\ell}] \int_{T_2} dt$$

$$\int_{A_{2,\ell}} dr\, \gamma^*(r,t)\Phi_{01,0}(r)]\}\rangle_{\{x_{2,\ell}\phi_{2,\ell}\}}^{x_1,\phi_1} \tag{3.24}$$

where we define the parameter ξ_ℓ

$$\xi_\ell = \int_{A_{2,\ell}} dr\, |\Phi_{01,0}(r)|^2. \tag{3.25}$$

The received envelope appears in (3.24) as a collection of correlation functionals (appropriately normalized)

$$\gamma_{\ell 0} \triangleq (T\xi_\ell)^{-1/2} \int_{T_2} dt \int_{A_{2,\ell}} dr\, \gamma(r,t)\Phi_{01,0}^{*}(r),$$

$$\ell = 1,2,\ldots,N_2, \tag{3.26}$$

which are a set of sufficient statistics for this formulation. An equivalent model is therefore given by

$$\gamma_{\ell 0} = \exp[\chi_1 + j\phi_1]\exp[\chi_{2,\ell} + j\phi_{2,\ell}]\alpha_0 b_0 E_{i1}\xi_\ell^{1/2} + n_{\ell 0},$$

$$\ell = 1,2,\ldots,N_2, \tag{3.27}$$

where $n_{\ell 0}$ is defined as follows

$$n_{\ell 0} = (T\xi_\ell)^{-1/2} \int_{T_2} dt \int_{A_{2,\ell}} dr\, n(r,t)\Phi_{01,0}^{*}(r),$$

$$\ell = 1,2,\ldots,N_2 \tag{3.28}$$

We assume that the N_2 pairs of turbulent random variables representing the process $\chi_2(r)+j\phi_2(r)$ are independent [33] (cf., Halme's discussion of independent samples [30]) and also that the real and imaginary parts of each pair are independent [1]. With the additional assumption that the distribution of any turbulent phase variable may be modeled as uniform [29], Equation 3.24 becomes

$$\Lambda = \Big\langle \prod_{\ell=1}^{N_2} \mathrm{Fr}([|b_0\alpha_0 E_{i1}|^2\xi_\ell \exp[2x_1]/N_0],[|\gamma_{\ell 0}|/N_0^{1/2}];\sigma_{2,\ell}^2)\Big\rangle_{x_1} \qquad (3.29)$$

where $\sigma_{2,\ell}^2$ $(= \sigma_2^2, \forall \ell)$ is the variance of $x_{2,\ell}$. The surface is again characterized by its coherent cross section $|b_0|$ which is to be estimated.

Standard estimation methods do not provide tractable estimators or bounds here so we must employ an indirect approach. Following the method described in Section 3.1.1, we obtain a tractable, unbiased estimator for $|b_0|^2$

$$|b_0|^2 = [1/N_2] \sum_{\ell=1}^{N_2} [|\gamma_{\ell 0}|^2 - N_0][|\alpha_0 E_{i1}|^2 \xi_\ell]^{-1} \qquad (3.30a)$$

The observation that $\Phi_{01,0}(r)$ is nearly a plane wave [8] over the aperture A_2 implies that the members of the set $\{\xi_\ell\}$ are nearly equal (cf., (3.25)) and hence that

$$\xi_\ell |\alpha_0|^2 \cong |\alpha_c|^2, \qquad \ell = 1,2,\ldots,N_2. \qquad (3.30b)$$

With the approximation, the estimator becomes

$$|b_0|^2 = [1/N_2] \sum_{\ell=1}^{N_2} [|\gamma_{\ell 0}|^2 - N_0] |\alpha_c E_{i1}|^{-2} \qquad (3.30c)$$

and it has normalized mean-square error

$$[\mathrm{Var}(|\hat{b}_0|^2)/|b_0|^4] = [1/N_2]\{(\exp[4\sigma^2]-1)+(N_2-1)(\exp[4\sigma_1^2]-1) +$$

$$[2/\Lambda_c] + [1/\Lambda_c^2]\}. \qquad (3.31a)$$

where we have utilized the parameter σ^2 which was defined in (3.15b). From (3.31a) we observe that the estimator error is minimized by utilizing every available receiver diversity element (coherence area). If we rewrite the error as follows, however,

$$[\mathrm{Var}(|\hat{b}_0|^2)/|b_0|^4] = (\exp[4\sigma_1^2]-1) + [1/N_2]\{(\exp[4\sigma^2]-\exp[4\sigma_1^2]) +$$

$$[2/\Lambda_c] + [1/\Lambda_c^2]\}. \qquad (3.31b)$$

the limiting effect of transmission path turbulence (via the term $(\exp[4\sigma_1^2]-1)$) on the performance of the estimator is apparent. The following selection, if possible, of N_2

$$N_2 = \sup(\lceil(\exp[4\sigma_1^2]-1)^{-1}\{\exp[4\sigma^2]-\exp[4\sigma_1^2] +$$

$$2\Lambda_c^{-1} + \Lambda_c^{-2}\}\rceil, 1) \qquad (3.32)$$

where $\lceil\cdot\rceil$ denotes the greatest integer contained in the enclosed expression provides an error approximately twice as large as the asymptotically $(N_2 \to \infty)$ achieved minimum. Such behavior corresponds to the

familiar economic law of diminishing returns. In Figure 3.3, for worst case fading ($\sigma^2 = .5$) which is arbitrarily divided equally ($\sigma_1^2 = \sigma_2^2 = .25$) between the transmission and reception paths, this error term is plotted as a function of Λ_c with N_2 as a parameter. For small SNR ($\Lambda_c << 1$), increasing N_2 supplies the usual diversity improvement in performance whereas, for large SNR ($\Lambda_c >> 1$), the improvement in performance becomes negligible after some fixed amount of diversity has been employed. For example, in Figure 3.3, when $\Lambda_c > 1$, we would never use more than 100 diversity elements (coherence areas).

The approach of Section 3.1.1 also leads to a lower bound for the CR bound

$$[\mathrm{Var}(|\hat{b}_0|^2)/|b_0|^4] \geq \sup([2/N_2\Lambda_c], 4\sigma_1^2(1+2\sigma_1^2) + [4\sigma_2^2/N_2](1+2\sigma_2^2), [1/N_2(2\Lambda_c^2+\Lambda_c^3)]). \quad (3.33)$$

In the same worst case analysis, the ratio of the estimator error to this bound exhibits a steadily decreasing variation with increasing N_2. For small N_2 (on the order of one or two), this ratio varies from 1.6 to 3.6 while, for large N_2 (on the order of 10^2), it ranges between 1.2 and 3.2. A comparison of this lower bound with its counterpart from Section 3.1.1 establishes that, excluding the term related to fading in the transmission channel, it also exhibits the

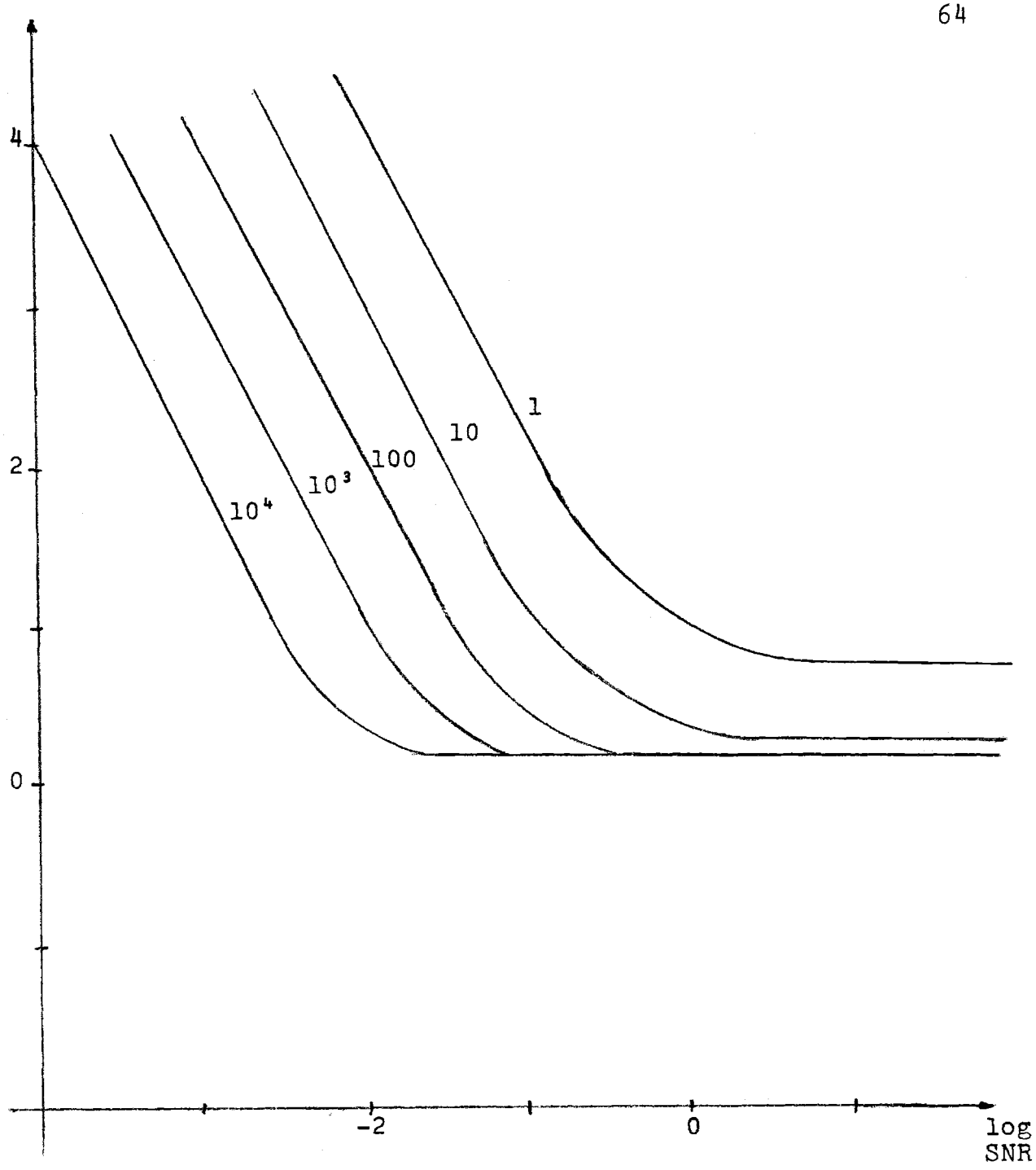

FIGURE 3.3: LOG-LOG PLOT OF NORMALIZED ERROR VERSUS SNR, Λ_c, FOR $\sigma^2 = .5$ (ARBITRARILY DIVIDED AS $\sigma_1^2 = \sigma_1^2 = .25$) WITH THE NUMBER OF RECEIVER DIVERSITY ELEMENTS, N_2, AS A PARAMETER

usual improvement in performance that is characteristic of diversity processing. The number of useful diversity elements, *i.e.*, the size of the receiving aperture, is therefore limited by the fading in the transmission channel. As in the preceding section and subject to the possible limitations discussed therein, all of the available temporal diversity is again utilized.

3.1.3 Transmitter Diversity Model (m1111)

Here apertures A_2 and P are contained within the appropriate coherence areas but aperture A_1 is not. Consequently, within a temporal coherence interval, the random variable approximation applies to the perturbation term $\chi_{2p}(r,r')+j\phi_{2p}(r,r')$ and the unilateral coherence approximation is valid for the term $\chi_{p1}(r',\hat{r})+j\phi_{p1}(r',\hat{r})$. The preceding approximations imply that the most general transmitted envelope with energy $|E_{i1}|^2$ is given by

$$E_{i1}(\hat{r},\hat{t}) = [1/\sqrt{T}]\, E_{i1}(\hat{r}), \qquad \hat{r} \in A_1,\ \hat{t} \in T_1, \tag{3.34a}$$

where T is the length of the transmission interval T_1 and where the spatial envelope satisfies the following requirement

$$\int_{A_1} d\hat{r}\, |E_{i1}(\hat{r})|^2 = |E_{i1}|^2. \tag{3.34b}$$

The transmission leads to the output envelope

$$\gamma(r,t) = E_{02}(r,t) + n(r,t) =$$

$$[1/\sqrt{T}] \{ \int_{A_1} d\hat{r}\, E_{i1}(\hat{r}) \exp[x_1(\hat{r}) + j\phi_1(\hat{r})]\, \hat{\Phi}_{i1,0}^*(\hat{r}) \}$$

$$\exp[x_2 + j\phi_2]\, \alpha_0 b_0 \Phi_{01,0}(r) + n(r,t),$$

$$r \in A_2,\ t \in T_2, \tag{3.35a}$$

where T_2 is a time-shifted (by $(L_1+L_2)c^{-1}$) version of T_1, where $\exp[x_2+j\phi_2]$, α_0, and b_0 were defined in (3.3) and where we now define

$$\exp[x_1(\hat{r})+j\phi_1(\hat{r})] = \exp[x_{p1}(0,\hat{r}) + j\phi_{p1}(0,\hat{r})]. \tag{3.35b}$$

Again we denote the height of the power spectrum for the additive noise as N_0 so that the likelihood ratio is given by

$$\Lambda = \langle \exp\{[-|\alpha_0 b_0|^2 \exp[2x_2]/N_0]$$

$$\left| \int_{A_1} d\hat{r}\, E_{i1}(\hat{r}) \exp[x_1(\hat{r})+j\phi_1(\hat{r})] \hat{\Phi}_{i1,0}^*(\hat{r}) \right|^2 \cdot$$

$$\exp\{[2/N_0]\, \mathrm{Re}[\alpha_0 b_0 \exp[x_2+j\phi_2] \left(\int_{A_1} d\hat{r}\, E_{i1}(\hat{r}) \exp[x_1(\hat{r})+j\phi_1(\hat{r})] \hat{\Phi}_{i1,0}^*(\hat{r}) \right)$$

$$[1/\sqrt{T}] \int_{T_2} dt \int_{A_2} dr\, \gamma^*(r,t) \Phi_{01,0}(r)]\} \rangle_{\substack{x_2,\phi_2 \\ x_1(\hat{r}),\phi_1(\hat{r})}} . \tag{3.36}$$

To facilitate the average with respect to the random process $\chi_1(\hat{r}) + \phi_1(\hat{r})$, we again employ the technique of splitting the aperture into coherence areas $\{A_{1,m}\}_{m=1}^{N_1}$ over each of which the process may be modeled as a random variable. Application of this technique leads to the equation

$$\Lambda = \langle \exp\{[-|\alpha_0 b_0|^2 \exp[2x_2]/N_0] \left| \sum_{m=1}^{N_1} \varepsilon_m \exp[x_{1,m}+j\phi_{1,m}] \right|^2 \}$$

$$\exp\{[2/\sqrt{T}\, N_0]\, \mathrm{Re}[\alpha_0 b_0 \exp[x_2+j\phi_2](\sum_{m=1}^{N_1} \varepsilon_m \exp[x_{1,m}+j\phi_{1,m}])$$

$$\int_{T_2} dt \int_{A_2} dr\, \gamma^*(r,t)\Phi_{01,0}(r)]\}\rangle_{\substack{x_2,\phi_2 \\ \{x_{1,m},\phi_{1,m}\}}} \tag{3.37a}$$

where ε_m is defined as follows

$$\varepsilon_m = \int_{A_{1,m}} d\hat{r}\, E_{i1}(\hat{r})\, \hat{\Phi}_{i1,0}^*(\hat{r}), \qquad m = 1,2,\ldots,N_1. \tag{3.37b}$$

The correlation function defined in (3.5) is a sufficient statistic and leads to the equivalent model

$$\gamma_0 = \exp[x_2+j\phi_2](\sum_{m=1}^{N_1} \varepsilon_m \exp[x_{1,m}+j\phi_{1,m}])\alpha_0 b_0 + n_0 \tag{3.38}$$

where n_0 was defined in (3.7). Since we can treat this problem

with the techniques introduced in Section 3.1.3, the quality of the estimator increases monotonically with the quantity

$$\left| \sum_{m=1}^{N_1} \varepsilon_m \exp[x_{1,m}+j\phi_{1,m}] \right| .$$

We must therefore determine how to distribute the available power among the parameters $\{\varepsilon_m\}$ in order to maximize this quantity.

We assume that the N_1 pairs of turbulent random variables representing the process $x_1(r)+j\phi_1(r)$ are independent [33] with each pair having independent real and imaginary parts [1]. The additional approximation that any turbulent phase variable is uniformly distributed [29] implies that the placement of the available energy within a single coherence area is the optimal transmission strategy in agreement with known results [34]. Since we are free to choose the transmitted envelope, the selection of a specific coherence area is immaterial. Because this strategy renders the formulation identical to that in Section 3.1.1, we conclude that there exists no purely spatial, nonadaptive modulation scheme which is capable of exploiting available transmitter diversity.

If, however, we employ time-varying spatial modulation within the interval T_1 which is contained in a temporal coherence interval, then we may utilize the available diversity. In N_3 successive, equal length (T/N_3) subintervals $\{T_{1,p}\}$, we transmit from distinct coherence areas the sequence of envelopes

$$E_{i1,p}(\hat{r}) = \begin{cases} E_{i1}\hat{\Phi}_{i1,0}(\hat{r})\Phi_p^{-1/2}[1/\sqrt{T}], & r \in A_{1,p},\ t \in T_{1,p} \\ 0 & \text{elsewhere,} \end{cases}$$

$$p = 1,2,\ldots,N_3, \qquad (3.39a)$$

where ξ_p is defined as follows (from conservation of the transmitted energy $|E_{i1}|^2$)

$$\xi_p = \int_{A_{1,p}} d\hat{r}\ |\hat{\Phi}_{i1,0}(\hat{r})|^2, \qquad p = 1,2,\ldots,N_3. \qquad (3.39b)$$

This transmission causes the sequence of received envelopes

$$\gamma_p(r,t) = E_{02,p}(r,t) + n_p(r,t) =$$

$$[1/\sqrt{T}]\ \alpha_0 b_0 E_{i1}\xi_p^{1/2}\exp[x_{1,p}+j\phi_{1,p}]\exp[x_2+j\phi_2]\Phi_{01,0}(r) + n_p(r,t),$$

$$r \in A_2,\ t \in T_{2,p},$$
$$p = 1,2,\ldots,N_3, \qquad (3.40)$$

where α_0 is the free space propagation parameter defined in (3.3), where $T_{2,p}$ is merely a time-shifted (by $(L_1+L_2)c^{-1}$) version of $T_{1,p}$, and where $n_p(r,t)$ is the usual additive noise process (*cf.*, Section 3.1.1) restricted to the *p*th reception subinterval $T_{2,p}$.

We again denote the height of the additive noise power spectrum as N_0 so that the likelihood ratio for this formulation is the following

$$\Lambda = < \prod_{p=1}^{N_3} \exp\{[-|\alpha_0 b_0 E_{i1}|^2 \exp[2x_2]\exp[2x_{1,p}]\xi_p/N_0N_3]\}$$

$$\exp\{[2/N_0\sqrt{T}]\ \mathrm{Re}[\alpha_0 b_0 E_{i1}\xi_p^{1/2}\exp[x_2+j\phi_2]\exp[x_{1,p}+j\phi_{1,p}]$$

$$\int_{T_{2,p}} dt \int_{A_2} dr\ \gamma_p^*(r,t)\phi_{01,0}(r)]\}>_{\substack{x_2,\phi_2 \\ \{x_{1,p},\phi_{1,p}\}}} . \qquad (3.41)$$

The sufficient statistics are a set of correlation functionals (appropriately normalized)

$$\gamma_{p0} \triangleq \int_{T_{2,p}} dt \int_{A_2} dr\ \gamma_p(r,t)\Phi_{01,0}^*(r)([T/N_3])^{-1/2},$$

$$p = 1,2,\ldots,N_3, \qquad (3.42)$$

and they lead to an equivalent model

$$\gamma_{p0} = \alpha_0 b_0 \exp[x_2+j\phi_2]\exp[x_{1,p}+j\phi_{1,p}]\xi_p^{1/2}E_{i1}N_3^{-1/2} + n_{p0},$$

$$p = 1,2,\ldots,N_3, \qquad (3.43)$$

where we define n_{p0}

$$n_{po} \triangleq \int_{T_{2,p}} dt \int_{A_2} dr\, n_p(r,t)\Phi_{01,0}^{*}(r)([T/N_3])^{-1/2},$$

$$p = 1,2,\ldots,N_3. \tag{3.44}$$

With the usual assumptions about the turbulent random variables, Equation 3.41 may be evaluated in terms of the frustration function

$$= < \prod_{p=1}^{N_3} Fr([|\alpha_0 b_0 E_{i1}|^2 \xi_p \exp[2x_2]/N_0 N_3], [|\gamma_{p0}|/(N_0)^{1/2}];$$

$$\sigma_{1,p}^{2})>_{x_2} \tag{3.45}$$

where $\sigma_{1,p}^{2}$ $(= \sigma_1^2, \forall p)$ is the variance of $x_{1,p}$. Again, the surface is completely characterized by $|b_0|$, its coherent cross section.

To circumvent the intractabilities associated with standard estimation procedures, we use the usual indirect approach to generate a tractable unbiased estimator for $|b_0|^2$

$$|b_0|^2 = [1/N_3] \sum_{p=1}^{N_3} [|\gamma_{p0}|^2 - N_0][|\alpha_0 E_{i1}|^2 \xi_p N_3^{-1}]^{-1} =$$

$$\sum_{p=1}^{N_3} [|\gamma_{p0}|^2 - N_0][|\alpha_0 E_{i1}|^2 \xi_p]^{-1}. \tag{3.46a}$$

The observation that $\hat{\Phi}_{i1,0}(\hat{r})$ is nearly a plane wave [8] over the aperture A_1 implies that the members of the set $\{\xi_p\}$ are nearly equal (cf., (3.39b)) and hence that

$$\xi_p|\alpha_0|^2 = |\alpha_c|^2, \qquad p = 1,2,\ldots,N_3. \tag{3.46b}$$

With this approximation, the estimator becomes

$$|b_0|^2 = \sum_{p=1}^{N_3} [|\gamma_{p0}|^2 - N_0]\left[|\alpha_c E_{i1}|^2\right]^{-1} \tag{3.46c}$$

and it has normalized mean-square error

$$[\mathrm{Var}(|b_0|^2)/|b_0|^4] = [1/N_3]\{(\exp[4\sigma^2]-1) + (N_3-1)(\exp[4\sigma_2{}^2]-1)$$

$$[2N_3/\Lambda_c] + [N_3{}^2/\Lambda_c{}^2]\} \tag{3.47}$$

where we again have utilized the parameter σ^2 which was defined in (3.15b). From Equation 3.47 we observe that the estimator error is minimized by the following selection for the transmitter diversity

$$N_3 = \sup(1, \lceil \Lambda_c \exp[2\sigma_2{}^2](\exp[4\sigma_1{}^2]-1)^{1/2} \rceil) \tag{3.48}$$

where $\lceil \cdot \rceil$ denotes the greatest integer in the enclosed expression. For fixed values of $\sigma_1{}^2$ and $\sigma_2{}^2$, this expression implies that, as Λ_c increases, the parameter N_3 initially remains constant (at one) and then increases linearly with Λ_c until reaching its maximum value N_1 (which is the number of available transmitter diversity elements). The following alternative form for the error term

$$[\mathrm{Var}(|\hat{b}_0|^2)/|b_0|^4] = (\exp[4\sigma_2^2]-1) +$$

$$[(\exp[4\sigma^2]-\exp[4\sigma_2^2])/N_3] + [2/\Lambda_c] + [N_3/\Lambda_c^2] \qquad (3.49)$$

illustrates the tradeoff in performance (degradations due to transmission path turbulence are diminished but degradations due to additive noise are exacerbated) obtained from the utilization of transmitter diversity and, hence, the necessity for its selective deployment. Also apparent from this expression is the limiting effect of reception path turbulence (via the term $(\exp[4\sigma_2^2]-1)$) on the performance of the estimator. In Figure 3.4 for worst case fading ($\sigma^2 = .5$) which is arbitrarily divided equally ($\sigma_1^2 = \sigma_2^2 = .25$) between the transmission and the reception paths, this error term is plotted as a function of Λ_c with N_3 as a parameter. From this figure we observe that the optimal utilization of available diversity follows the pattern previously described and that the improvement in performance becomes negligible after some fixed amount of diversity (approximately 100 elements here) has been employed because of the effects of reception path turbulence.

The approach of Section 3.1.1 also provides a lower bound for the CR bound

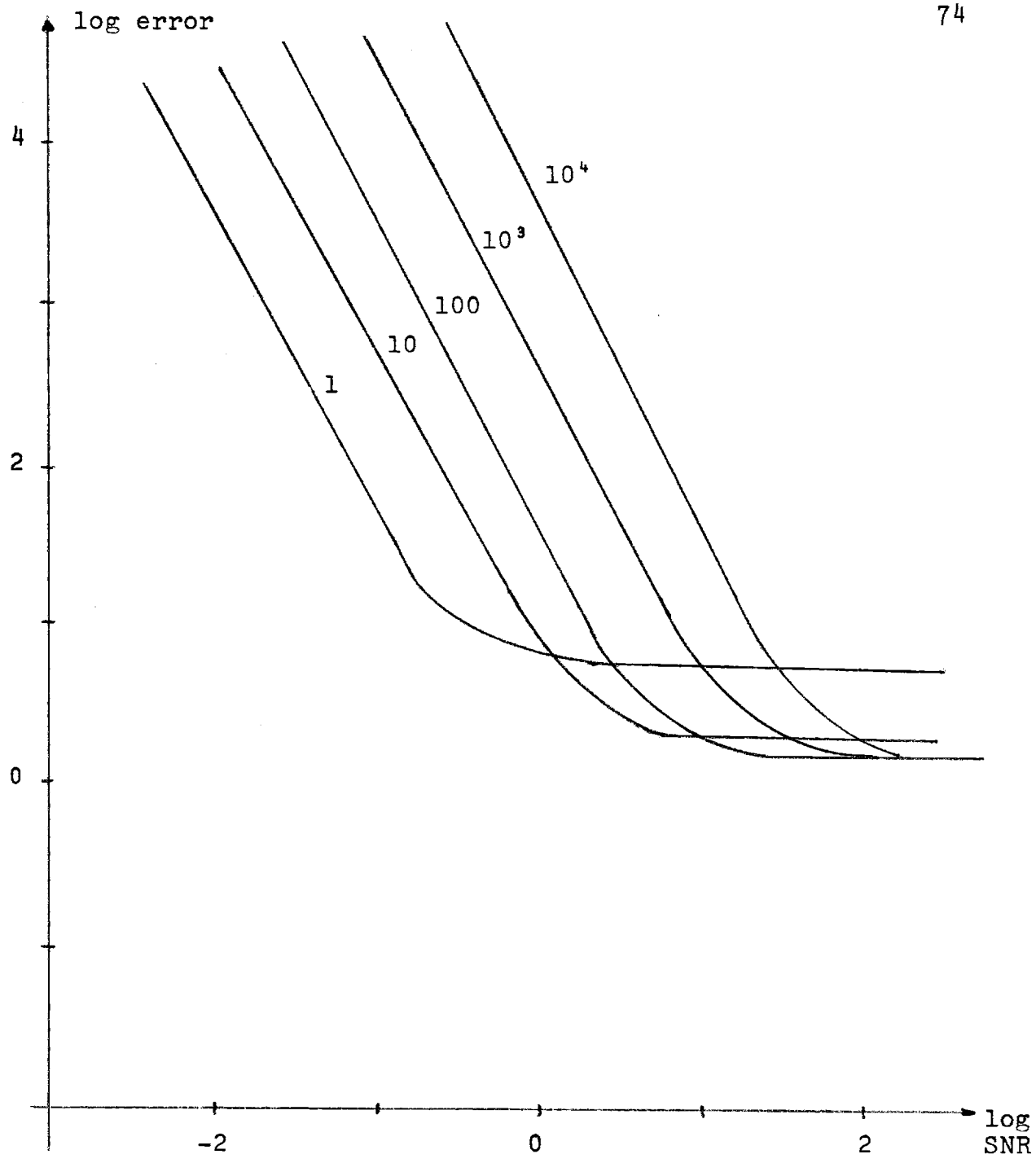

FIGURE 3.4: LOG-LOG PLOT OF NORMALIZED ERROR VERSUS SNR, Λ_c, FOR $\sigma^2 = .5$ (ARBITRARILY DIVIDED AS $\sigma_1^2 = \sigma_2^2 = .25$) WITH THE NUMBER OF TRANSMITTER DIVERSITY ELEMENTS, N_1, AS A PARAMETER

$$[\mathrm{Var}(|\hat{b}_0|^2)/|b_0|^4] \geq \sup\{[2/\Lambda_c],\ [4\sigma_1{}^2/N_3]\ (1+2\sigma_1{}^2) +$$

$$4\sigma_2{}^2(1+2\sigma_2{}^2),\ [N_3[2\Lambda_c{}^2+\Lambda_c{}^3N_3{}^{-1}]^{-1}\}. \qquad (3.50)$$

The same worst case analysis determines that the ratio of the estimator error to this bound varies from 1.6 to 3.6 for small N_3 (on the order of one or two) and from 1.2 to 3.8 for large N_3 (on the order of 10^2). Comparison of this bound with its counterpart from Section 3.1.1.establishes that it follows the same pattern of behavior as the error term, *i.e.*, degradations in performance due to transmission path turbulence are diminished by the characteristic diversity factor, part of the degradation due to additive noise as well as that attributed to reception path turbulence is unaffected while the remainder of the degradation due to noise is exacerbated by the same diversity factor. The number of useful diversity elements, *i.e.*, the size of the transmitting aperture is thus limited by both additive noise and fading in the reception channel. As previously discussed, temporal diversity is again utilized when it is available.

3.1.4 Transmitter and Receiver Diversity Model (mlllm)

Both A_1 and A_2 contain more than one coherence area while aperture P is contained within the appropriate coherence area. Within a temporal coherence interval, both perturbation terms thus require the unilateral coherence approximation. The most general trans-

mitted envelope with energy $|E_{i1}|^2$ remains that described in (3.34a) and (3.34b). This transmitted envelope produces the received envelope

$$\gamma(r,t) = E_{02}(r,t) + n(r,t) = [1/\sqrt{T}]\ \alpha_0 b_0$$

$$\{\int_{A_1} d\hat{r}\ E_{i1}(\hat{r})\exp[x_1(\hat{r})+j\phi_1(\hat{r})]\Phi_{i1,0}^{*}(\hat{r})\}$$

$$\exp[x_2(r)+j\phi_2(r)]\Phi_{01,0}(r) + n(r,t),$$

$$r \in A_2,\ t \in T_2, \tag{3.51}$$

where α_0, b_0, $\exp[x_1(\hat{r})+j\phi_1(\hat{r})]$, and $\exp[x_2(r)+j\phi_2(r)]$ were defined in (3.3a), (3.3b), (3.35), and (3.22), respectively, while T_1 and T_2 are the temporal intervals (of length T) previously described. Within this model, the surface is completely characterized by b_0 and the effects of transmitter and receiver diversity are uncoupled so that they may be treated separately in accordance with previously determined methods.

Although we can utilize available receiver diversity by means of spatial processing (Section 3.1.2), temporal processing is required to benefit from existing transmitter diversity (Section 3.1.3). Therefore, we partition the transmission interval into N_3 equal length (T/N_3) subintervals $\{T_{1,p}\}$ during which we sequentially transmit from distinct coherence areas the collection of equal energy envelopes

$$E_{il,p}(\hat{r}) = \begin{cases} E_{il}\xi_p^{-1/2}\hat{\Phi}_{il,0}(\hat{r})[1/\sqrt{T}], & r \in A_{1,p},\ t \in T_{1,p}, \\ 0, & \text{elsewhere} \end{cases}$$

$$p = 1,2,\ldots,N_3, \tag{3.52a}$$

where

$$\xi_p = \int_{A_{1,p}} d\hat{r}\ |\hat{\Phi}_{il,0}(\hat{r})|^2, \qquad p = 1,2,\ldots,N_3. \tag{3.52b}$$

This transmission causes the sequence of received envelopes

$$\gamma_p(r,t) = \alpha_0 b_0 \{ \int_{A_1} d\hat{r}\ E_{il,p}(\hat{r}) \exp[\chi_1(\hat{r}) + j\phi_1(\hat{r})] \hat{\Phi}_{il,0}^*(\hat{r}) \}$$

$$[1/\sqrt{T}]\ \xi_p^{1/2} \exp[\chi_2(r) + j\phi_2(r)] \Phi_{01,0}(r) + n_p(r,t),$$

$$r \in A_2,\ t \in T_{2,p},\ p = 1,2,\ldots,N_3, \tag{3.53}$$

where $n_p(r,t)$ is the additive noise process restricted to the p*th* subinterval.

To obtain a manageable likelihood ratio for this formulation, we must develop representations for the random processes describing the turbulence. We again employ the coherence area decomposition technique

thereby partitioning the apertures A_1 and A_2 into coherence areas $\{A_{1,m}\}_{m=1}^{N_1}$ and $\{A_{2,\ell}\}_{\ell=1}^{N_2}$ over each of which the appropriate process is modeled as a random variable. We assume that these $N_2 + N_1$ pairs of random variables are independent [33] (cf., Section 2.3.1) with each pair possessing independent real and imaginary parts [1]. Furthermore, any phase variable may be regarded as uniformly distributed. If N_0 denotes the spectral height of the additive noise, then these decompositions may be utilized to form the ensuing likelihood ratio

$$\Lambda = \Big\langle \prod_{p=1}^{N_3} \prod_{\ell=1}^{N_2} \exp\{[-|\alpha_0 b_0 E_{i1}|^2 \xi_p \xi_\ell \exp[2x_{1,p}]\exp[2x_{2,\ell}]/N_0 N_3]\} \cdot$$

$$\exp\{[2/N_0\sqrt{T}]\mathrm{Re}[\alpha_0 b_0 E_{i1} \xi_p^{1/2} \exp[x_{1,p}+j\phi_{1,p}]\exp[x_{2,\ell}+j\phi_{2,\ell}]$$

$$\int_{T_{2,p}} dt \int_{A_{2,\ell}} dr\, \gamma_p^*(r,t)\Phi_{01,0}(r)]\}\Big\rangle_{\substack{\{x_{1,p},\phi_{1,p}\} \\ \{x_{2,\ell},\phi_{2,\ell}\}}}, \qquad (3.54)$$

where ξ_ℓ was defined in (3.25). The received envelopes appear in (3.54) as a set of correlation functionals

$$\gamma_{p\ell 0} = \int_{T_{2,p}} dt \int_{A_{2,\ell}} dr\, \gamma_p(r,t)\, \Phi_{01,0}^*(r)\, ([T\xi_\ell/N_3])^{-1/2},$$

$$\ell = 1,2,\ldots,N_2,\ p = 1,2,\ldots,N_3, \qquad (3.55)$$

which are thus sufficient statistics. An equivalent model is the following

$$\gamma_{p\ell 0} = \exp[x_{1,p}+j\phi_{1,p}]\exp[x_{2,\ell}+j\phi_{2,\ell}]\alpha_0 b_0([\xi_\ell \xi_p/N_3])^{1/2} E_{i1} + n_{p\ell 0},$$

$$\ell = 1,2,\ldots,N_2,\ p = 1,2,\ldots,N_3, \qquad (3.56)$$

where we define $n_{p\ell 0}$ below

$$n_{p\ell 0} \triangleq \int_{T_{2,p}} dt \int_{A_{2,\ell}} dr\ n_p(r,t)\ \Phi_{01,0}^*(r)\ ([\xi_\ell T/N_3])^{-1/2},$$

$$\ell = 1,2,\ldots,N_2,\ p = 1,2,\ldots,N_3. \qquad (3.57)$$

Previous observations concerning the modes [8], $\hat{\Phi}_{i1,0}(\hat{r})$ and $\Phi_{01,0}(r)$, imply that

$$(\xi_p \xi_\ell)^{1/2}\ \alpha_0 = \alpha_c, \qquad \ell = 1,2,..,N_2,\ p = 1,2,\ldots,N_3, \qquad (3.58)$$

thereby simplifying this model (Equation 3.56) as follows

$$\gamma_{p\ell 0} = \exp[x_{1,p}+j\phi_{1,p}]\exp[x_{2,\ell}+j\phi_{2,\ell}]\alpha_c b_0 E_{i1}([1/N_3])^{1/2} + n_{p\ell 0},$$

$$\ell = 1,2,\ldots,N_2,\ p = 1,2,\ldots,N_3. \qquad (3.59)$$

Once again standard estimation procedures involve intractable expressions thereby prompting our use of Moldon's indirect technique. This method provides a tractable unbiased estimator for $|b_0|^2$

$$|\hat{b}_0|^2 = [1/N_3N_2]\{\sum_{p=1}^{N_3}\sum_{\ell=1}^{N_2}[|\gamma_{p\ell 0}|^2-N_0][|\alpha_c E_{i1}|^2 N_3^{-1}]^{-1}$$

$$= [1/N_2]\{\sum_{p=1}^{N_3}\sum_{\ell=1}^{N_2}[|\gamma_{p\ell 0}|^2-N_0]|\alpha_c E_{i1}|^2\} \qquad (3.60)$$

which has normalized mean-square error

$$[\mathrm{Var}(|\hat{b}_0|^2)/|b_0|^4] = [1/N_3N_2][(\exp[4\sigma^2]-1)+(N_2-1)(\exp[4\sigma_1{}^2]-1)+(N_3-1)$$

$$(\exp[4\sigma_2{}^2]-1)] + [2/N_2\Lambda_c] + [N_3/N_2\Lambda_c{}^2]. \qquad (3.61)$$

This quantity is minimized by choosing N_2 as large as possible and then selecting N_3 to satisfy the following

$$N_3 = \sup(1,\lceil\Lambda_c\{(\exp[4\sigma_1{}^2]-1)(\exp[4\sigma_2{}^2]-1+N_2)\}^{1/2}\rceil) \qquad (3.62)$$

where $\lceil\cdot\rceil$ denotes the greatest integer in the enclosed expression. This utilization of the available transmitter diversity is similar to that described in Section 3.1.3 although its detailed behavior depends on N_2. By rewriting the error in the following form

$$[\mathrm{Var}(|\hat{b}_0|^2)/|b_0|^4] = [1/N_2N_3][\exp[4\sigma^2]-\exp[4\sigma_1{}^2]-\exp[4\sigma_2{}^2]+1] +$$

$$[\exp[4\sigma_1{}^2]-1]N_3]^{-1}+[\exp[4\sigma_2{}^2]-1]N_2{}^{-1} + [2/N_2\Lambda_c] +$$

$$([N_3/N_2])\ [1/\Lambda_c{}^2] \qquad (3.63)$$

we observe that turbulence no longer absolutely limits the performance of the estimator in contrast to previous results. In Figure 3.5 worst case fading ($\sigma^2 = .5$) which is arbitrarily divided equally ($\sigma_1{}^2 = \sigma_2{}^2 = .25$) between the transmission and reception paths, this error term is plotted as a function of Λ_c with N_2 as a parameter and with N_3 chosen according to (3.62). For small SNR ($\Lambda_c << 1$), increasing N_2 provides the usual diversity improvement in performance (proportional to N_2) whereas, for large SNR ($\Lambda_c >> 1$), increasing N_2 provides an improvement which is proportional to $\sqrt{N_2}$. By comparison of this figure with Figures 3.3 and 3.4, we observe that the combination of transmitter and receiver diversity supplies a significant improvement over either type of diversity used alone.

The approach of Section 3.1.1 also leads to a lower bound for the CR bound

$$[\mathrm{Var}(|\hat{b}_0|^2)/|b_0|^4] \geq \sup([2/N_2\Lambda_c],$$

$$4([\sigma_1^2/N_3])(1+2\sigma_1^2) + 4([\sigma_2^2/N_2])(1+2\sigma_2^2),$$

$$[(N_3/N_2)/(2\Lambda_c^2+\Lambda_c^3 N_3^{-1})]). \qquad (3.64)$$

The same worst case analysis indicates that the ratio of the estimator error to this bound varies from 1.6 to 3.6 for small N_2 (on the order of one or two) and from 1.2 to 3.9 for large N_2 (on the order of 10^2). Comparison of this bound with its counterpart from Section 3.1.1 establishes that it exhibits the same improved quality as the error term. Consequently, the number of useful diversity elements, *i.e.*, the sizes of the apertures being used, is not absolutely limited as in previous sections. As previously discussed, all of the available temporal diversity is utilized in the appropriate manner.

3.1.5 Summary

Here we summarize our results for the coherent cross section group, *i.e.*, those models which involve far field propagation in both channels and a surface which is contained within the appropriate coherence area. The only available information concerning this surface is given by $|b_0|$, the coherent cross section defined in (3.3b) which is to be estimated. Although these models lead to estimation formulations of

varying complexity, we cannot determine explicit ML estimators or CR bounds for any of them. Consequently, we resort to an indirect technique due to Moldon which utilizes lower bounds for the CR bound and simple, tractable estimators in lieu of the ML estimators. Since the mean-square error associated with each of the estimators is not significantly different from the corresponding lower bound, these estimators are adequate albeit suboptimal.

The estimator (mean-square) errors corresponding to receiver diversity, transmitter diversity and both are plotted in Figures 3.3, 3.4, and 3.5, respectively, for worst case fading ($\sigma^2 = .5$) arbitrarily divided equally ($\sigma_1^2 = \sigma_2^2 = .25$) between the transmission and reception paths. As previously observed, the estimator error is minimized by utilizing every available receiver diversity element. For small SNR (*i.e.*, $\Lambda_c << 1$), this procedure supplies the usual diversity improvement in performance whereas for large SNR (*i.e.*, $\Lambda_c >> 1$) the supplied improvement becomes insignificant. This behavior is due to transmission path fading which is unaffected by receiver diversity and which, therefore, ultimately limits the quality of the estimator obtained when only receiver diversity processing is available.

We have already established that, for transmitter diversity processing, the estimator error is minimized by selecting the number of diversity elements (to be utilized) according to (3.48). This criterion results from the tradeoff in behavior of the error terms due to transmission path fading and background noise which can be

observed from Figure 3.4. Here, increasing the number of diversity elements improves performance for large SNR but degrades performance for small SNR. Even those improvements which can be obtained are modest, however, because reception path fading is independent of transmitter diversity and thus restricts the quality of estimators which utilize only this diversity.

When both types of diversity processing are available, we minimize estimator error by employing all receiver diversity elements and selecting N_3 according to (3.62). For small SNR, however, this procedure is equivalent to simple diversity reception which performs well under this restriction. For large SNR, however, this dual processing leads to substantial (proportional to $\sqrt{N_2}$) improvement in performance as indicated in Figure 3.5.

Finally, as already discussed, a collection of signalling intervals (temporal coherence intervals) may also be used to improve performance. In this case, the entire error is subjected to the usual diversity improvement. For small SNR and restricted apertures, this processing represents the only method for reaching desired performance levels.

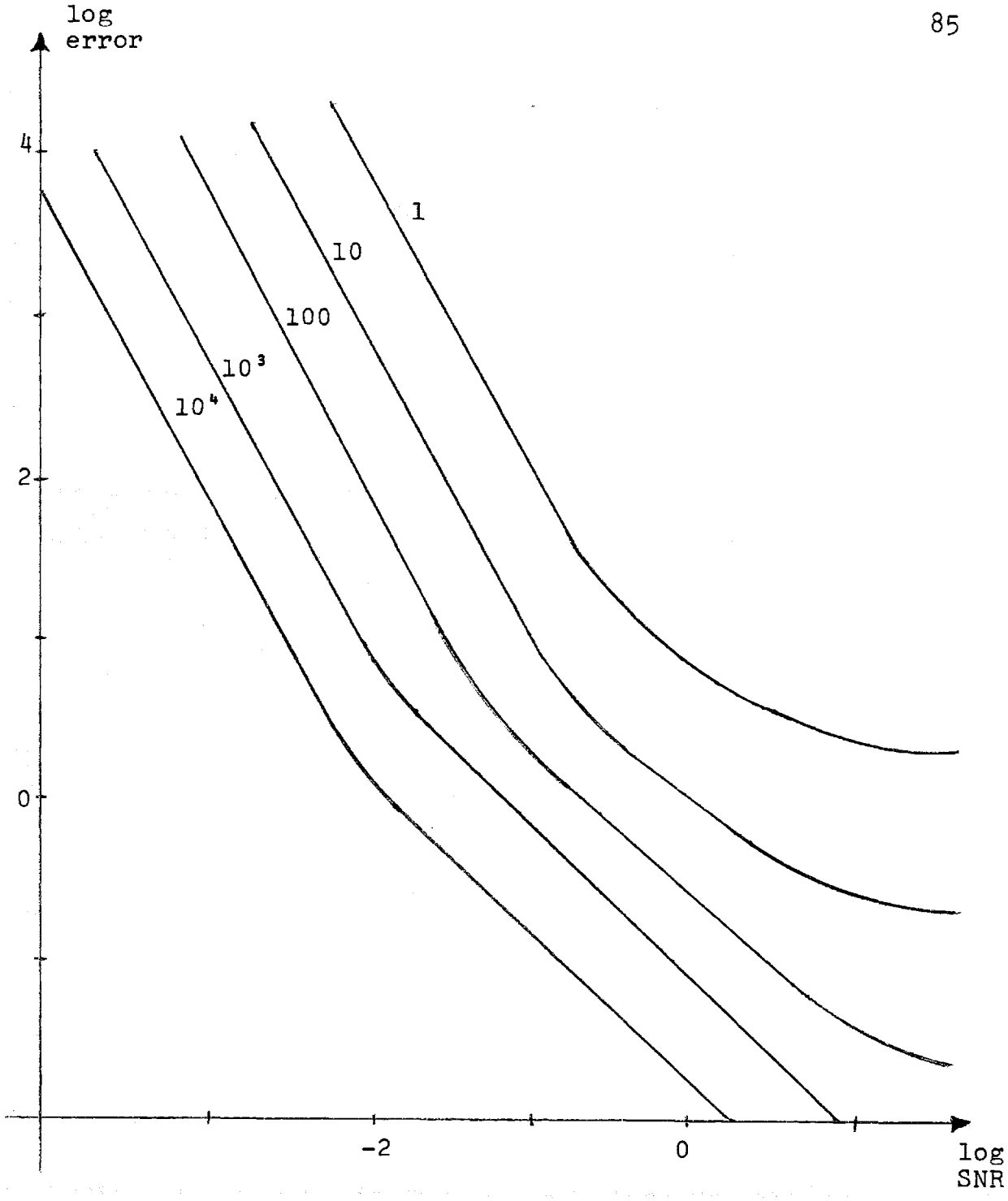

FIGURE 3.5: LOG-LOG PLOT OF NORMALIZED ERROR VERSUS SNR, Λ_c, FOR $\sigma^2 = .5$ (ARBITRARILY DIVIDED AS $\sigma_1^2 = \sigma_2^2 = .25$) WITH THE NUMBER OF RECEIVER DIVERSITY E ELEMENTS AS A PARAMETER AND WITH THE NUMBER OF TRANSMITTER DIVERSITY ELEMENTS CHOSEN ACCORDING TO CRITERION (3.62)

3.2 Coherent Imaging

In this section we consider those cases gathered in the coherent imaging group of Table 2.2. These models involve far field propagation in the transmission channel, near field propagation in the reception channel and a rough surface which is contained within the appropriate coherence area. In this case, the surface is completely characterized by its coherent image, *i.e.*, by the set of parameters related to those modes which are supported by the corresponding free space channels. Such formulations are related to the topic of passive imaging through turbulence which possesses an extensive literature summarized elsewhere [35, 36, 37].

3.2.1 Simple Imaging Model (111mm)

As in Section 3.1.2, apertures A_1 and P are contained within the appropriate coherence areas but aperture A_2 is not. Consequently, when the transmission interval is limited to a temporal coherence interval, we may approximate the perturbation term for the transmission channel as a random variable and the perturbation term for the reception channel as unilaterally coherent. The former channel remains in the far field regime so that its input mode and output mode are unaltered from the corresponding free space description. The former channel remains in the far field regime so that its input mode and output mode are unaltered from the corresponding free space description. The latter channel is in the near field regime and it

shares only input modes with the associated free space model.

The most general transmitted envelope with energy $|E_{i1}|^2$ is given by the following

$$E_{i1}(\hat{r},\hat{t}) = E_{i1}\,\hat{\Phi}_{i1,0}(\hat{r})\,[1/\sqrt{T}], \quad \hat{r} \in A_1, \hat{t} \in T_1, \tag{3.65}$$

where T is the length of the transmission interval T_1. This transmission produces the received envelope

$$\gamma(r,t) = E_{02}(r,t) + n(r,t) = \exp[x_1+j\phi_1]\exp[x_2(r)+j\phi_2(r)]\,[1/\sqrt{T}]$$

$$\{\sum_{\ell=1}^{\beta} n_{\ell,0} b_\ell \Phi_{0\ell,0}(r)\}\,\alpha_4 E_{i1} + n(r,t),$$

$$r \in A_2,\ t \in T_2, \tag{3.66}$$

where T_2 is a time-shifted (by $(L_1+L_2)c^{-1}$) version of T_1. Here $n_{\ell,0}$ is the eigenvalue corresponding to the ℓth mode in the decomposition for the free space reception channel, $\exp[x_1+j\phi_1]$ and $\exp[x_2(r)+j\phi_2(r)]$ were defined in (3.3) and (3.22), respectively, and we now define the following parameters

$$\alpha_4 \triangleq -\exp[jk(L_1+L_2)]\,[(PA_1)^{1/2}/\lambda L_1] =$$

$$-\exp[jk(L_1+L_2)](n_{1,0})^{1/2}; \tag{3.67a}$$

$$b_\ell \triangleq [1/P] \int_p dr'\ b(r')\ \Phi_{01,0}(r')\ \Phi_{i\ell,0}^{*}(r'); \tag{3.67b}$$

where $\hat{n}_{1,0}$ is the eigenvalue corresponding to the mode which is supported by the free space transmission channel. The parameter α_4 may be regarded as a free space propagation parameter and the parameters $\{b_\ell\}$ characterize the surface (target) completely.

Because the eigenvalues exhibit a clustering effect [8], *i.e.*, they tend to be near zero or one, Equation 3.66 reduces to

$$\gamma(r,t) = [1/\sqrt{T}]\ \exp[\chi_1 + j\phi_1]\exp[\chi_2(r) + j\phi_2(r)]$$

$$\left\{\sum_{\ell=1}^{D_{f02}} b_\ell \Phi_{0\ell,0}(r)\right\}\ \alpha_4 E_{i1} + n(r,t),$$

$$r \in A_2,\ t \in T_2, \tag{3.68}$$

where D_{f02}, the Fresnel number for the free space reception channel,

$$D_{f02} \triangleq [A_2 P/(\lambda L_2)^2], \tag{3.69}$$

is the number of modes supported by that channel (*i.e.*, with eigenvalues near one). Consequently, the received envelope only contains information about the parameters $\{b_\ell,\ \ell = 1,2,\ldots,D_{f02}\}$ which therefore completely characterize the surface in this formulation. Equation 3.68 may also be written in the form

$$\gamma(r,t) = [1/\sqrt{T}]\ \exp[x_1+j\phi_1]\ \exp[x_2(r)+j\phi_2(r)]\ d(r)\alpha_4 E_{i1} + n(r,t),$$

$$r \in A_2,\ t \in T_2, \qquad (3.70)$$

where $d(r)$ may be interpreted (to within a constant) as the envelope received at aperture A_2 when the envelope $b(r')\ \hat{\Phi}_{01,0}(r')$ is transmitted from aperture P through the free space channel.

From expressions (3.68) and (3.70), we observe that estimation of the surface parameters may be regarded as an exercise either in multiple nonrandom parameter estimation, $\{b_\ell,\ \ell = 1,2,\ldots,D_{f02}\}$ or in nonrandom waveform estimation, $\{d(r),\ r \in A_2\}$. Again the natural statistical technique [38] involves maximum likelihood (ML) estimators and Cramer-Rao (CR) bounds on the mean-square estimator error. From previous experience (Section 3.1) we expect that these quantities cannot be explicitly calculated because of intractabilities introduced both in the evaluation of the likelihood ratio and in the subsequent computation required to determine the estimators or bounds.

For the additive noise process previously described (cf., Sections 2.3.1 and 3.1.1), the likelihood ratio corresponding to the formulation (3.70) is given by

$$\Lambda = \langle \exp\{-[\exp[2x_1]|\alpha_4 E_{i1}|^2/N_0] \int_{A_2} dr \exp[2x_2(r)] |d(r)|^2\} \cdot$$

$$\exp|[2/\sqrt{T}\, N_0]\mathrm{Re}[\alpha_4 E_{i1}\exp[x_1+j\phi_1] \int_{T_2} dt \int_{A_2} dr$$

$$\gamma^*(r,t)\exp[x_2(r)+j\phi_2(r)]\, d(r)]\}\rangle_{\substack{x_1,\phi_1 \\ x_2(r),\phi_2(r)}} . \qquad (3.71)$$

To perform this averaging, we require a representation for the fading process $x_2(r)+j\phi_2(r)$. The issues of representing the fading process and evaluating the likelihood ratio have received a thorough examination, albeit, in a slightly different context, by Halme [30] and they are discussed in Appendix 3C. Here we utilize the sampling representation, which is an approximation that is exact for very large apertures, to obtain the following conditional likelihood ratio [30]

$$\Lambda = \langle \prod_{q=1}^{N_s} \exp\{[-|\alpha_4 E_{i1}|^2\exp[2x_{2,q}]\exp[2x_1]|d_q|^2/N_0]\} \cdot$$

$$\exp\{[2/N_0]\mathrm{Re}[\alpha_4 E_{i1}\exp[x_1+j\phi_1]\exp[x_{2,q}+j\phi_{2,q}]d_q\gamma_q^*]\}\rangle_{\substack{x_1,\phi_1 \\ \{x_{2q},\phi_{2q}\}}} , \qquad (3.72)$$

where N_s is the number of samples, $\{r_q\}_{q=1}^{N_s}$ are the sampling points

in the aperture A_2; γ_q is the q*th* sample of the received envelope

$$\gamma_q = [1/\sqrt{T}] \int_{T_2} dt\ \gamma(r_q,t), \quad q = 1,2,\ldots,N_s; \tag{3.73a}$$

d_q is the q*th* sample of the envelope $d(r)$

$$d_q = d(r_q)([1/\sqrt{T}] \int_{T_2} dt), \quad q = 1,2,\ldots,N_s; \tag{3.73b}$$

and $\chi_{2,q} + j\phi_{2,q}$ is the q*th* sample of the perturbation term

$$\chi_{2,q} + j\phi_{2,q} = \chi_2(r_q) + j\phi_2(r_q),$$

$$q = 1,2,\ldots,N_s. \tag{3.73c}$$

The conditioning may be removed from expression (3.72) by assuming that the fading samples $\{\chi_{2q}+j\phi_{2q}\}$ are independent. With the further assumption that the real and imaginary parts of each fading sample are also independent [1] and that the imaginary part is uniformly distributed [29], the likelihood ratio becomes the following

$$\Lambda = \Big\langle \prod_{q=1}^{N_s} Fr([|\alpha_4 E_{i1} d_q \exp[\chi_1]|^2/N_0],[|\gamma_q|/\sqrt{N_0}],\ \sigma_{2,q}{}^2)\Big\rangle_{\chi_1} \tag{3.74}$$

where $\sigma_{2,q}{}^2$ $(= \sigma_2{}^2, \forall q)$ is the variance of $\chi_{2,q}$.

Because (3.74) is similar to expressions previously obtained (cf., Sections 3.1.1 and 3.1.2), we are cognizant of the issues germane to the estimation of the parameters $\{d_q\}$. In particular, the estimator

$$|\hat{d}_q|^2 = [|\gamma_q|^2 - N_0]|\alpha_4 E_{il}|^{-2}, \qquad q = 1,2,\ldots,N_s \tag{3.75}$$

provides a suboptimal but adequate measure of the quantity $|d_q|^2$ while $\arg(d_q)$ is immeasurable because of the uniformly distributed fading phase. With the more realistic assumption that the fading phase is normally distributed (Section 2.1.1), the techniques of Section 3.1.1 may be applied to the estimation of $\arg d_q$. In Table 3.1 we present lower bounds (derived by utilizing (3.17)) on the mean-square error which may be achieved by unbiased estimators of $|d_q|^2$ and $\arg(d_q)$. From this table, we observe that the magnitude estimator (3.75) performs well as previously claimed but that any phase estimator will perform poorly (on an absolute scale) in view of the large size of the fading phase variances [29].

The usual sampling representation for $d(r)$, *i.e.*,

$$d(r) = \sum_{q=1}^{N_s} d_q \, \phi_{\text{inter},q}(r), \qquad r \in A_2, \tag{3.76}$$

where $\{\phi_{\text{inter},q}(r)\}$ are the interpolation functions associated with the sampling operation [30] along with the orthonormal property of

TABLE 3.1

Related Formulation	Amplitude Bound	Phase Bound
free space	$\frac{N_0}{\lvert\alpha_4 E_{i1}\rvert^2}$	$\frac{N_0}{\lvert\alpha_4 E_{i1}\rvert^2 \lvert d_q\rvert^2}$
noiseless	$\sigma_1^2+\sigma_2^2$	$\sigma_{\phi_1}^2+\sigma_{\phi_2}^2$
phase fading plus additive noise	$\frac{\frac{N_0^3}{4}}{2N_0\lvert\alpha_4 E_{i1}\rvert^4\lvert d_q\rvert^2+\lvert\alpha_4 E_{i1}\rvert^6\lvert d_q\rvert^4}$	$\frac{1}{2}(\sigma_{\phi_1}^2+\sigma_{\phi_2}^2)$

Lower bounds for the CR bound corresponding to the qth sample, d_q, of the received envelope, $d(r)$ derived by utilizing the inequality of Equation 3.17. Each pair of bounds is accompanied by the related simplified formulation (cf., Appendix 3A) from which they are obtained.

the free space eigenfunctions $\{\Phi_{0\ell,0}(r)\}$ yield the following relationship between the surface parameters $\{b_\ell\}$ and the samples of the received envelope $\{d_q\}$

$$b_\ell = \int_{A_2} dr\ \Phi_{0\ell,0}^{*}(r)\{\sum_{q=1}^{N_S} d_q \phi_{inter,q}(r)\}$$

$$= \sum_{q=1}^{N_S} d_q \{\int_{A_2} dr\ \Phi_{o\ell,0}^{*}(r)\ \phi_{inter,q}(r)\} \triangleq \sum_{q=1}^{N_S} d_q\ \Delta_{q\ell},$$

$$\ell = 1,2,\ldots,D_{f02}. \qquad (3.77)$$

Using this relationship, we can apply a known rule [28] to the derived bounds to determine similar bounds which correspond to the set $\{b_\ell\}$. We omit their complicated forms with the observation that they are typically large due primarily to the poor performance (large bounds) of the estimators for the sample phases, $\{\arg(d_q)\}$.

In view of results previously obtained concerning the estimation of the parameter b_0 in Section 3.1, these results for the set $\{d_q\}$ and hence for the set $\{b_\ell\}$ are not surprising because of the size of the fading phase variance. In many situations to which the formulation (3.70) is applicable, a sufficient target characterization may not require good estimates for the magnitude and phase of every parameter in the set $\{b_\ell\}$. For example, the familiar irradiance image, $|b(r')|^2$, requires only magnitude and relative phase estimates for $\{b_\ell\}$. The performance of relative phase estimators cannot be determined

from (3.72) due to the assumption of independent fading samples which was introduced to permit the evaluation of the likelihood ratio. Significant dependences among the fading samples would not imply that an accurate measurement of any particular sample phase could be made since the fading phase variance remains large. These dependences would imply, however, that more accurate measurements of relative sample phases (*e.g.*, $\arg(d_q)-\arg(d_p)$) could be achieved. Because no tractable method for treating the likelihood ratio (3.71) without the assumption of independent fading samples has been developed (*cf.*, Appendix 3C), we cannot evaluate lower bounds on the attainable performance for relative phase estimators by proceeding from the likelihood ratio. Intractabilities accordingly limit the usefulness of Moldon's technique in dealing with relative phase estimators and hence with irradiance images which are examined from a different viewpoint in Appendix 3B.

3.2.2 Imaging with Transmitter Diversity Model (mllmm)

Here, aperture P is contained within the appropriate coherence area whereas apertures A_1 and A_2 are not, so that the unilateral coherence approximation is required for both perturbation terms when the transmission interval does not exceed a temporal coherence interval. The transmission channel is in the far field regime so that its description is unaltered from Section 3.1.3 while the reception channel is in the near field thus retaining the description of the

preceding section. The most general transmitted envelope with energy $|E_{i1}|^2$ is given by

$$E_{i1}(\hat{r},\hat{t}) = [1/\sqrt{T}]\, E_{i1}(\hat{r}), \qquad \hat{r} \in A_1, \hat{t} \in T_1, \tag{3.78a}$$

where T is the length of the transmission interval T_1 and where the spatial envelope $E_{i1}(r)$ satisfies the following

$$\int_{A_1} d\hat{r}\, |E_{i1}(\hat{r})|^2 = |E_{i1}|^2. \tag{3.78b}$$

This transmission produces the received envelope

$$\gamma(r,t) = E_{02}(r,t) = \alpha_4\{\int_{A_1} d\hat{r}\, E_{i1}(\hat{r})\exp[\chi_1(\hat{r})+j\phi_1(\hat{r})]\hat{\Phi}_{i1,0}{}^*(\hat{r})\}$$
$$[1/\sqrt{T}]\exp[\chi_2(r)+j\phi_2(r)] \sum_{\ell=1}^{D_{f02}} b_\ell \Phi_{0\ell,0}(r) + n(r,t),$$
$$r \in A_2,\ t \in T_2, \tag{3.79}$$

where T_2 is a time-shifted (by $(L_1+L_2)c^{-1}$) version of T_1, where α_4, b_ℓ, and D_{f02} were defined in (3.67) and (3.69) and where the perturbation terms $\exp[\chi_1(\hat{r})+j\phi_1(\hat{r})]$ and $\exp[\chi_2(r)+j\phi_2(r)]$ were defined in (3.35) and (3.22), respectively. We observe that the effects of the transmitting and receiving apertures are uncoupled in Equation 3.79 so that both may be employed as previously determined

(cf., Sections 3.1.3 and 3.2.1).

Consequently, by means of temporal processing, the available transmitter diversity is selectively employed to combat the performance degradation that may be attributed to transmission channel fading. Quantitative results, *i.e.*, the usual collection of lower bounds, follow from the methods employed in the preceding section and they are displayed in Table 3.2. Once again the magnitude but not the phase of any sample $\{d_q\}$ can be measured accurately so that the surface parameters $\{b_\ell\}$ still experience severe measurement inaccuracies. As discussed in the preceding section, these results are not surprising in view of the assumptions that were used in their derivation. Since more realistic assumptions lead to analytical intractabilities, the usefulness of Moldon's technique is severely restricted in this context.

TABLE 3.2

Related Formulation	Amplitude Bound	Phase Bound
free space	$\frac{N_0}{\lvert\alpha_4 E_{i1}\rvert^2}$	$\frac{N_0}{\lvert\alpha_4 E_{i1}\rvert^2 \lvert d_q\rvert^2}$
noiseless	$\frac{\sigma_1^2}{N_3} + \sigma_2^2$	$\frac{\sigma_{\phi_1}^2}{N_3} + \sigma_{\phi_2}^2$
phase fading plus additive noise	$\frac{\frac{N_3 N_0^3}{4}}{2N_0\lvert\alpha_4 E_{i1}\rvert^4 \lvert d_q\rvert^2 + N_3^{-1}\lvert\alpha_4 E_{i1}\rvert^6 \lvert d_q\rvert^4}$	$\frac{1}{2}\left(\frac{\sigma_{\phi_1}^2}{N_3} + \sigma_{\phi_2}^2\right)$

Modifications of the lower bounds presented in Table 3.1 due to the utilization of N_3 transmitter diversity elements.

CHAPTER 4

Here we examine the simplest formulation in which the effective surface aperture is not necessarily contained within the appropriate turbulent coherence area. This case is the sole member of Group 5, the partially coherent cross section, in Table 2.2. In contrast to our usual approach, the chapter is split into two sections by separating the modeling and estimation aspects of this formulation because each entails lengthy discussions.

4.1 Partially Coherent Cross Section (11m11) Model

In this section we assume that both A_1 and A_2 are contained within the appropriate coherence areas but that the effective surface aperture P is not. We thus employ the usual approximation for each channel provided the transmission interval is limited to a temporal coherence interval. Accordingly the input mode for the transmission channel as well as the output mode for the reception channel are identical with their free space counterparts. The most general transmitted envelope with energy $|E_{i1}|^2$ thus has the form

$$E_{i1}(\hat{r},\hat{t}) = E_{i1}\,[1/\sqrt{T}]\,\hat{\Phi}_{i1,0}(\hat{r}), \quad \hat{r} \in A_1,\ \hat{t} \in T_1, \tag{4.1.}$$

where T is the length of the transmission interval. This transmission produces the following received envelope

$$\gamma(r,t) = E_{02}(r,t) + n(r,t)$$

$$= [1/\sqrt{T}]\,\alpha_0\beta_0 E_{i1}\Phi_{01,0}(r) + n(r,t),$$

$$r \in A_2,\ t \in T_2, \tag{4.2}$$

where T_2 is a time-shifted (by $(L_1+L_2)c^{-1}$) version of T_1. Here we have utilized α_0 which was defined in (3.3a) and β_0 which we now define as follows

$$\beta_0 = [1/P] \int_P dr'\ b(r')\exp[\chi_{P1}(r',0)+j\phi_{P1}(r',0)]$$

$$\exp[\chi_{2P}(0,r')+j\phi_{2P}(0,r')]\hat{\Phi}_{01,0}(r')\Phi_{i1,0}^{*}(r'). \qquad (4.3)$$

The parameter β_0 depends on both the surface (target) and the turbulence in contrast to previous formulations wherein the effects of the surface were conveyed by a distinct parameter (b_0) which was not affected by the turbulence.

For this model, the additive noise consists of background noise and an additional term that represents quantum effects (cf., Section 3.1.1). If N_0 denotes the height of the power spectrum for this additive noise, then the likelihood ratio for this formulation is given by

$$= \langle \exp[-[|\alpha_0 E_{i1}\beta_0|^2/N_0]]\exp[2/\sqrt{T}\ N_0$$

$$\cdot\ \mathrm{Re}\{\alpha_0 E_{i1}\beta_0 \int_{T_2} dt \int_{A_2} dr\ \gamma^{*}(r,t)\Phi_{01,0}(r)\}]\rangle_{\substack{\chi_{P1}(r',0),\phi_{P1}(r',0)\\ \chi_{2P}(0,r'),\phi_{2P}(0,r')}} \qquad (4.4)$$

where $\langle\cdot\rangle$ denotes an ensemble average over the turbulent processes. The received envelope appears in (4.4) only as a correlation

$$\gamma_0 \triangleq \int_{T_2} dt \int_{A_2} dr\ \gamma(r,t)\ \Phi_{01,0}^{*}(r)\ [1/\sqrt{T}] \tag{4.5}$$

which is thus a sufficient statistic [28]. An equivalent formulation is given by

$$\gamma_0 = \alpha_0\ E_{i1}\ \beta_0 + n_0 \tag{4.6}$$

where n_0 is defined as follows

$$n_0 \triangleq \int_{T_2} dt \int_{A_2} dr\ n(r,t)\ \Phi_{01,0}^{*}(r)\ [1/\sqrt{T}]. \tag{4.7}$$

The available information about the surface is conveyed via the parameter β_0 which we now analyze to determine what information it contains and whether this information can be extracted from it. Toward this goal, we rewrite β_0 in the form

$$\beta_0 = [1/P] \int_P dr'\ b'(r')\ \exp[\chi(r')+j\phi(r')] \tag{4.8}$$

which utilizes the definitions

$$\chi(r')+j\phi(r') \triangleq \chi_{P1}(r',0)+j\phi_{P1}(r',0)+\chi_{2P}(0,r')+j\phi_{2P}(0,r'),$$

$$r' \in P, \tag{4.9a}$$

$$b'(r') \triangleq b(r')\hat{\Phi}_{01,0}(r')\Phi_{i1,0}^{*}(r'),$$

$$r' \in P. \tag{4.9b}$$

The statistics of the composite process $\chi(r)+j\phi(r)$ follow from the joint statistics of the perturbation processes discussed in Sections 2.1.2 and 2.3.1. This process is a complex Gaussian which is characterized by its means and covariances.

If we follow the approach of Levitt [86] and apply the coherence area decomposition technique (*cf.*, Section 3.2.1) to Equation 4.8, we obtain the ensuing approximation

$$\beta_0 = \sum_{n=1}^{N_T} B_n \exp[\chi_n+j\phi_n] \tag{4.10}$$

where N_T is the number of coherence areas $\{P_n\}_{n=1}^{N_T}$, $\chi_n+j\phi_n$ is the value of the process $\chi(r')+j\phi(r')$ over the n*th* area and $\{B_n\}$ are given by

$$B_n = [1/P]\left(\int_{P_n} dr'\ b'(r')\right), \qquad n = 1,2,\ldots,N_T. \tag{4.11}$$

In accordance with previous assumptions, we model the fading log-amplitudes $\{\chi_n\}$ as normally distributed and the fading phases $\{\phi_n\}$ as uniformly distributed. These fading phases are assumed to be independent of one another and of the fading log-amplitudes which, however,

are dependent on each other. Provided the interdependence of the fading log-amplitudes is slight (see Appendix 4A) and the members of the set $\{B_n\}$ are comparable in magnitude (*i.e.*, $b(r')$ satisfies certain regularity conditions), we may employ results obtained by Levitt [86, 87] to determine the nature of the random variable β_0. These results indicate that β_0 possesses a log normally distributed amplitude and a uniformly distributed phase whenever the summation parameter N_T is sufficiently small and that β_0 possesses a Rayleigh distributed amplitude and a uniformly distributed phase whenever N_T is sufficiently large. Halme's simulations [30] have confirmed these results and, furthermore, they provide a quantitative indication (see Table 4.1) of the applicability of the log normal or the Rayleigh distributions for $|\beta_0|$. From Table 4.1, we observe that there exists only a narrow range of values (of N_T) for which neither of these distributions is suitable for $|\beta_0|$. Hence the preceding pair of distributions are an adequate characterization of the random variable β_0 for our purposes.

A Rayleigh variate is specified by its variance so that when this model is accurate, the available information about the surface is given by

$$b \triangleq \langle|\beta_0|^2\rangle = [1/P^2] \int_P dr' \int_P d\rho'\; b'(r')\; b'^{*}(\rho')$$

$$\exp[-(1/2)D(r'-\rho')] \qquad (4.12a)$$

TABLE 4.1

σ^2	N_L	N_U
.1	1	4
.5	1	4
1.0	4	64

The critical values of the summation parameter N_T (cf., (4.10)) as a function of the fading log-amplitude variance, σ^2. For $N_T \leq N_L$, the amplitude $|\beta_0|$ has a lognormal distribution whereas for $N_T \geq N_U$ it has a Rayleigh distribution.

where $D(\cdot)$ is the sum of the wave structure functions for the transmission and the reception paths

$$D(r'-\rho') = D_{p1}(r'-\rho',0) + D_{2p}(0,r'-\rho'),$$

$$r',\rho' \in P, \tag{4.12b}$$

A log normal variate, however, requires an additional moment to complete its specification so that when this model applies, the available information consists of b and an additional parameter. To ensure that tractable estimators for the characterizing parameters may be determined (cf., Section 4.2), we utilize the parameter b' defined below

$$b' \triangleq \langle|\beta_0|^4\rangle = [1/P^4] \int_P dr_1' \int_P d\rho_1' \int_P dr_2' \int_P d\rho_2' \exp[4\sigma^2]$$

$$b'(r_1')b'^*(\rho_1')b'^*(\rho_2')\, b'(r_2')$$

$$\exp[-(1/2)[D(r_1'-\rho_1')+D(r_1'-r_2')+D(r_1'-\rho_2')+$$

$$D(\rho_1'-r_2')+D(\rho_1'-\rho_2')+D(r_2'-\rho_2')] +$$

$$D_\phi(r_1'-r_2') + D_\phi(\rho_1'-\rho_2')] \tag{4.13a}$$

where $D_\phi(\cdot)$ is the corresponding summation of phase structure functions for the transmission and the reception paths

$$D_\phi(r'-\rho') = D_{\phi_{P1}}(r'-\rho',0) + D_{\phi_{2P}}(0,r'-\rho'),$$

$$r',\rho' \in P. \qquad (4.13b)$$

Estimation of these parameters from the received envelope is examined in Section 4.2.

To complete this discussion, we assume that the parameters which specify β_0 can be reliably recovered from the received envelope in order to determine when this information provides an accurate measurement of the sole surface parameter, the coherent cross section (*cf.*, Section 3.1.1)

$$|b_0|^2 = [1/P^2] \int_P dr' \int_P d\rho'\ b'(r')b'^*(\rho'). \qquad (4.14)$$

From Equation 4.12a and Equation 4.14, we observe that $|b_0|^2$ can be obtained from, and is nearly equal to, b whenever the term $\exp[-(1/2)D(\cdot)]$ has a negligible effect on the integrals contained in the former equation, *i.e.*, when the scale of the correlation function of $b'(r')$ is much smaller than the coherence distance of the turbulence. In this situation, b' is also directly related to $|b_0|^2$ so that the existence of two characterizing parameters for β_0 does not lead to any

inconsistency. When the correlation scale is nearly equal to the coherence distance, the unambiguous extraction of $|b_0|^2$ from b (or the set {b,b'}) is no longer possible. Finally, if the correlation scale is much larger than the coherence distance, then the recovered information characterizes the turbulence rather than the surface (target).

To provide a more physical interpretation, we recall from Section 2.2.2 that

$$b(r') = \alpha'(r')\exp[-2jkz'(r')], \qquad r' \in P, \tag{4.15}$$

where $z'(r')$ is the height of the surface and $\alpha'(r')$ represents its strength (*i.e.*, local coefficient of reflection). For most surfaces [20, 23, 53], $\alpha'(r')$ varies slowly and slightly over the effective aperture P whereas $kz'(r')$ exhibits large and rapid variations. Using Suzuki's definition [53] for the scale of the correlation function

$$A_{cor} \triangleq \frac{1}{P} \int_P dr' \int_P d\rho'\, b'(r')b'^*(\rho') = P|b_0|^2 \tag{4.16}$$

and recalling that the free space modes are nearly normal plane waves [8], we observe that the surface roughness as embodied in its height variations is the primary factor in determining whether the received information may be interpreted in terms of the coherent cross section. As long as the height variations are sufficiently uncorrelated, the

received information is representative of the surface. Otherwise, the surface parameter is masked by the turbulence and cannot be obtained from the received information.

4.2 Partially Coherent Cross Section (11m11)--Estimation

For the formulation developed in the preceding section

$$\gamma_0 = \alpha_0 E_{i1} \beta_0 + n_0 \tag{4.17}$$

we now consider the estimation of those nonrandom parameters which characterize β_0. In contrast to formulations that we have already encountered (*e.g.*, Equation 3.6), the nonrandom parameters being estimated do not explicitly appear in (4.17) because we are no longer able to separate turbulent and surface scattering effects. This behavior is in agreement with our previous observation that these parameters do not necessarily characterize the surface itself. Nonetheless, they completely characterize the received envelope (*cf.*, Section 4.1) and, thus, are the only quantities available for estimation.

We first examine the model wherein β_0 possesses a Rayleigh distribution amplitude and a uniformly distributed phase so that it is completely characterized by the parameter b defined in (4.12a). The likelihood ratio for this model follows directly

$$\Lambda = [N_0/N_0+|\alpha_0 E_{i1}|^2 b] \exp [|\gamma_0|^2|\alpha_0 E_{i1}|^2 b/N_0(N_0+|\alpha_0 E_{i1}|^2 b)] \tag{4.18}$$

and is amenable to the standard maximum likelihood techniques. The ML estimator for b

$$\hat{b} = (|\gamma_0|^2 - N_0)|\alpha_0 E_{i1}|^{-2} \tag{4.19}$$

is unbiased and efficient, *i.e.*, it achieves the CR bound on the mean-square error of an unbiased estimator

$$[\mathrm{Var}(\hat{b})/b^2] \geq 1 + [2N_0/|\alpha_0 E_{i1}|^2 b] + [N_0{}^2/|\alpha_0 E_{i1}|^4 b^2] \tag{4.20a}$$

$$\triangleq 1 + [2/\Lambda_2] + [1/\Lambda_2{}^2]. \tag{4.20b}$$

When M (temporally obtained) independent observations $\{\gamma_{0m}\}$ of the received parameter are available, the ML estimator becomes

$$\hat{b} = [1/M] \sum_{m=1}^{M} [|\gamma_{0m}|^2 - N_0]|\alpha_0 E_{i1}|^{-2} \tag{4.21}$$

which achieves the usual diversity reduction in the error

$$[\mathrm{Var}(\hat{b})/b^2] = [1/M]\,[1 + (2/\Lambda_2) + (1/\Lambda_2^2)]. \tag{4.22}$$

We next examine the model in which β_0 has a lognormal amplitude distribution and a uniform phase distribution so that its characterization requires two parameters, b and b' defined in (4.13a). Here the likelihood ratio may be expressed in terms of the Frustration function

$$\Lambda = \mathrm{Fr}[(|\alpha_0 E_{i1}|^2 b^2/N_0(b')^{1/2}),(|\gamma_0|/\sqrt{N_0});(1/4)\ell n\ b' - (1/2)\ell n\ b]. \tag{4.23}$$

As our previous experience with this function would suggest (cf., Section 3.1.1), the application of standard estimation (ML) techniques encounters intractabilities. Once again we resort to the development (Moldon's technique) of approximations for the ML estimators and lower bounds for the CR bounds. The simplest unbiased estimators provided by this approach are the following

$$\hat{b} = [|\gamma_0|^2 - N_0]|\alpha_0 E_{i1}|^{-2} \tag{4.24a}$$

$$\hat{b}' = [|\gamma_0|^4 - 4|\gamma_0|^2 N_0 + 2N_0^2]|\alpha_0 E_{i1}|^{-4}. \tag{4.24b}$$

Although tractability has been the primary factor in the determination of these forms, the former is identical with the estimator just derived

for the related Rayleigh model. The normalized mean-square errors associated with these estimators are given by

$$[\mathrm{Var}(\hat{b})/b^2] = ([b'/b^2]-1) + [2/\Lambda_2] + [1/\Lambda_2^2] \tag{4.25a}$$

$$\triangleq (\Delta - 1) + [2/\Lambda_2] + [1/\Lambda_2^2] \tag{4.25b}$$

$$[\mathrm{Var}(\hat{b}')/(b')^2] = (\Delta^4-1) + [8\Delta/\Lambda_2] + [20/\Delta\Lambda_2^2] +$$

$$[16/\Delta^2\Lambda_2^3] + [4/\Delta^2\Lambda_2^4]. \tag{4.25c}$$

Following Moldon's approach, we also develop a collection of lower bounds for the pair of CR bounds by means of a series of straightforward but tedious computations

$$[\mathrm{Var}(\hat{b})/b^2] \geq \sup[(2/\Lambda_2),(\ell n\Delta)(1+(1/2)\ell n\Delta),1/[2\Lambda_2^2+\Lambda_2^3)] \tag{4.26a}$$

$$[\mathrm{Var}(\hat{b}')/(b')^2] \geq \sup[(8/\Lambda_2),(4\ell n\Delta)(1+(1/2)\ell n\Delta),1/[2\Lambda_2^2+\Lambda_2^3)]. \tag{4.26b}$$

When M independent observations $\{\gamma_{0m}\}$ of the received parameter are available, the estimators given by

$$\hat{b} = [1/M] \sum_{m=1}^{M} [|\gamma_{0m}|^2-N_0]|\alpha_0 E_{i1}|^{-2} \tag{4.27a}$$

$$\hat{b}' = [1/M] \sum_{m=1}^{M} [|\gamma_{0m}|^4 - 4|\gamma_{0m}|^2 N_0 + 2N_0 + 2N_0^2] |\alpha_0 E_{ii}|^{-4} \qquad (4.27b)$$

achieve the diversity reduction in mean-square error. The calculated lower bounds also experience this reduction so that the relative (to the bound) performance of the estimators is unaltered by diversity even though their absolute performance (size of the mean-square error) is significantly improved.

Analysis of the relative performance of these estimators is complicated in general but simplifies in the specialized circumstances for which the coherent cross section of the surface may be obtained from the parameter set $\{b,b'\}$ (cf., Section 4.1). In this context, b and b' are directly related

$$b' = b^2 \exp[4\sigma^2] \qquad (4.28)$$

so that only the estimator (4.24a) is necessary. The associated mean-square error becomes

$$[\mathrm{Var}(\hat{b})/b^2] = (\exp[4\sigma^2]-1) + [2/\Lambda_2] + [1/\Lambda_2^2] \qquad (4.29)$$

while the lower bound is given by the following

$$[\mathrm{Var}(\hat{b})/b^2] \geq \sup[(2/\Lambda_2), 4\sigma^2(1+2\sigma^2), 1/[2\Lambda_2{}^2+\Lambda_2{}^3)]. \qquad (4.30)$$

The second term in Equation 4.30 provides the improved bound promised in Appendix 3A since this formulation subsumes the one employed there. Provided we relabel the axes (by replacing Λ_0 with Λ_2 and $|b_0|^{-4}\mathrm{Var}(|b_0|^2)$ with $b^{-2}\mathrm{Var}\ b$), Figure 3.1 supplies a graphic comparison of the error and the bound. As the ratio (see Figure 3.2) of these quantities varies modestly (1.6 to 3.6), this estimator possesses sufficient quality to justify its employment.

CHAPTER 5

In this chapter we discuss some imaging techniques which are useful in the more general formulations of Table 2.2, *e.g.*, the coherent scanning and imaging group or the general (partially coherent scanning and imaging) group. In view of the limited results that have been obtained for the relatively uncomplicated coherent imaging group (*cf.*, Section 3.2), we do not attempt to devise optimal transmission and reception processing for these complicated formulations. Instead, in Section 5.2, we utilize results obtained in Chapters 3 and 4 to develop techniques which provide adequate (radiance) images under suitably restricted circumstances. The topic of beam propagation which is relevant to these schemes is examined in Section 5.1.

5.1 Beam Propagation in the Clear, Turbulent Atmosphere

There exists considerable interest in this topic for which two distinct theoretical approaches based respectively on radiance statistics and mutual coherence functions have been developed. A partial bibliography along with an examination of the relative merits of these approaches vis-a-vis experimental results are presented elsewhere [54]. To avoid the uncertainties associated with the existence of focused beams in a turbulent environment [55, 56] we base our methods (for imaging) on the more pessimistic conclusions of the mutual coherence school.

As a quantitative framework for discussing these results, we employ the line-of-sight propagation model described in Section 2.1. The term beam refers to a complex envelope with a Gaussian profile characterized by its radius W_i and with a quadratic phase variation characterized by the focal length f_i so that the phrase "transmitted beam" indicates the following transmitted envelope

$$E_i(\hat{r}) = E_i([1/\pi W_i^2])^{1/2}\exp[-(|\hat{r}|^2/2)((1/W_i^2)+(jk/f_i))],$$

$$\hat{r} \in A_1, \tag{5.1}$$

where E_i is an energy parameter. When the focal length f_i is chosen to equal the pathlength L, the beam is said to be focused on aperture A_2. In a free space environment, this transmitted beam

causes the following received envelope provided the radius of aperture A_1 exceeds $\sqrt{2}\, W_i$ [14],

$$E_0(r) = E_i([1/\pi W_0^2])^{1/2}\exp[-(|r|^2/2)((1/W_0^2)+(jk/f_0))],$$

$$r \in A_2, \tag{5.2a}$$

where

$$W_0^2 = [L^2/k^2W_i^2] + W_i^2(1 - (L/f_i))^2 \tag{5.2b}$$

$$f_0 = [L\, W_0^2[(L/f_i)W_i^2(1-(L/f_i))-(L^2/k^2W_i^2)]]^{-1}. \tag{5.2c}$$

This envelope may be regarded as a beam with focal length f_0 and radius W_0 which is plotted in Figure 5.1 as a function of the parameters of the transmitted beam. For a focused transmission, the received beam has a spot size (area) given by

$$S_0 \triangleq 2\pi W_0^2 = [(\lambda L)^2/2\pi W_i^2]. \tag{5.3}$$

By using the appropriate set of linear phase variations in the transmitted envelope to displace the centroid of the received envelopes, we may cover the aperture A_2 with a collection of "physically orthogonal" beams [58]. This collection, henceforth designated the

scanning set, contains approximately N_{be} beams

$$N_{be} = [A_2/S_0] = [A_2(2\pi W_i^2)/(\lambda L)^2] =$$

$$[A_2 A_1/(\lambda L)^2] = D_{f0} \tag{5.4}$$

where D_{f0} is the free space Fresnel number (cf., Section 2.1.3).

In a turbulent environment, the received envelope due to a transmitted beam is obtained from the extended Huygens-Fresnel principle [21]

$$E_0(r) = \int_{A_1} d\hat{r}\, E_i(\hat{r}) h_0(r-\hat{r}) \exp[\chi_{21}(r,\hat{r}) + j\phi_{21}(r,\hat{r})]$$

$$r \in A_2, \tag{5.5}$$

where $E_i(r)$ is specified by Equation 5.1. The effects of turbulence are difficult to discern from this expression, but they may be analyzed by means of a familiar pair of approximations. First, we restrict the aperture A_1 as follows

$$\text{diam } A_1 \lesssim \rho_{sw} \tag{5.6a}$$

to employ the unilateral coherence approximation (cf., Section 2.4) which yields

$$E_0(r) = \exp[\chi_{21}(r,0)+j\phi_{21}(r,0)]E_{0f}(r),$$

$$r \in A_2, \tag{5.6b}$$

where $E_{0f}(r)$ is the corresponding received envelope in a free space environment. Since $E_0(r)$ is merely a corrupted version of $E_{0f}(r)$, its (long exposure) properties are similar. For example, the restriction of the size of the transmitter aperture limits the minimum spot size achieved by the mean irradiance, $<|E_0(r)|^2>$,

$$S_T \geq [(\lambda L)^2/\pi(\rho_{SW}/2)^2]. \tag{5.7}$$

This limitation on the minimum spot size may also be interpreted (via the relationship given in (5.4)) as a limitation on the number of members in the scanning set in a turbulent environment.

To permit smaller spot sizes to be achieved, we utilize a slight generalization of the preceding approximation (previously examined in Appendix 2A)

$$\chi_{21}(r,\hat{r})+j\phi_{21}(r,\hat{r}) = \chi_{21}(r,0)+j\phi_{21}(r,0)-j[\Delta\cdot(r-\hat{r})][k/L],$$

$$\hat{r} \in A_1,\ r \in A_2, \tag{5.8}$$

which permits a slight increase in the size of aperture A_1

$$\text{diam } A_1 \lesssim 1.9\, \rho_{SW}. \tag{5.9a}$$

From the resultant form of the received envelope

$$E_0(r) = \exp[\chi_{21}(r,0)+j\phi_{21}'(r,0)]E_{0f}(r-\Delta),$$

$$r \in A_2, \tag{5.9b}$$

we observe that the received beam is a corrupted version of the free space reception, $E_0(r)$, which also executes a random walk (beam wander) over the aperture A_2. Once again the restriction on the size of the transmitter aperture (Equation 5.9a) limits the minimum spot size of the mean received irradiance

$$S_T' \geq [(\lambda L)^2/\pi(1.9\, \rho_{SW}/2)^2]. \tag{5.10}$$

Although the decreased spot size (relative to S_T) appears to imply that the turbulent scanning set has been enlarged, the "physical orthogonality" of its members is assured only if we increase this minimum spot size (by an amount sufficient to ensure that beam wander effects do not significantly alter the orthogonal relationships. The necessary computation (performed in Appendix 5A) indicates that the effective minimum spot size, *i.e.*, S_T' suitably incremented, remains unchanged at S_T. This result has previously been established by

Yura [57] via an examination of the average received irradiance with no initial limitation on the transmitter aperture. Thus, for a fixed receiving aperture (or a fixed target size) we are interpreting the effects of the turbulent environment in terms of a limitation on the number of members in the scanning set. Although this crude interpretation is adequate for our purposes, it must be carefully evaluated for use elsewhere.

5.2 Imaging Techniques

In this section we describe some techniques which provide (radiance) images for selected surfaces under suitably restricted conditions. Although a variety of such methods can be employed in a free space environment, the presence of turbulence severely degrades the images supplied by some of these approaches. Those techniques which retain their utility in the turbulent environment exploit the special characteristics of the relevant class of surfaces to circumvent the turbulent degradations.

The decision to utilize radiance images ($|b(r')|$ or $|b(r')|^2$) rather than coherent images ($b(r')$) also exploits characteristics of the class of surfaces (targets) to which the radar model developed in Chapter 2 is applicable. From Section 2.2 we recall that the rough surface is described by the multiplicative operator

$$b(r') = \alpha'(r') \exp[-2jkz'(r')] I_p(r'), \qquad r' \in P, \tag{5.12}$$

where we have explicitly included the indicator function for the effective surface aperture defined by the following

$$I_p(r') = \begin{cases} 1 & r' \in P \\ 0 & r' \notin P \end{cases}. \tag{5.13}$$

In view of prior assumptions concerning the nature of the surface roughness, the function $b(r')$ exhibits rapid variations due principally to the phase term which involves the surface height [13,17,18]. We observe that the surface radiance image

$$|b(r')| = \alpha'(r')I_p(r'), \qquad r' \in P, \tag{5.14}$$

does not involve this rapidly varying term but depends only on $\alpha'(r')$ which varies smoothly and slowly [13,17]. Because the resolution of rapid surface variations is seriously impaired by both diffractive and turbulent effects (*cf.*, Appendix 3D) and since an absolute phase reference cannot be established for a turbulent path (*cf.*, [29] and Section 3.2.1), we are content here to treat the radiance image as an adequate characterization of the surface (target).

In the ensuing subsections we examine three distinct techniques which provide radiance images (henceforth designated as images, for convenience) of suitably chosen classes of surfaces (targets). The first technique, surface decomposition, is based on the observation that standard passive imaging methods such as those discussed in Appendix 3D can be utilized whenever the effective source, *i.e.*, the illuminated region of the surface, lies within an isoplanatic patch. If we therefore sequentially illuminate the target with a scanning set of appropriate spot size, the resulting images may be recombined to form a surface image. This technique is obviously dependent on our ability to focus a transmitted beam (*cf.*, Section 5.1), *i.e.*, to ensure that the illuminated

region is sufficiently small and also encounters the familiar turbulent degradations experienced by passive imaging methods (*cf.*, Appendix 3D) so that its use is limited to an appropriately (spatial-frequency) band-limited class of surfaces.

The second technique, surface sampling, is based on the previous observation that $|b(r')|$ varies slowly and smoothly. Accordingly, this function may be regarded as (spatial-frequency) bandlimited so that it admits a sampling representation. In this case we sequentially illuminate the target with a collection of focused beams of minimal spot size centered at the respective sampling points. The received envelopes are then processed according to the methods developed in Chapters 3 and 4 to obtain a collection of high quality sample estimates which may be used to construct an image. The applicability of this technique is again dependent on our ability to focus a transmitted beam, *i.e.*, to ensure that the sampling pulse (beam) is suitably narrow.

The third technique, surface approximation, is also based on the observation that $|b(r')|$ exhibits smooth variations. Here we model this function as spatially uniform, *i.e.*, $|b(r')|$ equals either zero or a fixed value. In this case, we sequentially illuminate the target with the scanning set of minimal spot size (*cf.*, Section 5.1). For each received envelope, we then utilize the methods of Chapters 3 and 4 to decide whether the transmitted beam has been reflected by the target. This collection of decisions may then be combined to generate an

image of the surface. The quality of this image is also affected by our ability to focus a transmitted beam since beams that are partially reflected from the target lead to ambiguous decisions.

These techniques are examined in a quantitative manner in the following subsections. In all cases, if more optimistic predictions concerning beam focusing in a turbulent environment prove to be justified (*cf.*, Section 5.1), the technique of interest can be applied to a less restricted class of surfaces thus enhancing its utility.

5.2.1 Surface Decomposition

The formulation corresponding to a surface which contains many coherence areas is sufficiently complicated that the usual imaging techniques (*cf.*, Appendix 3D) are no longer appropriate. Consequently, to utilize these methods, we employ a transmission scheme which sequentially illuminates sections of the surface that permit the strict isoplanatic and the unilateral coherence approximations, *i.e*, that are contained within a turbulent coherence area. An obvious selection for the sequence of transmitted envelopes is the scanning set $\{E_{il,\ell,0}(r)\}$ of "physically orthogonal" beams described in Section 5.1. Here the subscripts il indicate an input to the first (transmission) channel, the subscript ℓ indicates the ℓth member of the scanning set and the subscript 0 indicates that the form is identical to its free space counterpart (*cf.*, Section 3.1.1). Provided it produces a suitable spot size on the surface (an issue that we temporarily avoid), the ℓth such

envelope causes the following received envelope at aperture A_2 (cf., Equation 5.5b)

$$E_{02,\ell}(r) = E_{02,\ell,0}(r)\exp[x_\ell(r)+j\phi_\ell(r)] + n_\ell(r),$$

$$\ell \in 1,2,\ldots,D_{f01},$$
$$r \in A_2. \qquad (5.15a)$$

Here $n_\ell(r)$ is the usual background noise restricted to the ℓth reception interval (cf., Section 3.1.1); $E_{02,\ell,0}(r)$ is the received envelope for the corresponding free space system (in view of the limits on A_1 and the spot size)

$$E_{02,\ell,0}(r) = \int_p dr' \; E_{01,\ell,0}(r')b(r')h_0(r,r'),$$

$$\ell \in 1,2,\ldots,D_{f01},$$
$$r \in A_2, \qquad (5.15b)$$

and $x_\ell(r)+j\phi_\ell(r)$ is defined by

$$x_\ell(r)+j\phi_\ell(r) = x_{P1}(r_\ell',0)+j\phi_{P1}(r_\ell',0)+x_{2P}(r,r_\ell')+j\phi_{2P}(r,r_\ell'),$$

$$\ell \in 1,2,\ldots,D_{f01},$$
$$r \in A_2, \qquad (5.15c)$$

wherein we have again utilized the limitations on the transmitting aperture and the scanning spot size.

We then process each of these received envelopes with a thin lens that has focal length L_2 (which is the pathlength in the reception channel) and transmission function $w(r)$ to obtain the following set of image spectra (*i.e.*, image Fourier transforms)

$$O_\ell(f) = \int_{A_2} dr \{w(r)w^*(r-\lambda L_2 f)\}$$

$$\{E_{02,\ell,0}(r)\exp[x_\ell(r)+j\phi_\ell(r)]+n_\ell(r)\}$$

$$\{E_{02,\ell,0}^*(r-\lambda L_2 f)\exp[x_\ell(r-L_2 f)-j\phi_\ell(r-\lambda L_2 f)]$$

$$+ n_\ell^*(r-L_2 f)\}, \quad \ell \in 1,2,\ldots,D_{fOI}, \tag{5.16}$$

where f is the transformation variable which may be interpreted as a spatial frequency. For a lens of sufficient quality, the uncorrupted image spectra

$$I_{\ell,0}(f) = \int_{A_2} dr \{w(r)w^*(r-\lambda L_2 f)E_{02,\ell,0}(r)E_{02,\ell,0}^*(r-\lambda L_2 f)\},$$

$$\ell \in 1,2,\ldots,D_{fOI}, \tag{5.17}$$

are adequate representations [14,15] for the respective transmitted

radiances to which they correspond, *i.e.*, $\{|E_{01,\ell,0}(r')b(r')|^2\}$. For each of these received envelopes, we combine many short exposures images (to form a long exposure image) in order to counteract the noise terms, *i.e.*, we form the following set of image spectra

$$I_\ell(f) \triangleq \langle O_\ell(f)\rangle = I_{\ell,0}(f)\exp[-(1/2)D_2(\lambda L_2 f)] + N_0 \int_{A_2} dr\ |w(r)|^2,$$

$$\ell \in 1,2,\ldots,D_{f01}, \tag{5.18}$$

where $D_2(\cdot)$ is the wave structure function for the reception channel (*cf.*, Section 2.1.2) and where N_0 is the height of the power spectral density of the background noise (*cf.*, Section 2.3.1). We then superimpose these long exposures and subtract the (constant) noise-dependent term to obtain an image which has the following spectrum

$$I(f) = \{\sum_{\ell=1}^{D_{f01}} I_{\ell,0}(f)\}\exp[-(1/2)D_2(\lambda L_2 f)]$$

$$\triangleq I_0(f)\ \exp[-(1/2)\ D_2(\lambda L_2 f)], \tag{5.19}$$

which is a spatial-frequency-limited version of the free space image spectrum, $I_0(f)$. This technique is therefore suitable for treating transmitted envelopes with images which are bandlimited to a spatial frequency bandwidth B' that satisfies the following requirement

$$B'/2 \leq [\rho_{SW,2}/\lambda L_2], \tag{5.20}$$

where $\rho_{SW,2}$ is the spherical wave coherence distance for the reception channel.

To obtain an image of the surface itself, we must eliminate the effects of the scanning beams from this (long exposure)image which, as previously mentioned, depends on both the surface and the beams incident on it. In other words, we have formed a bandlimited version of the image given by the following expression

$$Im_0(r') = \sum_{\ell=1}^{D_{f01}} Im_{\ell,0}(r') = \sum_{\ell=1}^{D_{f01}} |E_{01,\ell,0}(r')b(r')|^2,$$

$$\ell \in 1,2,\ldots,D_{f01},$$

$$r' \in P, \tag{5.21}$$

from which we wish to recover the surface image, $|b(r')|^2$. If this surface image is bandlimited to a spatial frequency band (with bandwidth B) then the following restriction

$$\max[B/2,[\rho_{SW,1}/2\sqrt{2}\,\lambda L_1]] \leq [\rho_{SW,2}/\lambda L_2], \tag{5.22}$$

where $\rho_{SW,1}$ is the spherical wave coherence distance for the transmission channel ensures that the surface image can be obtained, *i.e.*, that the recovered image includes the relevant spatial frequency con-

tent of both the scanning beam and the surface image.

The class of surfaces which satisfy the requirement (5.22) is typically quite limited in comparison to the class for which the uncorrupted (diffraction-limited) image spectrum, $I_0(f)$, adequately represents the spectrum of the transmitted radiance. For this reason, much effort [36] has been devoted to searching for alternative processing techniques that provide images for a broader class of surfaces. For example, provided that the background noise is negligible, Hufnagel [36] has calculated the number of short exposure images (of an isoplanatic target) that must be taken in order to ensure (within an acceptable tolerance, *e.g.*, 1%) that a diffraction-limited one is obtained. Once a suitable collection (one for each isoplanatic region contained in the target) of such images is available, we superimpose them to form a diffraction-limited image from which the effects of the scanning beams must be removed. Of course, this technique tacitly assumes that we recognize (by some means) a diffraction-limited short exposure when it occurs.

For the context of negligible background noise, the novel processing technique (M-diversity processing) described in Appendix 3D is appropriate. Using M-diversity processing with a well corrected lens, we obtain the following collection of long exposure image spectra (defined to be the average of the Fourier transform of the intensity in the focal plane of the lens)

$$I_{\ell}(f) = I_{\ell,0}(f)\ \exp[-(1/2M)\ D_2(\lambda L_2 f)],$$

$$\ell = 1,2,\ldots,D_{f01}. \tag{5.23}$$

In this context, we select M to eliminate the (spatial-frequency) bandlimiting effects of the turbulence thereby ensuring the formation of diffraction-limited images, *i.e.*, the ℓth image thus obtained is given by the following

$$Im_{\ell}(r') = Im_{\ell,0}(r') \triangleq |E_{01,\ell,0}(r')b(r')|^2,$$

$$\ell = 1,2,\ldots,D_{f01},$$
$$r' \in P. \tag{5.24}$$

We then spatially limit the ℓth such image to a region P determined by but not equal to the spot size of the ℓth transmitted beam [59]. The effects of this transmission are easily removed so that the ℓth image is now a replica of the appropriate section of the surface

$$Im_{\ell}(r') = |b(r')|^2, \qquad \ell \in 1,2,\ldots,D_{f01},$$
$$r' \in P_{\ell}. \tag{5.25}$$

These images may be linearly combined to reconstruct the image of the entire surface. In a noiseless context, we therefore conclude that we

can form an image of any surface (that fits in the model given in Chapter 2) to which the surface decomposition technique can be applied.

A final relevant question thus concerns the applicability of the surface decomposition technique. From Section 5.1, we recall that the transmitting aperture is restricted to a coherence region (cf., Equation 5.6a) so that the scanning spot size satisfies the following

$$S_T \geq (\lambda L_1)^2/2\pi(\rho_{SW,1}/2)^2 . \tag{5.26}$$

To utilize the model (Equation 5.15) employed in this section, we further require that this scanning spot size is contained within a turbulent coherence region, *i.e.*,

$$S_T \leq \pi(\rho_{SW}/2)^2, \tag{5.27a}$$

where the coherence distance, ρ_{SW}, for the composite process (cf., Chapter 4) may be approximated as follows [83]

$$\rho_{SW}^2 = [\rho_{SW,1}^2 \, \rho_{SW,2}^2]/[\rho_{SW,1}^2+\rho_{SW,2}^2]. \tag{5.27b}$$

Accordingly, the surface decomposition technique may be utilized for those pathlengths, L_1 and L_2, which satisfy the requirement (recall that $\rho_{SW,i}$ depends on L_i, $i = 1,2$, as indicated in (2.12))

$$[(\lambda L_1)^2/2\pi(\rho_{SW,1}/2)^2 \leq (\pi/4)\ \rho_{SW,1}^2\,\rho_{SW,2}^2[\rho_{SW,1}^2+\rho_{SW,2}^2]^{-1} \quad (5.28)$$

In the case where the radar is monostatic (*i.e.*, L_1 and L_2 are equal), routine manipulation of Equation 5.28 yields

$$1 \leq [\pi\rho_{SW,1}^2/4\lambda L_1]^2. \quad (5.29)$$

This requirement is similar to the one (Equation 2.13) which justifies the random variable approximation. Consequently, those pathlengths for which the surface decomposition technique is appropriate are comparable to the results presented in Table 2.1. We have previously disregarded such pathlengths because of their restricted sizes (cf., Appendix 2C) so that this decomposition technique is not interesting within our formulation.

5.2.2 Surface Sampling

When the function that characterizes the surface, $b(r')$, is spatial-frequency bandlimited (as it can always be regarded since evanescent waves do not propagate in this channel [8,14]), it admits a sampling representation [60],

$$b(r') = \sum_{m=1}^{\infty} b(r_m')\phi_{inter}'(r'-r_m'),$$

$$r' \in P, \quad (5.30)$$

where $\{r_m'\}$ are the sampling points and $\phi_{inter}'(\cdot)$ is the usual [60] interpolation function. Because of the rapid variations exhibited by $b(r')$, the set of requisite samples are closely-spaced. A radiance image of the surface, however, involves only $|b(r')|$ which displays much smoother variations so that the necessary samples possess much larger spatial separations, *i.e.*, the sampling distances are equal to $(2B_M)^{-1}$ where B_M is the bandwidth of $|b(r')|^2$. In this case, the sampling representation becomes

$$|b(r')|^2 = \sum_{\ell=1}^{\infty} |b(r_\ell')|^2 \phi_{inter}(r'-r_\ell'), \qquad r' \in P, \tag{5.31a}$$

which, in view of Equation (5.12), may be rewritten as follows

$$|b(r')|^2 = \sum_{\ell=1}^{\infty} \alpha'(r_\ell')^2 \phi_{inter}(r'-r_\ell'), \qquad r' \in P. \tag{5.31b}$$

Again, $\{r_\ell'\}$ are the sampling points and $\phi_{inter}(\cdot)$ is the appropriate interpolation function [60]. Although this representation requires an infinite collection of samples (as indicated in the preceding equations), a representation that utilizes a (suitably large) finite number of samples, N_S

$$|b(r')|^2 = \sum_{\ell=1}^{N_s} \alpha'(r_\ell')^2 \phi_{inter}(r'-r_\ell'),$$

$$r' \in P, \tag{5.32}$$

often supplies an accurate approximation [30].

We restrict consideration to the class of bandlimited surfaces for which the sampling distance exceeds the minimum attainable spot size diameter

$$B_M^{-1} \gtrsim [2\sqrt{2}\, \lambda L_1/\rho_{SW,1}]. \tag{5.33}$$

If we now sequentially transmit a set of beams that are focused on the individual sample points, $\{r_\ell'\}$, then the received envelope due to the ℓth such transmission (in view of the limitation on the size of the transmitting aperture) becomes the following

$$E_{02,\ell}(r) = \int_P dr' \{\alpha'(r')\exp[-2jkz'(r')]E_{01,\ell,0}(r')h_0(r,r')$$

$$\exp[\chi_{P1}(r',0)+j\phi_{P1}(r',0)+\chi_{2P}(r,r')+j\phi_{2P}(r,r')]\} + n(r),$$

$$r \in A_2$$

$$\ell \in 1,2,\ldots,N_{sample}. \tag{5.34}$$

This envelope thus contains information about the ℓth sample value, *i.e.*,

$$E_{02,\ell}(r) = \alpha'(r_\ell') \int_P dr' \{\exp[-2jkz'(r')] E_{01,\ell,0}(r') h_0(r,r')$$

$$\exp[x_{p1}(r',0)+j\phi_{p1}(r',0)+x_{2p}(r,r')+j\phi_{2p}(r,r')]\} + n(r),$$

$$r \in A_2$$

$$\ell \in 1,2,\ldots,N_{sample}, \qquad (5.35)$$

where the approximation utilizes the restriction given in (5.33). Accordingly, this envelope may be processed to obtain an estimate for the ℓth sample. When the sampling distance and the spot size radius are comparable, it becomes necessary to account for the finite sample pulse width (*e.g.*, see Monroe [61]). Since the mathematics associated with finite sampling pulses is complicated, we do not pursue this issue.

To determine a (suboptimal) estimator for the ℓth sample, we split the receiving aperture into coherence areas $\{A_{2,p}\}$ in order to utilize the techniques developed in Chapter 4. We denote the modal decomposition corresponding to the free space channel from the ℓth illuminated surface area, P_ℓ, to the pth coherence area as $\{\Phi_{ip\ell,m,0}(r'), \Phi_{Op\ell,m,0}(r), \eta_{p\ell,m,0}\}$ and let $D_{fOp\ell}$ represent the number of modes which efficiently transfer their energy. These modes are

are correlated with the received envelope

$$\gamma_{p\ell,m} = \int_{A_{2,p}} dr\, E_{02,\ell}(r)\Phi_{0p\ell,m,0}^{*}(r),$$

$$m \in 1,2,\ldots,D_{f0p\ell}, \tag{5.36}$$

to provide the parameters $\{\gamma_{p\ell,m}\}$ which are used in the estimator. An obvious modification of the results in Chapter 4 (cf., Equations 4.19 and 4.24 which apply to $\alpha'(r_\ell')^2$) provides the following estimator for $\alpha'(r_\ell')^2$

$$\hat{\alpha'(r_\ell')^2} = [1/N_{\ell,0}] \sum_{p=1}^{N_2} \sum_{m=1}^{D_{f0p\ell}} \{|\gamma_{p\ell,m}|^2 - N_0\}(|\alpha_{0p\ell}E_{i1}|^2 <|\beta_{p\ell,m}|^2>)^{-2},$$

$$\ell \in 1,2,\ldots,N_{sample}. \tag{5.37}$$

Here $|E_{i1}|^2$ is the transmitted energy and we define the following parameters

$$N_{\ell,0} = \sum_{p=1}^{N_2} D_{f0p\ell}, \qquad \ell = 1,2,\ldots,N_{sample}, \tag{5.38a}$$

$$\alpha_{0p\ell} = [-\exp[jkL_2]/j\lambda L_2](P_\ell A_{2,p})^{1/2},$$

$$p \in 1,2,\ldots,N_2,$$

$$\ell \in 1,2,\ldots,N_{sample}, \tag{5.38b}$$

$$\beta_{p\ell,m} = [1/P_\ell] \int_p dr' \; E_{01,\ell,0}(r')\exp[-2jkz'(r')]\Phi_{ip\ell,m,0}^{*}(r')$$

$$\exp[\chi_{p1}(r',0)+j\phi_{p1}(r',0)+\chi_{2p}(r_p,r')+j\phi_{2p}(r_p,r')],$$

$$p \in 1,2,\ldots,N_2$$

$$\ell \in 1,2,\ldots,N_{sample}$$

$$m \in 1,2,\ldots,D_{fOp\ell}. \qquad (5.38c)$$

where r_p denotes a fixed point in the p*th* coherence area, $A_{2,p}$. The collection $\{\alpha_{Op\ell}\}$ may be interpreted as free space propagation parameters while the parameters $\{\beta_{p\ell,m}\}$ depend on both the channel turbulence and the surface height variations (*cf.*, the analogs of parameters defined and discussed in Chapter 4).

The performance of this unbiased estimator may be calculated directly or adapted from previous results, *i.e.*, the associated normalized mean-square error is the following

$$[\mathrm{Var}(\hat{\alpha'}(r_\ell')^2)/\alpha'(r_\ell')^4] = [1/N_\ell] \sum_{p=1}^{N_2} \sum_{n=1}^{D_{fOp\ell}} \{[<|\beta_{p\ell,m}|^4>/<|\beta_{p\ell,m}|^2>^2]$$

$$- 1 + [2N_0/\alpha'(r_\ell')^2|\alpha_{Op\ell}E_{i1}|^2<|\beta_{p\ell,m}|^2>] +$$

$$[N_0^2/\alpha'(r_\ell')^4|\alpha_{Op\ell}E_{i1}|^4<|\beta_{p\ell,m}|^2>^2]\};$$

$$\ell = 1,2,\ldots,N_{sample}. \qquad (5.39)$$

This expression can be simplified whenever the random variables $\{\beta_{p\ell,m}\}$ can be described by either of the two models (lognormal or Rayleight amplitude and uniform phase) discussed in Chapter 4. Even when the value of this error term is excessive, however, since we realize that temporal diversity may be utilized to achieve satisfactory performance (sufficiently small mean-square error) for the estimator, (5.37).

These sample estimates are then combined according to the sampling representation

$$|\hat{b}(r')|^2 = \sum_{\ell=1}^{N_s} \alpha'(r_\ell')^2 \phi_{inter}(r'-r_\ell'), \qquad r' \in P, \tag{5.40}$$

to form an image of the target which is unbiased, *i.e.*,

$$\langle |\hat{b}(r')|^2 \rangle = |b(r')|^2, \qquad r' \in P, \tag{5.41}$$

where $|b(r')|^2$ is given by (5.32). As previously observed, temporal diversity can be employed to ensure that the error associated with $|\hat{b}(r')|^2$ is tolerably small. We therefore conclude that the surface sampling technique provides (radiance) images for the class of surfaces which satisfy the bandlimiting requirement of Equation 5.33.

5.2.3 Surface Approximation

In this section we restrict consideration to those surfaces which possess nearly uniform reflectivity functions

$$\alpha'(r') = \alpha_0', \qquad r' \in P \tag{5.42}$$

The (radiance) image of such a target

$$|b(r')|^2 = |\alpha'(r')|^2 = (\alpha_0')^2, \qquad r' \in P, \tag{5.43}$$

is accordingly determined by its effective surface aperture, P. When this target is known to be contained within a region P', then we may obtain an approximate image by splitting this region into subregions P_m' which are included (or excluded) entirely in (from) the approximation

$$|b(r')|^2 = (\alpha_0')^2 \sum_{m=1}^{N_{reg}} H_m I_{P_m'}(r'),$$

$$r' \in P', \tag{5.44a}$$

where H_m indicates whether the region P_m' is included, *i.e.*,

$$H_m = \begin{cases} 1 & P_m' \in P \\ 0 & P_m' \notin P \end{cases} \qquad m = 1,2,\ldots,N_{reg}, \tag{5.44b}$$

and where $I_{P_m'}$ is the indicator function for P_m'

$$I_{P_m'}(r') = \begin{cases} 1 & r' \in P_m' \\ 0 & r' \in P_m' \end{cases} \qquad \begin{matrix} m = 1,2,\ldots,N_{reg} \\ r' \in P'. \end{matrix} \tag{5.44c}$$

The quality of this approximation is dependent on the number of subregions, N_{reg}, as well as their shapes.

We now sequentially transmit a set of beams that are focused on the members of the set of subregions $\{P_m'\}$. Each of these subregions must therefore exceed the minimum scanning spot size determined in Section 5.1 (*cf.*, Equation 5.7). In view of the turbulent limitation on the size of the transmitting aperture, the received envelope due to the m*th* such transmission is given by

$$E_{02,m}(r) = \int_{P} dr' \{\exp[-2jkz'(r')] E_{01,m,0}(r') h_0(r,r')$$

$$\exp[\chi_{P1}(r',0) + j\phi_{P1}(r',0)]$$

$$\exp[\chi_{2P}(r,r') + j\phi_{2P}(r,r')]\} + n_m(r),$$

$$r \in A_2, \quad m = 1,2,\ldots,N_{reg}, \tag{5.45a}$$

when the surface is illuminated and

$$E_{02,m}(r) = n_m(r), \qquad r \in A_2,$$
$$m = 1,2,\ldots,N_{reg}, \tag{5.45b}$$

when it is not illuminated. In these expressions, $n_m(r)$ is the usual additive noise (*cf.*, Sections 2.3.1 and 3.1.1) for the *mth* reception interval. The preceding pair of equations constitute a standard binary hypothesis formulation [28]. Accordingly, the techniques of decision theory may be employed here. From the discussion in the preceding section, we know that accurate decisions can be achieved for each of the N_{reg} formulations by appropriately processing the received envelopes to utilize the available diversity. Again, it may be necessary to employ temporal diversity to attain the desired level of performance.

To obtain an image of the target, we interpolate this set of decisions according to the representation given in (5.44a), *i.e.*, if H_m represents the *mth* decision, then we construct the following image

$$|\hat{b}(r')|^2 = (\alpha_0')^2 \sum_{m=1}^{N_{reg}} \hat{H}_m \, I_{P_m'}(r'),$$
$$r' \in P'. \tag{5.46}$$

In view of the accuracy of the individual decisions $\{\hat{H}_m\}$, the preceding image provides an accurate reconstruction of the surface image given in expression (5.44a). The latter image, however, misrepresents those sur-

face areas which only partially intercept the illuminating beam. These areas are either included or excluded in toto from this image so that it does not converge to the surface image per se (*i.e.*, (5.43)). Nonetheless, this image can still be useful in determining certain gross surface characteristics such as shape or size. For example, we expect to notice any surface appendage which possesses a minimum dimension that exceeds the turbulent spot size.

5.2.4. Summary

A comparison of the imaging techniques just described is an appropriate summary for this chapter. Because the surface decomposition technique and the surface sampling technique apply to related classes of targets (*i.e.*, both classes satisfy (spatial-frequency) bandlimiting assumptions which are given in Equations 5.22 and 5.33, respectively), the comparison is confined to these techniques.

Both techniques supply accurate images within their range of applicability as indicated in Equations 5.21 and 5.41, respectively. In this sense, the surface decomposition technique is slightly superior because it applies to a broader class of targets. To obtain these images, both methods have effectively counteracted the additive background noise. On this point, the techniques are indistinguishable since both perform well.

Quantum effects, on the other hand, provide an interesting contrast since the processing involved in the surface decomposition technique

includes them only with difficulty. As previously discussed in Chapter 3, the processing utilized in the surface sampling technique can be adapted to account for quantum effects and the resulting estimators effectively counteract them. In this sense, the surface sampling technique is more adaptable.

The most important comparison concerns the applicability of these techniques. The surface decomposition technique can be utilized only for a restricted collection of pathlengths (cf., Equation 5.29). Because the surface sampling technique encounters no limitation of this nature, it may be employed within formulations of interest.

Re-examination of Sections 5.2.1 and 5.2.2 reveals that the surface decomposition technique does not properly utilize the available receiver and temporal diversity whereas the surface sampling technique does. The superior performance of the latter technique arises because it does not restrict the scanning spot to a turbulent coherence area and since it permits diversity processing at the receiver.

CHAPTER 6

We now examine some practical applications of the laser radar system which has been analyzed in the preceding chapters. In Section 6.1, we discuss insect detection and identification which is related to the material in Chapter 3. In Section 6.2, we consider ocean roughness measurement which utilized the results developed in Chapter 4. While both of these applications have been considered previously for microwave radars, they represent novel utilizations of an optical radar. Furthermore, the limitations imposed by turbulence on these applications have not been previously presented.

6.1 Insect Detection and Identification

Although radar systems have been employed almost from their inception for ornithological purposes [62,63], it is only recently that their use as an entomological tool has been seriously considered. Prior to the development of high-powered microwave radars in the mid-60's, the small cross sections possessed by most insects made reliable detection impossible even for modest ranges [64]. Even at this juncture, the realization that such applications existed was accidental as it resulted from examinations of radar "angels," *i.e.*, radar echoes received from a supposedly clear atmosphere. With the determination that many of these echoes could be attributed to insects [65], research concerned with the entomological uses of microwave radars was begun. In view of the difficulties associated with an exact theoretical analysis of this topic, the preponderance of the available research has been directed toward the measurement of those parameters required to utilize standard statistical radar models (*e.g.*, see [38]).

Provided we neglect the usual radar information concerning target range and radial velocity which is irrelevant to this application, the radar cross section represents a complete description of an insect (target) for transmissions of short temporal duration. In this situation, the cross section is the sole identification of an observed insect so that most of the ongoing experimental research concerns the measurement both in the laboratory [66] and in the field under controlled conditions [67,68] of radar cross sections for insects typically present in the

lower atmosphere. For lengthier transmissions, a temporal record of the radar cross section constitutes the entire available information about the insect. From such a record, items of entomological interest such as the flight pattern [67] (*i.e.*, flying or coasting-conditions which, because of wing movement, correspond to different cross sections) may be obtained.

A survey of insect dimensions [69] establishes that the vast majority of them are contained within a single turbulent coherence area for any atmospheric pathlength to which the Rytov approximation can be applied (*cf.*, Section 2.1.2). Consequently, the statistical model developed in Section 3.1 is appropriate for entomological applications of a laser radar system. Provided both apertures (receiving and transmitting) are likewise contained within turbulent coherence areas, this formulation may be expressed as follows

$$\gamma_0 = \exp[x_1+j\phi_1]\exp[x_2+j\phi_2]\alpha_0 E_{i1} b_0 + n_0, \tag{6.1}$$

where γ_0 is a sufficient statistic derived from the received envelope (*cf.*, Equation 3.5) and n_0 is the analogous statistic obtained from the noise envelope (which can be adapted to include quantum effects). Also α_0 is a free space propagation parameter defined by the following

$$\alpha_0 = -\exp[jk(L_1+L_2)]P(A_1A_2)^{1/2}/\lambda^2 L_1 L_2. \tag{6.2}$$

$|E_{i1}|^2$ is the transmitted energy, b_0 is the radar cross section, $x_1+j\phi_1$ is the turbulent random variable corresponding to the transmission channel and $x_2+j\phi_2$ is the turbulent random variable associated with the reception channel. The unbiased estimator for the (magnitude squared of the) cross section

$$|\hat{b}_0|^2 = [|\gamma_0|^2 - N_0]|\alpha_0|^{-2}|E_{i1}|^{-2}, \tag{6.3}$$

has normalized mean-square error

$$\mathrm{Var}(|\hat{b}_0|^2)/|b_0|^4 = (\exp[4\sigma^2]-1) + 2N_0/|\alpha_0 b_0 E_{i1}|^2 + N_0^2/|\alpha_0 b_0 E_{i1}|^4. \tag{6.4}$$

As in Chapter 3, available diversity (receiver, transmitter or temporal) may be employed to reduce the size of this error.

To illustrate the utilization of these results, we consider the measurement (estimation) of the radar cross section of a worker honeybee with a physical cross section of approximately $2cm^2$ [69]. Here the signal-to-noise ratio

$$\mathrm{SNR} = |\alpha_0 b_0 E_{i1}|^2/N_0 = [|E_{i1}|^2/N_0] \cdot P^2|b_0|^2 A_1 A_2/(\lambda L_1)^2(\lambda L_2)^2, \tag{6.5}$$

determines whether noise or turbulence is limiting the performance of the estimator previously selected. In order to numerically evaluate the signal-to-noise ratio, we require an approximate value for the cross section of this insect. To our knowledge, such data is not available in the literature so that we must judiciously extrapolate from the data that is available [66,67,68] to obtain representative values for the necessary radar cross sections. Following the suggestion of Hardy and Katz [64], we approximate the cross section of an insect with the cross section of a water drop that has similar dimensions. This technique indicates that $|b_0|$ is approximately 10^{-1} (and dimensionless as we recall from its definition in Chapter 3). If we further assume (for convenience) that the pathlengths and the apertures are identical, the SNR becomes

$$SNR = (10^{-2}) \left[(|E_{i1}|^2)/(N_0)\right] \left[(A_1 P)/(\lambda L_1)^2)\right]^2. \qquad (6.6)$$

For a laser system operating at a wavelength of 1.06u, the factor $(|E_{i1}|^2)/N_0$ typically exceeds 10^6 [71,3] so that the SNR becomes

$$SNR = 4 \cdot 10^{20} \left[(A_1^2)/(L_1^4)\right]. \qquad (6.7)$$

With a worst case turbulence model [71], the turbulent coherence area at a range of one kilometer has a radius of one centimeter so that

$$SNR = 36. \tag{6.8}$$

This result implies that turbulence rather than noise is limiting the performance of the estimator given in (6.3) under those circumstances for which the model developed in Chapter 3 is applicable. By simply utilizing the available temporal diversity we can ensure that the estimator error is sufficiently small, *e.g.*, by the employment of seven temporal measurements (of duration equal to the temporal coherence interval), we can achieve an error on the order of the size of the coherent cross section itself (*cf.*, (6.4)). We therefore conclude that the in situ measurement of a honeybee's cross section is feasible with existing systems over (Rytov-regime) pathlengths in those environments that we are likely to encounter.

Furthermore, under uncontrolled conditions, clutter from other insects as well as the land or sea background [67] may seriously degrade the system performance. The possibility of clutter points out the principal advantage of a laser system, namely, much smaller resolution cell size (proportional to λ^2) in the target plane. This advantage is limited but not eliminated by the turbulent restrictions on the transmitting aperture discussed in Chapter 5. For example, the aperture of 1 centimenter radius used to transmit at a wavelength of 1.06u achieves the same resolution cell size (at a fixed pathlength) as an aperture of 100m radius transmitting at a wavelength of 1.06cm.

We draw two conclusions based on the discussion and the example which have been given in this section. While the appropriate utilization of available diversity for a specific insect will depend on its SNR, the measurement of radar cross sections for many common insects is within the capability of state-of-the-art devices (laser systems). Furthermore, the improved resolution cell size of such a system significantly enhances the possibility of in situ measurements as well as tracking applications.

6.2 Ocean Roughness Measurement

There has long been considerable interest [72,73] in the measurement of ocean-surface parameters (such as wave height or wind speed) for subsequent utilization in applications like routing of marine vessels or weather prediction. The physical isolation of a significant portion of the earth's oceans has prompted the recent development of techniques designed for remote sensing [72,74] of the necessary information about the ocean surface. Many of these techniques have employed microwave devices (radars, scatterometers, radiometers, etc.) to gather their data so that accurate models of the sea at radio frequencies have been developed [75]. These techniques are primarily useful for measuring ocean-surface temperature which may also be obtained by means of a variety of techniques involving passive infrared spectrometers [76]. Thus far, utilization of laser radars has been restricted to wave profiling [73] with simple altimeters. Here we shall consider the possibility, first suggested by Beckmann [77,78], that active laser radars can provide information concerning ocean-surface roughness.

Typically, the radar system will be located in an aircraft or a satellite so that the system apertures will possess modest dimensions. Consequently, if we again neglect the usual radar information (which is irrelevant), the radar cross section completely describes the target (ocean) for transmissions of short temporal duration. Experiments designed to measure this cross section are being conducted in several laboratories [79,80]. For lengthier transmissions, a temporal record

of the behavior of the radar cross section constitutes the available information from which items of oceanographic interest may be determined.

An examination of existing systems [71] establishes that each of the system apertures (receiving and transmitting) is contained within a turbulent coherence area for those atmospheric paths to which the Rytov approximation can be applied. Therefore, the statistical model developed in Section 4.1 is suitable for this application, namely

$$\gamma_0 = \alpha_0 E_{i1} \beta_0 + n_0, \tag{6.9}$$

where γ_0 is a sufficient statistic derived from the received envelope (cf., Equation 4.5) and n_0 is the analogous statistic obtained from the noise envelope (which includes quantum effects). Also α_0 is a free space propagation parameter defined in (6.2), $|E_{i1}|^2$ is the transmitted energy and β_0 is a random variable which includes both (target) scattering; *i.e.*,

$$\beta_0 = [1/P] \int_b dr' \; b(r') \hat{\Phi}_{01,0}(r') \Phi_{i1,0}^{*}(r')$$

$$\exp[\chi_{p1}(r',0)+j\phi_{p1}(r',0)+\chi_{2p}(0,r')+j\phi_{2p}(0,r')]. \tag{6.10}$$

A discussion relating to the extraction of target information (*i.e*, the radar cross section) from this quantity has been given in Chapter 4. The roughness of the ocean surface [77,78] typically satisfies the

criterion established therein so that the associated, unbiased estimator for $<|\beta_0|^2>$, namely

$$(<|\hat{\beta}_0|^2>) = (|\gamma_0|^2 - N_0)/(|\alpha_0|^2 |E_{i1}|^2), \tag{6.11}$$

provides an estimate of the (magnitude squared of the) target cross section, $|b_0|^2$. Because large pathlengths are usually involved in this application, the illuminated region of the ocean surface will contain enough turbulent coherence areas so that the Rayleigh model for β_0 is appropriate (*cf.*, Section 4.1). Accordingly, the estimator (6.11) has normalized mean square error

$$[\mathrm{Var}(|\hat{b}_0|^2)/|b_0|^4] = 1 + [(2N_0)/(|\alpha_0 b_0 E_{i1}|^2)] + [(N_0^2)/(|\alpha_0 b_0 E_{i1}|^4)]. \tag{6.12}$$

Once again, temporal diversity may be utilized to reduce the error by the usual diversity factor.

As an example, we consider the measurement (estimation) of the radar cross section of the ocean surface for a calm sea (*i.e.*, a class 1 sea state). The signal-to-noise ratio previously defined in (6.5) again determines the quality of this measurement. For convenience, we assume that the apertures and pathlengths are similar so that the SNR becomes

$$SNR = [(|E_{i1}|^2)/N_0]\ [(P^2 A_1^2 |b_0|^2)/(\lambda L_1)^4]. \tag{6.13}$$

Provided we transmit a Gaussian-shaped beam focused on the ocean surface (cf., Chapter 5), the illuminated region will have a spot size

$$P = (\lambda L_1)^2/A_1 \tag{6.14}$$

so that the SNR becomes the following

$$SNR = [(|E_{i1}|^2)/N_0]\ |b_0|^2. \tag{6.15}$$

If we again operate the laser system at 1.06u, then $|E_{i1}|^2 N_0^{-1}$ exceeds 10^6 so that the SNR can be bounded as follows

$$SNR \geq 10^6\ |b_0|^2. \tag{6.16}$$

In order to complete this evaluation, we must determine a typical value for $|b_0|^2$ in sea state 1. Recalling the definition of the correlation scale of the ocean surface (Equation 4.16), we may rewrite $|b_0|^2$ as follows

$$|b_0|^2 = [A_{cor}/P] = [A_{cor} A_1/(\lambda L_1)^2] \tag{6.17}$$

to utilize Barrick's [88] estimate of A_{cor} ($= 10^{-4}$) corresponding to sea state 1. The resultant SNR

$$SNR \geq 10^2 \left[A_1/(\lambda L_1)^2\right] \tag{6.18}$$

indicates estimator performance as a function of aperture size and pathlength. For example, an aperture of radius one centimeter operating over a 10 kilometer path achieves a signal-to-noise ratio

$$SNR \geq 3 \cdot 10^4. \tag{6.19}$$

The preceding SNR indicates that, even without temporal diversity, the estimator error will be of the same order as the (normalized) coherent cross section itself (*cf.*, (6.12)). We thus conclude that in situ measurement of ocean surface roughness is feasible with existing systems in those contexts to which our model can be applied.

There exist related applications concerned with the measurement of the roughness of natural terrain [74] or sea ice [81]. The feasibility of these applications can be determined by the technique utilized in this section to discuss the measurement of ocean surface roughness.

CHAPTER 7

Here we summarize those results which we have obtained for the radar model of Section 2.3.1 and the related simplifications described in Section 2.3.2 (cf., Table 2.2). These results can be separated into four categories associated with Sections 3.1, 3.2, 4.2, and 5.2, respectively.

7.1 Summary

First, we have thoroughly analyzed the performance of the laser radar system for an isoplanatic target which is completely characterized by its coherent cross section. Our analysis indicates that we always utilize the available receiver diversity but that we selectively employ the available transmitter diversity (according to the rule given in Equation 3.48) in order to provide a high quality measurement of the target parameter. When the transmitter diversity is utilized, we obtain satisfactory measurements (*i.e.*, those possessing suitably small mean-square errors) in significantly shortened measurement intervals (*i.e.*, less temporal diversity is necessary).

Second, we have similarly analyzed the performance of this system for those (isoplanatic) targets which are completely characterized by their coherent images. In this case, the quality of the resultant image is poor despite the utilization of transmitter diversity. For this class of targets, we have also developed a method for obtaining diffraction-limited radiance images in the related noiseless context but have been unable to ascertain the merits of this technique in the (noisy) context of interest.

Third, we have thoroughly described the performance of this system for non-isoplanatic targets which are completely

characterized by their cross sections. Since the target parameter may be masked by turbulent effects in this context, we have determined a criterion (involving the coherence radius of the turbulence and the correlation distance of the target) which indicates when the system can recover this parameter. Furthermore we have developed an estimator which provides a satisfactory measurement of the target cross section provided it can be recovered from the received signal.

Fourth, by generalizing the results obtained in the three preceding contexts, we have devised some suboptimal imaging techniques which are applicable in the general formulation. By scanning certain classes of targets, we effectively employ the available transmitter diversity to form radiance images that cannot be obtained by other available imaging methods. By analyzing the performance of the radar system when such techniques are utilized, we have determined that the resulting images provide adequate descriptions of the relevant targets.

APPENDIX 2A

As an example of a higher order approximation related to the random variable approximation, we develop a physical interpretation of the linear phase approximation for the spherical wave perturbation term

$$\chi_{21}(r,\hat{r})+j\phi_{21}(r,\hat{r}) = \chi_0+j\phi_{00}+j(\phi_{10}\cdot r)+j(\phi_{01}\cdot\hat{r}),$$

$$r \in A_2,\ \hat{r} \in A_1. \qquad (2.A1)$$

Employment of this approximation restricts the dimensions of both apertures thus limiting the pathlength over which energy may be effectively transferred between these apertures. If we recast this approximation into the form

$$\chi_{21}(r,\hat{r})+j\phi_{21}(r,\hat{r}) = \chi_0+j(\phi_0+[k/2L]|\Delta|^2)+j(\phi_1\cdot r)-j[\Delta\cdot(r-\hat{r})]\frac{k}{L},$$

$$r \in A_2,\ \hat{r} \in A_1, \qquad (2.A2)$$

the atmospheric impulse response is given by

$$h_{21}(r,\hat{r}) = h_0(r-\hat{r}-\Delta)\{\exp[\chi_0+j\phi_0+j(\phi_1\cdot r)]\},$$

$$r \in A_2,\ \hat{r} \in A_1, \qquad (2.A3)$$

provided the paraxial approximation is used for $h_0(r-\hat{r})$.

The physical interpretation is straightforward: Δ is a random vector representing beam wander (deviation of the transmission from the normal line-of-sight) and ϕ_1 is a random vector representing image dancing (deviation of the transmission from the nominal tilt, which leads to a dancing effect in the focal plane of a lens). In other words, both the output and its Fourier transform are executing two-dimensional random walks. As long as the beam wander effect does not cause the output to miss the receiver, neither effect will degrade the quality of an image formed by a thin lens over short temporal intervals as compared to the corresponding free space image. These effects will, however, degrade time-averaged images. Interestingly, higher order perturbation effects necessarily degrade image quality [12] including short exposures. The results also provide some insight into the approximations of Section 2.1.4. The assumption of spatial invariance precludes image dancing whereas the assumption of unilateral coherence prevents beam wander. Since these assumptions place similar restrictions on the system of Figure 2.1, experiments comparing beam wander and image dancing effects may yield a measure of the validity of these approximations vis-à-vis one another. For example, if beam wander effects were to predominate in a given experiment, then the isoplanatic approximation would be more appropriate in that context.

APPENDIX 2B

We define the average unilateral coherence index, Δ_{uc}, by

$$\Delta_{uc} = \inf_{E_i(\hat{r})} \left[\int_{A_1} d\hat{r} |E_i(\hat{r})|^2 / \int_{A_2} dr \langle |E_0(r) - E_0'(r)|^2 \rangle \right], \qquad (2.B1)$$

where $E_0(r)$ is obtained from the channel input-output relationship, Equation 2.4,

$$E_0(r) = \int_{A_1} d\hat{r}\, E_i(\hat{r})\, h_{21}(r,\hat{r}), \qquad r \in A_2, \qquad (2.B2)$$

and $E_0'(r)$ is given by the unilateral coherence approximation to this relationship

$$E_0'(r) = \int_{A_1} d\hat{r}\, E_i(\hat{r})\, h_0(r-\hat{r}) \exp[x_{21}(r,0) + j\phi_{21}(r,0)],$$

$$r \in A_2. \qquad (2.B3)$$

The quantity Δ_{uc} is an inverse measure of the normalized mean square error that results when Equation 2.B3 replaces Equation 2.B2. From (2.B1) we observe that Δ_{uc} equals λ_{luc}^{-1} where λ_{luc} is the maximum eigenvalue of the kernel

$$K_{uc}(\hat{r}_1,\hat{r}_2) = \int_{A_2} dr \langle \{h_{21}^*(r,\hat{r}_1)-h_0^*(r-\hat{r}_1)\exp[x_{21}(r,0)-j\phi_{21}(r,0)]\}$$

$$\{h_{21}(r,\hat{r}_2)-h_0(r-\hat{r}_2)\exp[x_{21}(r,0)+j\phi_{21}(r,0)]\}\rangle,$$

$$\hat{r}_1,\hat{r}_2 \in A_1. \tag{2.B4}$$

Exact evaluation of λ_{1uc} appears hopeless, but the upper bound

$$\lambda_{1uc} \leq \int_{A_1} d\hat{r}\, K_{uc}(\hat{r},\hat{r}), \tag{2.B5}$$

leads to the following lower bound on Δ_{uc},

$$\Delta_{uc} \geq \left| [A_2/(\lambda L)^2] \int_{A_1} d\hat{r}\, (1-\exp[-\tfrac{1}{2} D(0,\hat{r})]) \right|^{-1} \tag{2.B6}$$

when the apertures A_1 and A_2 are circular. Preliminary work with this bound indicates that the unilateral coherence distance is approximately equal to the spherical-wave phase coherence length. For example, if we utilize the criterion

$$\Delta_{uc} \geq 10 \tag{2.B7}$$

and Yura's [83] square law approximation for the wave structure function

$$D(r,\hat{r}) = \left[|r|^2 + r\cdot r + |r|^2\right]\rho_{sw}^{-2},$$

$$r \in A_2,\ \hat{r} \in A_1, \qquad (2.B8)$$

then the bound in Equation 2.B6 requires that the diameter of the transmitting aperture satisfy the following

$$\text{diam } A_1 \leq 1.2\ \rho_{sw} \qquad (2.B9)$$

so that $1.2\ \rho_{sw}$ is the unilateral coherence distance. Because the development in this appendix exactly parallels its isoplanatic counterpart, we expect that other results that may be derived for the isoplanatic approximation can also be adapted to the unilateral coherence approximation (cf., [10]).

Although these results are sufficient for our purposes, more accurate descriptions of the behavior of the eigenvalue λ_{1uc} are available [10]. In particular, stronger, albeit more complicated, bounds for the eigenvalue exist and a thorough description of the behavior of its mean value has been presented.

APPENDIX 2C

Within the context of a line-of-sight propagation path, we consider the two formulations, lml and mlm, which were disallowed in Section 2.3.3. The former admits the random variable approximation (Equation 2.22) so that the number of modes $\langle D_f \rangle$ satisfies Equation 2.13

$$\langle D_f \rangle = D_{f_0} = [\pi \rho^2_{PW}/4\lambda L]^2. \tag{2.C1}$$

Pathlengths for which this approximation is valid are obtained by recalling that

$$\rho_{PW} = (2.92\ k^2 C_n^2 L)^{-3/5} \tag{2.C2}$$

and requiring that $\langle D_f \rangle$ satisfy Equation 2.C1 to ensure that the appropriate number of modes efficiently transfer their energy. It then follows that the formulation lml will be valid only for pathlengths which are shorter (by a factor of $D_{f_0}^{1/2}$) than those given in Table 2.1. Since this formulation is restricted to paths which are uninteresting in a radar context, we may disregard it as a matter of convenience.

For the latter case, we employ Shapiro's [8] observation that the turbulent channel possesses a single mode if and only if the eigenvalues satisfy the relationship

$$\langle(\sum_n \eta_n)^2\rangle = \sum_n \langle\eta_n{}^2\rangle. \qquad (2.C3)$$

By evaluating this equation, we determine the equivalent condition

$$\exp[-D(0,\hat{r}_1-\hat{r}_2)-D(r_1-r_2,0)+[1/2]D(r_1-r_2,\hat{r}_1-\hat{r}_2)+[1/2]D(r_2-r_1;\hat{r}_1-\hat{r}_2)] = 1 \qquad (2.C4)$$

where $D(r,\hat{r})$ is the wave structure function [11] for the turbulence. From the preceding expression, it follows that the initial restriction (2.C3) may be interpreted in terms of restrictions on the apertures

$$\text{diam } A_1 \leq 1.3\ \rho_{PW} \qquad (2.C5a)$$

$$\text{diam } A_2 \leq 1.3\ \rho_{PW} \qquad (2.C5b)$$

which implies that they may not exceed the coherence area which has a diameter of approximately $1.8\ \rho_{PW}$. Consequently, the formulation mlm may be disregarded without any loss of generality since it cannot occur.

APPENDIX 3A

In this appendix, we examine the derivation of the lower bounds of Section 3.1.1. The general inequality (3.17) is proven, applied to the formulation of that section to obtain (3.18a) and then extended to biased estimators. The development of the improved bound, (3.18b) is also discussed.

The derivation follows from the observation that an unbiased estimator, $\hat{\beta}(\gamma)$, satisfies the ensuing equation

$$0 = \int d\gamma(\hat{\beta}(\gamma)-\beta)\ p(\gamma|\beta) \tag{3.A1}$$

into which we introduce the supplementary vector Δ

$$0 = \int d\gamma(\hat{\beta}(\gamma)-\beta) \int d\Delta\ p(\gamma|\beta,\Delta)\ p(\Delta) \tag{3.A2}$$

and interchange the order of integration

$$0 = \int d\Delta\ p(\Delta) \int d\gamma\ p(\gamma|\beta,\Delta)\ [\hat{\beta}(\gamma)-\beta]. \tag{3.A3}$$

We next differentiate with respect to the parameter β to obtain

$$0 = [\partial/\partial\beta]\{\int d\Delta\ p(\Delta) \int d\gamma\ p(\gamma|\beta,\Delta)[\hat{\beta}(\gamma)-\beta]\}$$

$$= -1 + \int d\Delta\ p(\Delta) \int d\gamma [[\partial/\partial\beta]p(\gamma|\beta,\Delta)](\hat{\beta}(\gamma)-\beta) \qquad (3.A4)$$

which may be rearranged as follows

$$1 = \int d\Delta\ p(\Delta) \int d\gamma(\hat{\beta}(\gamma)-\beta)\ p(\gamma|\beta,\Delta)$$

$$[[\partial/\partial\beta]\ \ell n\ p(\gamma|\beta,\Delta)]. \qquad (3.A5)$$

Because $p(\Delta)$ is nonnegative, we may apply the Schwartz inequality to the inner integral

$$1 \leq \int d\Delta\ p(\Delta)(\{\int d\gamma(\hat{\beta}(\gamma)-\beta)^2 p(\gamma|\beta,\Delta)\}^{1/2} \cdot$$

$$\{\int d\gamma([\partial/\partial\beta]\ \ell n\ p(\gamma|\beta,\Delta))^2 p(\gamma|\beta,\Delta)\}^{1/2}). \qquad (3.A6)$$

We again employ this inequality to obtain the expression

$$1 \leq \{\int d\Delta\ p(\Delta) \int d\gamma(\hat{\beta}(\gamma)-\beta)^2 p(\gamma|\beta,\Delta)\}^{1/2} \cdot$$

$$\{\int d\Delta\ p(\Delta) \int d\gamma([\partial/\partial\beta]\ \ell n\ p(\gamma|\beta,\Delta))^2 p(\gamma|\beta,\Delta)\}^{1/2} \qquad (3.A7)$$

which, when squared, leads to the inequality

$$\mathrm{Var}[\beta(\gamma)] = \langle(\hat{\beta}(\gamma)-\beta)^2\rangle \geq$$

$$\langle\langle([\partial/\partial\beta] \ln p(\gamma|\beta,\Delta))^2\rangle_{\gamma|\Delta}\rangle_{\Delta}^{-1}. \tag{3.A8}$$

To arrive at (3.16), we use the relationship [28]

$$\langle\langle([\partial/\partial\beta] \ln p(\gamma|\beta,\Delta))^2\rangle_{\gamma|\Delta}\rangle_{\Delta} =$$

$$-\langle\langle[\partial^2/\partial\beta^2] \ln p(\gamma|\beta,\Delta)\rangle_{\gamma|\Delta}\rangle_{\Delta}. \tag{3.A9}$$

The results obtained by applying this bound to the formulation of Section 3.1.1 are gathered in Table 3.A1 which also contains the related results due to Moldon [29]. These latter results were determined via a collection of tedious computations so that, in some instances (*e.g.*, bounds 3 and 4 in Table 3A.1), they represent approximations to rather than lower bounds for the CR bound. Our technique therefore permits the necessary refinement of Moldon's original results. As an illustration of the utilization of this technique, we here present the computation which uses the fading parameters as the supplementary vector:

TABLE 3A.1

mentary ables	Related Formulation	Lower Bound	Moldon's Bound
$,\phi_1,\phi_2$	free space	$[2/\Lambda_0]$	$[2/\Lambda_0]$
)	noiseless	$4\sigma^2$	$4\sigma^2$
$,x_2$	---	$(1/[2\exp(4\sigma^2)\Lambda_0{}^2+2\exp(12\sigma^2)\Lambda_0{}^3+\exp(24\sigma^2)\Lambda_0{}^4])$	$(1/[2\Lambda_0{}^2+2\Lambda_0{}^2+\Lambda_0{}^4]$
$,x_2$	---	$(1/[\Lambda_0+\Lambda_0{}^2])$	$(1/[\Lambda_0{}^2])$
--	phase fading	$(1/[2\Lambda_0{}^2+\Lambda_0{}^3])$	---

Lower bounds generated by expression (3.17) for the formulation (3.6) and related approximate bounds obtained by Moldon [29].

$$\ell n\ p(\gamma_0|b_0,x_1,x_2,\phi_1,\phi_2) =$$

$$-\ell n(\pi N_0)-[1/N_0]|\gamma_0-\alpha_0 b_0 E_{i1}\exp[x_1+j\phi_1]\exp[x_2+j\phi_2]|^2; \qquad (3.A10)$$

$$[\partial^2/(\partial|b_0|^2)^2]\ell n\ p(\gamma_0|b_0,\cdot) =$$

$$[-\gamma_0{}^*\alpha_0 b_0 E_{i1}\exp[x_1+j\phi_1]\exp[x_2+j\phi_2]/4N_0|b_0|^4] +$$

$$[-\gamma_0{}^*\alpha_0{}^* b_0{}^* E_{i1}{}^*\exp[x_1+j\phi_1]\exp[x_2+j\phi_2]/4N_0|b_0|^4]; \qquad (3.A11)$$

$$<[\partial^2/(\partial|b_0|^2)^2]\ \ell n\ p(\gamma_0|b_0,\cdot)>_{\gamma_0|\cdot} =$$

$$[-|\alpha_0 E_{i1}|^2\exp[2x_1]\exp[2x_2]/2N_0|b_0|^2]; \qquad (3.A12)$$

$$<<[\partial^2/(\partial|b_0|^2)^2]\ \ell n\ p(\gamma_0|b_0,\cdot)>_{\gamma_0|\cdot}>_{\cdot} =$$

$$[-|\alpha_0 E_{i1}|^2/2N_0|b_0|^2]; \qquad (3.A13)$$

$$[-1/|b_0|^4](<<[\partial^2/(\partial|b_0|^2)^2]\ \ell n\ p(\gamma_0|b_0,\cdot)>_{\gamma_0|\cdot}>_{\cdot})^{-1} =$$

$$[2N_0/|\alpha_0 b_0 E_{i1}|^2]. \qquad (3.A14)$$

The remaining computations are similar although those that use only the fading amplitudes as the supplementary vector involve further ap-

proximations. The bound (3.18a) is then reached by observing that α_0 becomes α_c and hence Λ_0 becomes Λ_c for the relevant geometry (*c.f.*, discussion following Equation 3.15b).

While this inequality has been developed for unbiased estimators, it can be extended to include biased ones. If $\hat{\beta}(\gamma)$ is a biased estimate of β with bias $B(\beta)$, *i.e.*,

$$\langle\hat{\beta}(\gamma)\rangle = \beta + B(\beta) \tag{3.A15}$$

then Equation 3.A1 is replaced by the expression

$$B(\beta) = \int d\gamma(\beta(\gamma)-\beta)\ p(\gamma|\beta). \tag{3.A16}$$

The subsequent steps in the derivation follow in exactly the same order and they lead to this generalization

$$\mathrm{Var}(\beta(\gamma)-\beta) \geq \langle\langle([\partial/\partial\beta]\ \ell n\ p(\gamma|\beta,\Delta))^2\rangle_{\gamma|\Delta}\rangle_{\Delta}^{-1} \cdot \left|1 + [\partial B(\beta)/\partial\beta]\right|^2. \tag{3.A17}$$

We do not require the other extensions of the inequality (3.1) so we do not pursue such issues here.

The bound (3.18a) was subsequently tightened by the development of replacements for two of the three component bounds. The first of

these is derived in Chapter 4 where we establish the bound $4\sigma^2(1+2\sigma^2)$ to replace the term $4\sigma^2$. The other follows from the observation that the related formulation which involves only phase fading

$$\gamma_0 = \exp[j\phi_1+j\phi_2]\alpha_0 b_0 E_{i1} + n_0 \tag{3.A18}$$

also provides lower bounds to the CR bound because the amplitude fading does not alter the average received energy and cannot improve the attainable performance. This result provides the lower bound,

$$[\mathrm{Var}(|b_0|^2)/|b_0|^4] \geq 1/[2\Lambda_0^2+\Lambda_0^3], \tag{3.A19}$$

which completes the development of (3.18b). This discussion also introduces the concept that many of the lower bounds generated by (3.17) can be interpreted as CR bounds for simpler yet related formulations. For example, the term $2\Lambda_0^{-1}$ is the CR bound for the free space formulation

$$\gamma_0 = \alpha_0 b_0 E_{i1} + \mathbf{n_0} \tag{3.A20}$$

whereas $4\sigma^2$ is the CR bound for the noiseless formulation

$$\gamma_0 = \exp[x_1+j\phi_1]\exp[x_2+j\phi_2]\alpha_0 b_0 E_{i1}. \tag{3.A21}$$

APPENDIX 3B

In order to obtain information about the quality of irradiance images corresponding to the formulation of Equation (3.70), we utilize a concept introduced in Appendix 3A. There we observed that the lower bounds on the CR bound could be identified as exact CR bounds for related, albeit simplified, formulations. Furthermore, these simplifications provide estimators which, although suboptimal, often exhibit interesting behavior. Here we examine the free space formulation

$$\gamma(r,t) = [1/\sqrt{T}]\ \alpha_4 E_{i1} d(r) + n(r,t),$$

$$r \in A_2,\ t \in T_2, \tag{3.B1}$$

and the noiseless formulation

$$\gamma(r,t) = \exp[x_1 + j\phi_1]\exp[x_2(r) + j\phi_2(r)][1/\sqrt{T}]\alpha_4 E_{i1} d(r),$$

$$r \in A_2,\ t \in T_2, \tag{3.B2}$$

but we neglect the simplification involving both phase fading and additive noise

$$\gamma(r,t) = \exp[j\phi_1 + j\phi_2(r)][1/\sqrt{T}]\ \alpha_4 E_{i1} d(r) + n(r,t),$$

$$r \in A_2,\ t \in T_2, \qquad (3.B3)$$

since it is intractable.

Throughout we consider the estimation of the envelope $d(r)$ because estimators and bounds for this quantity lead directly to estimators and bounds for the coherent image, $b(r')$, or the irradiance image, $|b(r')|^2$, [28]. In particular, from the relationship

$$d(r) = \int_P dr'\ h_0(r,r')\ b(r'), \qquad r \in A_2, \qquad (3.B4)$$

it follows that an ML estimate for $d(r)$ provides an ML estimate for $b(r')$, namely

$$b(r') = \int_{A_2} dr\ d(r)\ h_1(r',r), \qquad r' \in P, \qquad (3.B5)$$

where $h_1(r',r)$ is the inverse filter for $h_0(r,r')$, *i.e.*,

$$\int_{A_2} dr\ h_1(r_1',r)\ h_0(r,r_2') = u_0(r_1'-r_2'),\ r_1',r_2' \in P. \qquad (3.B6)$$

For this channel, Shapiro [43] has determined that the conjugate filter, which corresponds to a thin lens for this formulation, supplies an estimate

$$\tilde{b}(r') = \int_{A_2} dr\, \hat{d}(r)\, h_0^*(r,r'), \qquad r' \in P, \tag{3.B7}$$

which does not differ significantly from the preceding ML estimate. Similarly, the estimate for $|b(r')|^2$ may be generated with a conjugate filter rather than an inverse filter. The relationship (3.B4) may also be used to generate CR bounds for $b(r')$ or $|b(r')|^2$ from the corresponding CR bounds for $d(r)$ although this calculation is often difficult (*cf.*, [28]).

The free space model (3.B1) is well understood so we merely appropriate available results. The ML estimate for the envelope $d(r)$ [28]

$$\hat{d}(r) = [1/\sqrt{T}] \int_{T_2} dt\, \gamma(r,t)(\alpha_4 E_{i1})^{-1}, \qquad r \in A_2 \tag{3.B8}$$

is unbiased and efficient with mean-squared-interval error $D_{f02}N_0|\alpha_4 E_{i1}|^{-2}$ since only D_{f02} modes are reconstructed (*cf.*, Section 3.2.1). When a collection of independent temporal observations $\{\gamma_m(r,t)\}_{m=1}^{M}$ are available (*cf.*, Section 3.1.1), we combine them in the usual manner

$$\hat{d}(r) = [1/M] \sum_{m=1}^{M} \hat{d}_m(r), \qquad r \in A_2, \tag{3.B9}$$

to achieve the usual diversity reduction (M^{-1}) in the estimator error. Interestingly, the introduction into this model of a uniformly distributed fading phase variable destroys the quality of the estimators $\hat{d}(r)$ and $\hat{b}(r')$ but does not affect the quality of the estimator $|\hat{b}(r')|^2$ [44].

Because there exists no closed-form likelihood ratio [30] for the formulation (3.B2), we cannot directly derive bounds or estimators for the envelope $d(r)$ in this context. Results obtained by applying ML techniques to the related sampling representation suggest the following biased and inefficient estimator (using σ^2 from (3.15b))

$$\hat{d}(r) = [1/\sqrt{T}] \int_{T_2} dt\, \gamma(r,t)(\alpha_4 E_{i1})^{-1} \exp[\sigma^2], \qquad r \in A_2. \tag{3.B10}$$

Here, when a set of independent temporal observations are available, they are combined multiplicatively

$$\hat{d}(r) = [\prod_{m=1}^{M} \hat{d}_m(r)]^{1/M}, \qquad r \in A_2, \tag{3.B11}$$

rather than additively. For this context, we have been unable to determine the CR bound for the envelope $d(r)$.

While we have obtained only a partially complete set of results in this appendix, they possess interesting implications. To facilitate

comparison with the literature, the behavior of the irradiance images provided by estimators (3.B9) and (3.B11) are examined in the context of passive imaging over a line-of-sight propagation in Appendix 3D. The results therein described may be straightforwardly adapted to the formulation utilized in this discussion.

APPENDIX 3C

We now consider the issues pertinent to the evaluation of the likelihood ratio for the formulation (3.70)

$$\gamma(r,t) = [1/\sqrt{T}]\ \exp[\chi_1+j\phi_1]\exp[\chi_2(r)+j\phi_2(r)]d(r)\alpha_4 E_{i1} + n(r,t),$$

$$r \in A_2,\ t \in T_2. \tag{3.C1}$$

To limit the complexity of this discussion, we assume that the additive noise process consists only of the background noise described in Section 2.1.1. Inclusion of quantum effects, when they are significant, can be accomplished with the approach described in Section 3.1.1. If we denote the height of the power spectrum of the background noise as N_b, then the likelihood ratio associated with (3.C1) is the following (cf., Equation 3.71)

$$\Lambda = \langle \exp\{-[\exp 2\chi_1]|\alpha_4 E_{i1}|^2/N_b] \int_{A_2} dr\ \exp[2\chi_2(r)]|d(r)|^2\} \cdot$$

$$\exp\{[2/N_b]\ \mathrm{Re}(\alpha_4 E_{i1}\exp[\chi_1+j\phi_1] \int_{A_2} dr\ \gamma_{co}^*(r)d(r)$$

$$\exp[\chi_2(r)+j\phi_2(r)])\}\rangle_{\substack{\chi_1,\phi_1 \\ \chi_2(r),\phi_2(r)}} \tag{3.C2}$$

where we have introduced the notation corresponding to the obvious temporal correlator

$$\gamma_{co}(r) = [1/\sqrt{T}] \int_{T_2} dt\, \gamma(r,t), \qquad r \in A_2. \tag{3.C3}$$

To obtain an explicit evaluation of Λ, we must perform the averaging operation indicated in (3.C2). Although this averaging cannot be determined for the general case, there exist a variety of techniques which permit it to be accomplished for special cases.

First, we examine some techniques which facilitate this averaging operation without recourse to a representation for the received envelope. For sufficiently large apertures, *i.e.*, those containing enough coherence areas, Harger [39] has employed the central limit theorem to claim that the argument of the exponential term of Λ may be modeled as a Gaussian random variable. The averaging of the reception path fading variables is accomplished via a theorem due to Fried [40] and along with the usual assumption of uniform phase distribution yields the following LR

$$\Lambda_g = \langle \exp\{\exp[2\chi_1][|\alpha_4 E_{i1}|^2/N_b] \int_{A_2} dr \int_{A_2} d\rho \; d(r)$$

$$d^*(\rho)\, \gamma_{co}{}^*(r)\, \gamma_{co}(\rho) \exp[-(1/2)D_2(r-\rho)]\}$$

$$\exp\{-\exp[2\chi_1][|\alpha_4 E_{i1}|^2/N_b] \int_{A_2} dr\, |d(r)|^2\}$$

$$\exp\{-\exp[4\chi_1][|\alpha_4 E_{i1}|^4/2N_b{}^2](\int_{A_2} dr\, |d(r)|^2)\}$$

$$\exp\{\exp[4\chi_1][|\alpha_4 E_{i1}|^4/2N_b{}^2]\exp[4\sigma_2{}^2] \int_{A_2} dr \int d\rho$$

$$|d(r)\, d^*(\rho)|^2 \exp[-2D\chi_2(r-\rho)]\}\rangle_{\chi_1} \qquad (3.C4)$$

where $D_{\chi_2}(\rho)$ is the structure function for $\chi_2(r)$; $D_{\phi_2}(\rho)$ is the structure function for $\phi_2(r)$; and D_2 is the wave structure function for the perturbation term $\chi_2(r)+j\phi_2(r)$ which is defined as follows (cf., Section 2.1.2)

$$D_2(r-\rho) = D_{\chi_2}(r-\rho) + D_{\phi_2}(r-\rho), \qquad r,\rho \in A_2. \qquad (3.C5)$$

Available results [30,41] indicate that a more accurate approximation would contend that the argument of the second exponential term in (3.C2) tends to a Gaussian random variable and that the remainder is better modeled as a lognormal random variable. This approximation involves a more difficult averaging operation which can be

performed by means of an independence assumption for these two variables

$$\Lambda_{\ell g} = \exp[\exp[2\chi_1][|\alpha_4 E_{i1}|^2/N_b{}^2] \int_{A_2} dr \int_{A_2} d\rho$$

$$d(r)\, d^*(\rho)\, \gamma_{co}{}^*(r)\, \gamma_{co}{}^*(r)\, \gamma_{co}(\rho)\, \exp[-(1/2)D_2(r-\rho)]]$$

$$Fr(\exp[2\chi_1]\Delta_1, 0; \Delta_2)>_{\chi_1} \qquad (3.C6a)$$

where we define the auxiliary parameters Δ_1 and Δ_2 as follows

$$\Delta_1 = |\alpha_4 E_{i1}|^2 \exp[-2\sigma_2{}^2] N_b{}^{-1} \left(\int_{A_2} dr\, |d(r)|^2 \right)^2$$

$$\left(\int_{A_2} dr \int_{A_2} d\rho\, d(r) d^*(\rho) \gamma_{co}{}^*(r) \gamma_{co}(\rho) \exp[-(1/2)D_2(r-\rho)] \right)^{-1/2};$$

(3.C6b)

$$\Delta_2 = \sigma_2{}^2 + (1/4)\ell n\left(\int_{A_2} dr \int_{A_2} d\rho\, d(r) d^*(\rho) \gamma_{co}{}^*(\rho) \gamma_{co}(\rho) \exp[-(1/2)D_2(r-\rho)] \right)$$

$$- [1/2]\, \ell n\left(\int_{A_2} dr\, |d(r)|^2 \right). \qquad (3.C6c)$$

Despite the difficult averages remaining in both expressions, (3.C6) is less manageable than (3.C4), thereby illustrating the tradeoff between accuracy and tractability involved in such approximations.

We may also employ standard approximation techniques [30, 42], *i.e.*, series expansions, to facilitate the necessary averaging operation. For any series, by increasing the number of terms retained in the expansion, we can generate a hierarchy of increasingly accurate and complicated approximations. The most useful approximation here is a Taylor series for the exponential term present in the conditional LR. For example, the first and second order approximations of this type for Λ are given by

$$\Lambda_1 = 1 - [|\alpha_4 E_{ij}|^2/N_b] \int_{A_2} dr\ |d(r)|^2; \tag{3.C7a}$$

$$\Lambda_2 = \Lambda_1 + [|\alpha_4 E_{ij}|^2/N_b^2] \int_{A_2} dr \int_{A_2} d\rho\ d(r)\ d^*(\rho)$$

$$\gamma_{co}{}^*(r)\ \gamma_{co}(\rho)\ \exp[-(1/2)D_2(r-\rho) +$$

$$[|\alpha_4 E_{ij}|^4 \exp[4\sigma^2]/2N_b^2] \int_{A_2} dr \int_{A_2} d\rho\ \ d(r)d^*(\rho)|^2 \exp[-2D_{\chi_2}(r-\rho)]. \tag{3.C7b}$$

Other possible expansions (*e.g.*, those due to Harger [39]) usually involve only a part of the argument of the exponential term present in (3.C6) and they encounter the same difficulties in performing the averaging operation as the statistically motivated techniques just discussed.

Next, we consider techniques which accomplish the averaging operation in (3.C2) by utilizing a representation for the received envelope.

Halme [30] has thoroughly examined this issue and has concluded that only the sampling representation yields tractable likelihood ratios. One of these forms, obtained by conditioning on the fading parameters, has already been presented in Section 3.2.1.

$$\Lambda_{sf} = \Big\langle \prod_{q=1}^{N_s} \exp\{-[|\alpha_4 E_{i1}|^2 \exp[2x_1]|d_q|^2 \exp[2x_{2,q}]/N_b]\} \cdot \exp\{[2/N_b]\mathrm{Re}(\alpha_4 E_{i1} \exp[x_1 + j\phi_1] \exp[x_{2,q} + j\phi_{2,q}] d_q \gamma_q^*)\} \Big\rangle_{\substack{x_1,\phi_1 \\ \{x_{2,q},\phi_{2,q}\}}} \tag{3.C8}$$

wherein the terminology of that section is retained and where the likelihood ratio is subscripted to denote its genesis. The conditioning may be removed from this expression with the assumption of independent fading samples $\{x_{2,q}+j\phi_{2,q}\}_{q=1}^{N_s}$. The second LR is obtained by conditioning on the noise

$$\Lambda_{sn} = \langle \exp[-\sum_{q=1}^{N_s}\sum_{p=1}^{N_s} \ell n|[\gamma_q - n_q/\alpha_4 E_{i1} d_q]| + \sigma^2 K_\chi^{-1}(q,p)$$

$$\{\ell n|[\gamma_p - n_p/\alpha_4 E_{i1} d_p]| + \sigma^2\}]$$

$$\exp[\sum_{q=1}^{N_s}\sum_{p=1}^{N_s} \{\ell n|[\gamma_q/\alpha_4 E_{i1}]+\sigma^2\}K^{-1}(q,p)\{\ell n|[\gamma_p/\alpha_4 E_{i1}] +\sigma^2\}]$$

$$\exp[\sum_{q=1}^{N_s}\sum_{p=1}^{N_s}\{\arg([\gamma_q - n_q/\alpha_4 E_{i1} d_q])\}K_\phi^{-1}(q,p)\{\arg([\gamma_p - n_p/\alpha_4 E_{i1} d_p])\}]$$

$$\exp[\sum_{q=1}^{N_s}\sum_{p=1}^{N_s} \arg([\gamma_q/\alpha_4 E_{i1}])K_\phi^{-1}(q,p)\arg([\gamma_p/\alpha_4 E_{i1}])]\rangle_{\{n_q\}}. \tag{3.C9}$$

Here n_q is the q sample of the background noise, K_χ is the covariance matrix for the fading amplitudes $\{\chi_1+\chi_{2,q}\}_{q=1}^{N_s}$, and K_ϕ is the covariance matrix for the fading phases $\{\phi_1+\phi_{2,q}\}_{q=1}^{N_s}$. This averaging over noise samples can be performed with the assumptions of independent reception path fades and relatively weak noise.

At this point, we pause to comment on the representation of the received envelope that we employed in Section 3.1; namely the coherence area decomposition technique wherein we separate the receiver aperture into a collection of coherence areas over each of which the fading process is modeled as a complex random variable. This technique is not an accurate representation for the received envelope but a heur-

istic corruption of Halme's sampling representation. This inaccuracy is unimportant in the models for which the technique was employed.

When the assumption of independent fading samples is not appropriate (*cf.*, Section 3.2.1), the averaging operations in Equations 3.C8 and 3.C9 cannot be accomplished. To partially circumvent this intractability, we apply the series expansion techniques previously discussed to these expressions. The results thus obtained for Λ_{sf} are similar to those ((3.C7a) and (3.C7b)) previously developed. When Λ_{sn} is approximated by this method, however, a large signal approximation is also necessary

$$\ell n|\gamma_q - n_q| = \ell n|\gamma_q| - [n_q/\ell_q], \qquad q = 1,2,\ldots,N_s, \tag{3.C10}$$

to obtain manageable results, *e.g.*, the first order approximation

$$\begin{aligned} \text{snl} = 1 &- [N_b/2] \sum_{q=1}^{N_s} [K_\chi^{-1}(q,q)+K_\phi^{-1}(q,q)/|\gamma_q|^2] - \\ &\sum_{q=1}^{N_s}\sum_{p=1}^{N_s} \{\ell n|d_q|K_\chi^{-1}(q,p)[\ell n|[d_p\alpha_4 E_{i1}/\gamma_p]|-\sigma^2] \\ &- (\ell n|[\gamma_q/\alpha_4 E_{i1}]|+\sigma^2)K_\chi^{-1}(q,p)\ell n|d_p|\} \\ &- \sum_{q=1}^{N_s}\sum_{p=1}^{N_s} \{\arg(d_q)K_\phi^{-1}(q,p)\arg([d_p\alpha_4 E_{i1}/\gamma_p]) - \\ &\arg([\gamma_q/\alpha_4 E_{i1}])K_\phi^{-1}(q,p)\arg(d_p)\}. \end{aligned} \tag{3.C11}$$

Because ML estimators cannot be directly calculated for the formulation (3.C1), we can apply the usual maximum likelihood approach to the approximate likelihood ratios just derived. Although the estimators thus generated are not ML, we expect that they will resemble the ML estimator whenever the relevant approximation is accurate. Because the approximate likelihood ratios derived via statistical means possess complicated forms, they yield estimator equations which require further approximation. For example, Λ_g (Equation 3.C4) leads to the following equation

$$0 = <\Lambda_{g|x_1}[-\exp[2x_1] \int_{A_2} dr|d(r)|\{1+[\exp[2x_1]2|E_{i1}\alpha_4|^2/N_b] \int_{A_2} d\rho|d(\rho)|^2\}$$

$$+ \exp[2x_1]([1/N_b]) \int_{A_2} dr \int_{A_2} d\rho\gamma_{co}{}^*(r)\gamma_{co}(\rho)\exp[-(1/2)D_2(r-\rho)]$$

$$\{\exp[j\arg d(r)]d^*(\rho)+\exp[-j\arg d(\rho)]d(r)\} +$$

$$2\exp[4x_1]\exp[4x_2{}^2][|E_{i1}\alpha_4|^2/N_b] \int_{A_2} dr \int_{A_2} d\rho\ d(r)||d(\rho)|^2$$

$$\exp[-2D_{x_1}(r-\rho)]]>_{x_1} . \qquad (3.C12)$$

To evaluate this expectation, we must approximate the term $\Lambda_{g|x_1}$. The obvious means is a Taylor series which leads to a hierarchy of estimators including the following first order ones

$$\arg \hat{d}(r) = \arg \gamma_{co}(r) + \text{cnst}, \qquad r \in A_2, \tag{3.C13a}$$

$$N_b + 2|\alpha_4 E_{i1}|^2 \exp[4\sigma_1^2] \int_{A_2} d\rho\, |\hat{d}(\rho)|^2 =$$

$$2|\gamma_{co}(r)| \int_{A_2} d\rho\, \exp[-(1/2)D_2(r-\rho)]\ \gamma_{co}(\rho)| +$$

$$2\exp[4\sigma^2]|\alpha_4 E_{i1}|^2 \int_{A_2} d\rho \exp[-2D_x(r-\rho)|\hat{d}(\rho)|^2,$$

$$r \in A_2. \tag{3.C13b}$$

It is difficult to solve this integral equation for an explicit estimator $|\hat{d}(r)|$ and higher order approximations for $\Lambda_{g|x_1}$ lead to more complicated forms. Similar results can be obtained for $\Lambda_{\ell g}$.

ML techniques may also be applied to the Taylor series approximations for the LR to generate a hierarchy of results. In particular applications of these techniques to Λ_1 yields

$$\hat{d}(r) = \exp[-(1/2)(\sigma^2+K_\phi(0))](\alpha_4 E_{i1})^{-1}\gamma_{co}(r) = 0,$$

$$r \in A_2, \tag{3.C14}$$

where the latter approximation follows from the usual assumption of a large fading phase variance $(K_\phi(0) >> 1)$. The second order LR, Λ_2, leads to an estimate for $\arg \hat{d}(r)$ and an integral equation for $|\hat{d}(r)|$

$$\arg \hat{d}(r) = \arg \gamma_{co}(r) - \arg(\alpha_4 E_{i1}),$$

$$r \in A_2, \tag{3.C15a}$$

$$N_b|\hat{d}(r)| = |\gamma_{co}(r)| \int_{A_2} d\rho\, |\gamma_{co}(\rho)| \exp[-(1/2)D_2(r-\rho)]|\hat{d}(\rho)| +$$

$$|\alpha_4 E_{i1}|^2 \exp[4\sigma^2]|d(r)| \int_{A_2} d\rho \exp[-2D_{x_1}(r-\rho)]|\hat{d}(\rho)|^2,$$

$$r \in A_2. \tag{3.C15b}$$

Use of Λ_{sf1} provides an analogous result

$$\hat{d}_q = \exp[-(1/2)(\sigma^2+K_\phi(0))](\alpha_4 E_{i1})^{-1}\gamma_q = 0,$$

$$q = 1,2,\ldots,N_s \tag{3.C16}$$

as does the utilization of $_{sf2}$

$$\arg \hat{d}_q = \arg \gamma_q - \arg(\alpha_4 E_{i1}), \qquad q = 1,2,\ldots,N_s, \tag{3.C17a}$$

$$N_b|\hat{d}_q| = |\gamma_q| \sum_{p=1}^{N_s} |\gamma_p \hat{d}_p| \exp[-(1/2)D_2(q,p)] +$$

$$|\alpha_4 E_{i1}|^2 \exp[4\sigma^2]|\hat{d}_q| \sum_{p=1}^{N_s} |\hat{d}_p \hat{d}_q| \exp[-2D_{\chi_2}(q,p)],$$

$$q = 1,2,\ldots,N_s. \qquad (3.C17b)$$

On the other hand, the first order estimates provided by $_{snl}$ are given by

$$\hat{d}_q = (\alpha_4 E_{i1})^{-1} \exp[\sigma^2] \exp[\cdot <\ell n(\gamma_q - n_q)>] = (\alpha_4 E_{i1})^{-1} \exp[\sigma^2] \gamma_q$$

(3.C18)

where the last approximation follows from the assumption of a large signal (cf., Equation 3.C10). Using this same assumption, we determine that the second order estimates satisfy the following collection of coupled equations

$$\ell n\left|\frac{\hat{d}_q\alpha_4 E_{il}}{\gamma_q}\right|\{1 - N_b \sum_{p=1}^{N_s}\frac{K_\phi^{-1}(p,p)+K_\chi^{-1}(p,p)}{|\gamma_p|^2}\} =$$

$$\frac{N_b}{|\gamma_q|^2}\sum_{p=1}^{N_s} K_\chi^{-1}(q,p)\ \ell n\left|\frac{d_p\alpha_4 E_{il}}{\gamma_p}\right|$$

$$+ \ell n\left|\frac{\hat{d}_q\alpha_4 E_{il}}{\gamma_q}\right| \sum_{p=1}^{N_s}\sum_{m=1}^{N_s}\left|\ell n\,|\hat{d}_p|\,K_\chi^{-1}(p,m)\ \ell n\left|\frac{\hat{d}_m\alpha_4 E_{il}}{\gamma_m}\right|\right.$$

$$\left. + \arg\hat{d}_p\ K_\phi^{-1}(p,m)\ \arg\left(\frac{\hat{d}_m\alpha_4 E_{il}}{\gamma_m}\right)\right|\},$$

$$q = 1,2,\ldots,N_s \qquad (3.C19a)$$

$$\arg\left(\frac{\hat{d}_q\alpha_4 E_{il}}{\gamma_q}\right)\{1 - N_b \sum_{p=1}^{N_s}\frac{K_\phi^{-1}(p,p)+K_\chi^{-1}(p,p)}{|\gamma_p|^2}\} =$$

$$\frac{N_b}{|\gamma_q|^2}\sum_{p=1}^{N_s} K_\phi^{-1}(q,p)\ \arg\left(\frac{\hat{d}_p\alpha_4 E_{il}}{\gamma_p}\right) + \arg\left(\frac{\hat{d}_q\alpha_4 E_{il}}{\gamma_q}\right)$$

$$\{\sum_{p=1}^{N_s}\sum_{m=1}^{N_s}\arg(\hat{d}_p)K_\phi^{-1}(p,m)\ \arg\left(\frac{\hat{d}_m\alpha_4 E_{il}}{\gamma_m}\right) + \ell n|\hat{d}_p|\,K_\chi^{-1}(p,m)\ell n\left(\frac{\hat{d}_m\alpha_4 E_{il}}{\gamma_m}\right)\}$$

$$q = 1,2,\ldots,N_s. \qquad (3.19b)$$

Higher order estimates are determined by yet more complicated pairs of coupled equations. As expected for the ML approach [32], first order estimates depend only on the received envelope and the parameters of the process upon which we have conditioned the calculation of the appropriate likelihood ratio (*e.g.*, $\chi_1+j\phi_1+\chi_2(r)+j\phi_2(r)$ for Λ). The second order estimates also depend on the covariance function of this conditioning process.

Excluding the trivial cases, the application of ML techniques to approximate likelihood ratios, whether they are derived by statistical arguments or by series expansions, leads to estimators that are specified by means of coupled or integral equations from which we may deduce the structure of the processor [28] designed to form these estimators from the received envelope. Analytic difficulties associated with the solution of these equations, however, prevent explicit evaluation of the estimators or their mean-square errors so that we are unable to ascertain the quality of such processors.

APPENDIX 3D

Using the line-of-sight propagation model described in Section 2.1, we examine passive irradiance imaging in a turbulent but noiseless environment. In the original formulation for point sources [31, 45], the received envelope consists of the (free-space) propagated form of the transmitted envelope along with a multiplicative disturbance due to the turbulence, *i.e.*,

$$\gamma(r) = \{\int_{A_1} dr'\ b(r')h_0(r-r')\}\exp[x_{21}(r-r_0')+j\phi_{21}(r-r_0')],$$

$$r \in A_2, \tag{3.D1}$$

where r_0' is the location of the point source in the aperture A_1. The generalization of this model to include extended sources [29, 46] usually employs the isoplanatic assumption

$$\gamma(r) = \int_{A_1} dr'\ b(r')h_0(r-r')\exp[x_{21}(r-r',0)+j\phi_{21}(r-r',0)],$$

$$r \in A_2, \tag{3.D2}$$

so that turbulent effects are included in a convolutional form. As previously discussed, the equally useful assumption of unilateral coherence (*cf.*, Section 2.1.4) may be used to obtain a model which retains the

multiplicative representation for turbulent effects

$$\gamma(r) = \int_{A_1} dr'\ b(r')h_0(r-r')\exp[\chi_{21}(r,0)+j\phi_{21}(r,0)]$$

$$\triangleq d(r)\exp[\chi(r,0)+j\phi(r,0)], \quad r \in A_2. \tag{3.D3}$$

Despite the exclusion of background noise, the resulting formulations (3.D2) and (3.D3) are still not amenable to standard analytical methods. We next examine several techniques that have been developed for circumventing the relative intractability of these models.

The imaging properties [15] of a thin lens make it an obvious choice (*cf.*, Appendix 3B) for processing the received envelope, a selection strengthened by the occurence, albeit irregular and infrequent, of "good seeing" phenomena. Employment of a thin lens with focal length L (the length of the propagation path) and the transmission function $w(r)$ provides the following image spectrum, *i.e.*, the Fourier transform of the intensity in the focal plane of the lens

$$O(f) = \int_{A_2} dr\{w(r)w^*(r-\lambda Lf)d(r)d^*(r-\lambda Lf)$$

$$\exp[\chi(r)+j\phi(r)+\chi(r-\lambda Lf)-j\phi(r-\lambda Lf)], \tag{3.D4}$$

where f is the transformation variable which may be interpreted as a spatial frequency. For a lens of sufficient quality, the uncorrupted

image spectrum

$$I(f) = \int_{A_2} dr\{w(r)w^*(r-\lambda Lf)d(r)d^*(r-\lambda Lf)\} \tag{3.D5}$$

is an adequate representation [14, 15] of the object spectrum. Linear combination of many of these short exposure image spectra leads to the well-known [31, 45] long exposure image spectrum

$$O_{LE}(f) = \langle O(f)\rangle = I(f)\tau_{LE}(f), \tag{3.D6}$$

where $\langle\cdot\rangle$ denotes an ensemble average over the turbulence and where $\tau_{LE}(f)$ is the long exposure turbulent mutual coherence function (MCF),

$$\tau_{LE}(f) = \exp[\chi(r)+j\phi(r)]\exp[\chi(r-\lambda Lf)-j\phi(r-\lambda Lf)] =$$

$$\exp[-(1/2)D(\lambda Lf)]. \tag{3.D7}$$

which utilized $D(\cdot)$, the wave structure function defined in Section 2.1.1. The presence of this term in Equation 3.D6 severely degrades high spatial frequencies present in the object spectrum so that much subsequent effort [35] has been expended in the development of techniques for the recovery of this high frequency information.

Those advances which have been achieved are usually counterbalanced by some restriction of the image. As an example we consider the

technique of speckle interferometry [48-51] which has recently evolved in connection with the measurement of stellar diameters. This method involves post-lens processing based on the observation that the average of the modulus-squared MCF, *i.e.*,

$$\langle |O(f)|^2 \rangle = |I(f)|^2 \langle |\tau(f)|^2 \rangle \tag{3.D8}$$

remains modestly attenuated for all spatial frequencies within the diffraction limit of the lens. Appropriate processing [48] leads to the recovery of the moduli of these spatial frequencies which represent sufficient information for the previously described objective.

The restrictions imposed by this technique include the absence of phase information for the recovered frequencies which eliminates its application to imaging since, in general, there exists no method for reconstructing an image from the amplitude of its spectrum. Furthermore, the modest attenuation of the recovered amplitudes may be a factor of nearly 10^3 so that the presence of noise will necessitate many additional measurements at higher spatial frequencies to achieve an equivalent SNR. These restrictions illustrate the tradeoffs which may be utilized to obtain specialized information as opposed to a complete image.

Another technique for circumventing model intractabilities, homomorphic processing (see [52] for a discussion), is based on the observation that certain nonlinear estimation problems can be cast into a linear form by means of reversible nonlinear operations. This linear form is

processed with standard techniques and subsequently passed through the inverse nonlinear operation to obtain an estimator. While analysis of this method is unduly complicated, there exists ample experimental evidence [52] to verify its utility.

Application of this method along with a maximum likelihood criteria for the linear processing yields precisely the estimator suggested in Appendix 3B; namely,

$$\hat{d}(r) = \exp[\sigma^2]\Big[\prod_{m=1}^{M} \gamma_m(r)\Big]^{1/M}, \qquad r \in A_2 \tag{3.D9}$$

where $\{\gamma_m(r)\}$ are M independent (temporally obtained) received envelopes. When this quantity is passed through a lens, the image spectrum becomes the following

$$O(f) = \int_{A_2} dr\{w(r)w^*(r-\lambda Lf)d(r)d^*(r-\lambda Lf)\} \cdot$$

$$\Big[\prod_{m=1}^{M}\prod_{\ell=1}^{M} \exp\{\chi_m(r)+j\phi_m(r)+\chi_\ell(r-\lambda Lf)-j\phi_\ell(r-\lambda Lf)\}\Big]^{1/M}. \tag{3.D10}$$

When many of these (M-diversity) short-term exposures are combined to form a long exposure image spectrum, we obtain the following result

$$\langle O(f)\rangle = I(f)\exp[(2\sigma^2/M)]\exp[-(1/2M)D(\lambda Lf)]. \tag{3.D11}$$

As indicated in expression (3.D11), for the proper selection of M, we may form diffraction-limited images for any lens through a turbulent environment by means for non-adaptive pre-processing. For the Kolmogorov spectrum [11], this effect is illustrated in Figure 3.6 wherein we plot the normalized M-diversity MCF, $\exp[-(1/2M)D(\lambda Lf)]$ for a receiver aperture which contains 100 turbulent coherence areas. In this context, M-diversity processing increases the cutoff frequency (the maximum resolvable frequency according to an arbitrary criterion [31]) by a factor of $M^{3/5}$. In view of the diffraction-limited image provided by (the appropriate) M-diversity long exposure, it has pointed out [85] that relatively few of the constituent M-diversity short exposures can supply images that are significantly inferior to the diffraction-limited one. This behavior may be attributed to the formation of the M-diversity short exposure since this procedure introduces an averaging effect.

There remain two major difficulties associated with utilization of the estimator (3.D9). First, we have not determined a method for implementing the necessary pre-processing because of the troublesome but crucial *Mth* root operation (holograms can be used to realize the required multiplication). Second, inclusion of background noise in this model has not yet been accomplished and appears to involve intractabilities due to the form of the estimator. Furthermore, but common to all previous approaches, the unilateral coherence (or isoplanatic) approximation severely restricts the class of "imageable" sources.

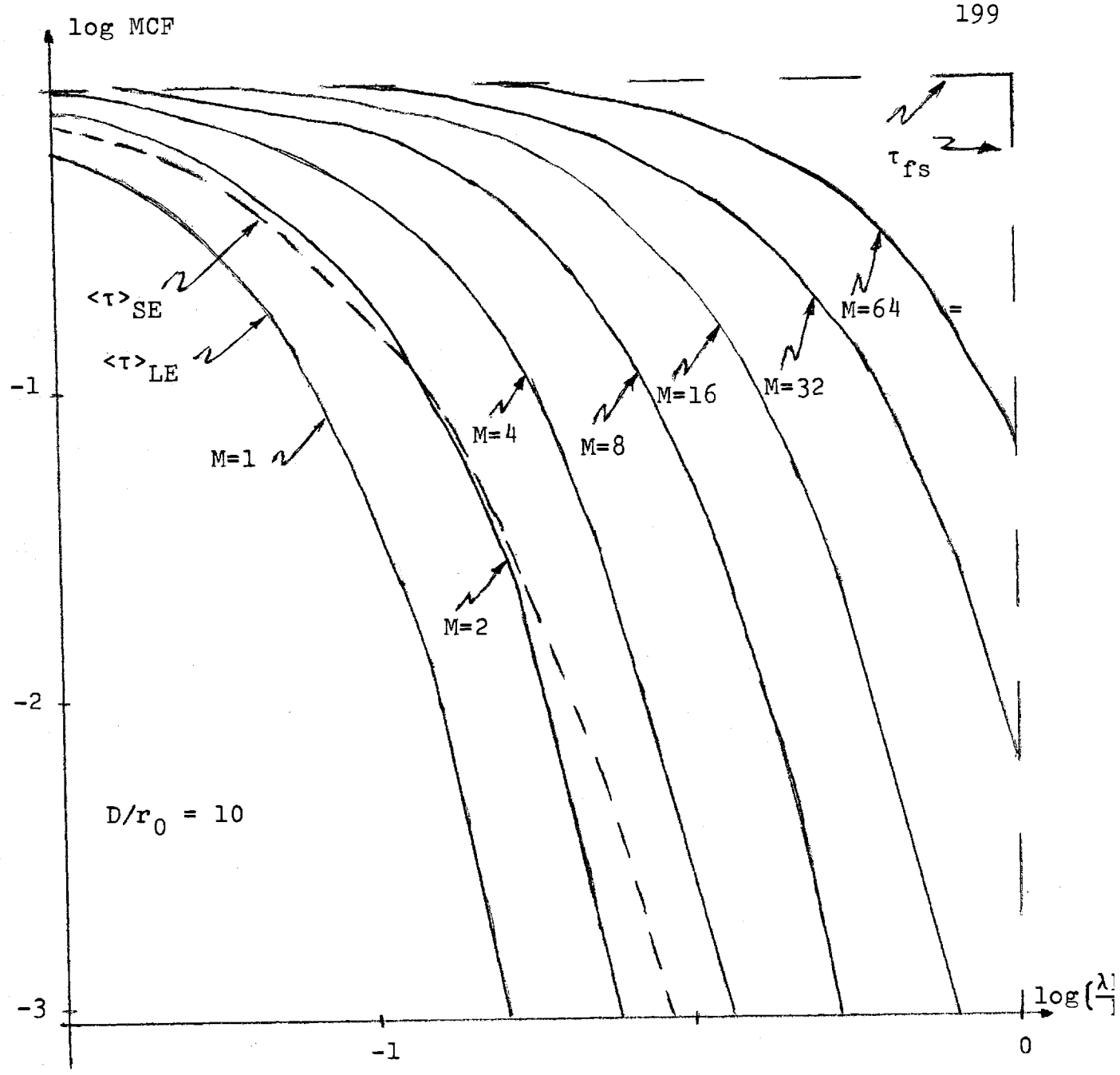

LEGEND: D IS A APERTURE DIAMETER

r_0 IS TURBULENT COHERENCE LENGTH

$\langle\tau\rangle_{SE}$ & $\langle\tau\rangle_{LE}$ ARE FRIED'S MCF'S [31]

τ_{fs} IS THE FREE SPACE MCF

FIGURE 3.6: THE MUTUAL COHERENCE FUNCTION (MCF) OBTAINED BY M-DIVERSITY PROCESSING IN COMPARISON TO BOTH THE FREE SPACE MCF AND FRIED'S MCF'S FOR AN APERTURE WHICH CONTAINS 100 COHERENCE AREAS

APPENDIX 4A

In this appendix we reexamine approximation (4.10) which replaces the integral definition of β_0 with a sum of random variables

$$\beta_0 = \sum_{n=1}^{N_T} B_n \exp[x_n + j\phi_n]. \tag{4.A1}$$

Specifically we are interested in the mutual dependences of the random fading amplitudes $\{x_n\}$. For previous approximations of this type (cf., Section 3.1), these random variables were associated with a single perturbation process which also determined the coherence areas (or the sampling distances) so that the slight dependences existing among them could be neglected [3, 30, 33]. In this case, however, the fading amplitudes are attributed to a composite process which is the summation of two perturbation processes so that significant dependences can arise. For example, when these processes possess coherence areas of vastly different sizes, the smaller one effectively determines the coherence area for the composite process so that the part of the fading amplitude due to the process with the larger coherence area will retain a high degree of correlation over these areas.

Although analysis of the general formulation is complicated, there exist several specializations for thich these dependences are slight enough to permit the use of Levitt's results (cf., Section 4.1). For the statistically homogeneous and isotropic turbulence which we

have previously employed, the restriction to near equality of the involved pathlengths will ensure that the perturbation processes possess coherence areas of nearly equal size. Each process now may be modelled as a random variable over each coherence area so that

$$\beta_0 = \sum_{n=1}^{N_T} B_n \exp[x_{1,n}+j\phi_{1,n}]\exp[x_{2,n}+j\phi_{2,n}]. \qquad (4.A2)$$

In accordance with our usual assumptions, the sets $\{x_{1,n}\}$ and $\{x_{2,n}\}$ are independent and the members of each set exhibit only negligible dependences [30, 33]. Consequently, the composite fading amplitudes $\{x_n\}$ are independent thereby justifying the use of available results.

Another relevant specialization occurs when one or the other of these processes has only one coherence area. Equation 4.A1 here reduces to the following expression

$$\beta_0 = \exp[x_1+j\phi_1] \sum_{n=1}^{N_T} B_n \exp[x_{2,n}+j\phi_{2,n}] \qquad (4.A3)$$

From which we observe that Levitt's results may be applied to the summation. The random variable $|\beta_0|$ is then lognormally distributed whenever the magnitude of the summation is also lognormally distributed. Otherwise neither the Rayleigh nor the lognormal distribution can be accurately assigned to $|\beta_0|$.

The final specialization requires that both perturbation terms possess a large number of coherence areas but does not restrict their relative sizes. Assuming that the larger of the coherence areas corresponding to the perturbation processes contains N_p of the smaller coherence areas, we may rewrite Equation 4.A1 as follows

$$\beta_0 = \sum_{n=1}^{N_T/N_p} \exp[x_{2,n}+j\phi_{2,n}] \sum_{\ell=N_p(n-1)+1}^{N_p n} B_\ell \exp[x_{1,\ell}+j\phi_{1,\ell}] \tag{4.A4a}$$

$$\triangleq \sum_{n=1}^{N_T/N_p} s_n. \tag{4.A4b}$$

The random variables $\{s_n\}$ exhibit negligible dependences and each of them possesses a well-behaved distribution (*i.e.*, they have finite moments). Consequently, we may invoke the Central Limit Theorem [28, 32, 38] whenever N_T/N_p is sufficiently large to argue that β_0 has a uniformly distributed phase and a Rayleigh distributed amplitude.

The preceding specializations have indicated some circumstances under which the models examined in Chapter 4 accurately describe the random variable β_0. Further specializations will not be examined here since we have already demonstrated the utility of the models that were analyzed.

APPENDIX 5A

In this appendix, we calculate the increment in the radius of the minimum spot size required to offset the effects of beam wander and, hence, to preserve the "physical orthogonality" of the turbulent scanning set. The criterion [58] employed to determine the members of the scanning set requires that each member have a fraction of its energy no larger than $\exp[-2]$ outside of its spot size. For example, in the free space context, the radius, R, of the spot size follows directly from the application of this criterion to (5.2a)

$$\int_{|r|\geq R} dr\ (1/\pi W_0^2)\exp[-[|r|^2/W_0^2] \leq \exp[-2] \tag{5.A1}$$

since the preceding expression implies that

$$R \geq \sqrt{2}\ W_0. \tag{5.A2}$$

In the case where beam wander effects are significant, we generalize the criterion of "physical orthogonality" to require that, on the average, each member have no more than $\exp[-2]$ of its energy outside of its effective spot size (which exceeds its actual spot size in order to counteract the wandering of the beam). For the received envelope given by (5.9b), this criterion implies that the radius, R', of the effective spot size satisfies the following

$$< \int_{|r| \geq R'} dr \; (1/\pi W_0'^2) \exp[-(|r-\Delta|^2/W_0'^2)] >_{\Delta} \leq \exp[-2]. \qquad (5.A3)$$

The beam wander parameter Δ is a zero-mean Gaussian random vector [12] with independent components that have identical variances (denoted by σ_{BW}^2). The use of these statistics in the evaluation of (5.A3) indicates that

$$R' = \sqrt{2}\,[W_0'^2 + \sigma_{BW}^2]^{1/2}. \qquad (5.A4)$$

Since the reduction in spot size (from S_T to S_T') was due solely to the removal of beam wander effects, it follows that

$$W_0^2 = W_0'^2 + \sigma_{BW}^2 \qquad (5.A5)$$

in agreement with Yura [57]. Hence, as we claimed in Section 5.1, the effective spot size is unchanged.

ACKNOWLEDGEMENT

It is with great pleasure that I express my gratitude to Professor Estil V. Hoversten who supervised the research reported here. The guidance that he provided throughout my graduate studies has been invaluable. In addition, I gratefully acknowledge the many contributions of Professor Jeffrey H. Shapiro who assisted in the supervision of my research. Professor Robert S. Kennedy, who served as a thesis reader, also deserves mention.

I also wish to thank the National Science Foundation for the support that I received during the period of my graduate studies.

REFERENCES

1. R. S. Lawrence and J. W. Strohbehn, Proc. IEEE, 58, 1970, p. 1523.

2. J. W. Strohbehn, Proc. IEEE, 56, 1968, p. 1301.

3. E. V. Hoversten, R. O. Harger, and S. J. Halme, Proc. IEEE, 58, 1970, p. 1626.

4. E. Brookner, IEEE Trans, Com. Tech., COM-18, 1970, p. 396.

5. J. H. Shapiro, J. Opt. Soc. Am., 61, 1971, p. 492.

6. J. H. Shapiro, "Optimal Spatial Modulation for Reciprocal Channels," Technical Report 476, Research Laboratory of Electronics, M.I.T., Cambridge, Mass., 1970.

7. N. S. Kopeika and J. Bordogna, Proc. IEEE, 58, 1970, p. 1571.

8. J. H. Shapiro, "Normal mode approach to wave propagation in the turbulent atmosphere," App. Opt., 13, 1974, p. 2614.

9. D. Korff and G. Dryden, "Isoplanicity--the translation invariance of the atmospheric Green's function," submitted to J. Opt. Soc. Am.

10. J. H. Shapiro, J. Opt. Soc. Am., 64, 1974, p. 540A.

11. V. I. Tatarski, Wave Propagation in a Turbulent Medium, McGraw-Hill Book Co., New York, 1961.

12. D. L. Fried, J. Opt. Soc. Am., 55, 1965, p. 1427.

13. P. Beckmann and A. Spizzichino, The Scattering of Electromagnetic Waves from Rough Surfaces, Pergamon Press, Oxford, 1963.

14. J. W. Goodman, Introduction to Fourier Optics, McGraw-Hill Book Co., San Francisco, 1968.

15. M. Born and E. Wolf, Principles of Optics, Pergamon Press, Oxford, 1970.

16. J. V. Evans and T. Hagfors, Radar Astronomy, McGraw-Hill Book Co., New York, 1968.

17. L. I. Goldfischer, J. Opt. Soc. Am., 55, 1965, p. 247.

18. J. W. Goodman, Proc. IEEE, 53, 1965, p. 1688.

19. L. H. Enloe, Bell Sys. Tech. J., , 1967, p. 1479.

20. B. Eliasson and F. M. Mottier, J. Opt. Soc. Am., 61, 1971, p. 559.

21. R. F. Lutomirski and H. T. Yura, App. Opt., 10, 1971, p. 1652.

22. N. Fernelius and C. Tome, J. Opt. Soc. Am., 61, 1971, p. 566.

23. J. Bulabois, M. E. Guillaume and J. C. Vienot, App. Opt., 12, 1973, p. 1686.

24. P. L. Bender, Proc. IEEE, 55, 1967, p. 1039.

25. K. E. Golden, D. E. Kind, S. L. Leonard and R. C. Ward, App. Opt., 12, 1973, p. 1447.

26. A. J. Hughes and E. R. Pike, App. Opt., 12, 1973, p. 597.

27. J. C. Owens, Proc. IEEE, 57, 1969, p. 530.

28. H. L. Van Trees, Detection, Estimation and Modulation Theory, Part I, John Wiley and Son, New York, 1968.

29. J. C. Moldon, "Imaging of Objects Viewed through a Turbulent Atmosphere," Technical Report 469, Research Laboratory of Electronics, M.I.T., Cambridge, Mass., 1969.

30. S. J. Halme, "Efficient Optical Communication in a Turbulent Atmosphere" Technical Report 474, Research Laboratory of Electronics, M.I.T., Cambridge, Mass., 1970.

31. D. L. Fried, J. Opt. Soc. Am., 56, 1966, p. 1372.

32. D. Middleton, An Introduction to Statistical Communication Theory, McGraw-Hill Book Co., New York, 1960.

33. R. S. Kennedy and E. V. Hoversten, IEEE Trans. Inf. Th., IT-14, 1968, p. 716.

34. J. P. Moreland and S. A. Collins, J. Opt. Soc. Am., 59, 1969, p. 10.

35. Restoration of Atmospherically Degraded Images, 3 Vols., Nat. Acad. Sci., Woods Hole Summer Study, 1966.

36. Evaluation of Motion Degraded Images, Nat. Aero. and Space Admin. Seminar, 1968.

37. T. S. Huang, W. F. Schreiber and O. J. Tretiak, Proc. IEEE, 59, 1971, p. 1586.

38. H. L. Van Trees, Detection and Estimation and Modulation Theory, Part 3, John Wiley and Son, New York, 1971.

39. R. O. Harger, IEEE Trans. Aero. Elec., AES-3, 1967, p. 819.

40. D. L. Fried, Proc. IEEE, 55, 1967, p. 57.

41. R. L. Mitchell, J. Opt. Soc. Am. 58, 1968, p. 1267.

42. F. B. Hildebrand, Introduction to Numerical Analysis, McGraw-Hill Book Co., New York, 1974.

43. J. H. Shapiro, "Optimum Adaptive Imaging through the Turbulent Atmosphere," App. Opt., 13, 1974, 2609. (Nov., 1974).

44. R. O. Harger, IEEE Trans. Aero. Elec., AES-3, 1967, p. 681.

45. R. E. Hugnagel and N. R. Stanley, J. Opt. Soc. Am., 54, 1964, p. 52.

46. R. F. Lutomirski and H. T. Yura, App. Opt., 13, 1974, p. 431.

47. H. S. Lin, "Communication Model for the Turbulent Atmosphere," Ph.D. Thesis, CWRU, 1973.

48. D. Korff, J. Opt. Soc. Am., 63, 1973, p. 971.

49. M. G. Miller and D. Korff, J. Opt. Soc. Am., 64, 1974, p. 155.

50. C. Y. C. Liu and A. W. Lohmann, Opt. Comm., 8, 1973, p. 372.

51. C. P. Wang, Opt. Comm., 10, 1974, p. 253.

52. A. V. Oppenheim, R. W. Schafer and T. G. Stockham, Proc. IEEE, 56, 1968, p. 1264.

53. T. Suzuki and R. Hioki, Jap. J. App. Phys., 5, 1966, p. 807.

54. J. A. Dowling and P. M. Livingston, J. Opt. Soc. Am., 63, 1973, p. 846.

55. J. R. Kerr and R. Eiss, J. Opt. Soc. Am., 62, 1972, p. 682.

56. J. R. Kerr and J. R. Dunphy, J. Opt. Soc. Am., 63, 1973, p. 1.

57. H. T. Yura, J. Opt. Soc. Am., 63, 1973, p. 567.

58. D. Gabor, "Light and Information," in Progress in Optics, Vol. 1, North-Holland, Amsterdam, 1961.

59. D. P. Petersen and D. Middleton, Info. and Cont., 5, 1962, p. 279.

60. B. P. Lathi, Signals, Systems and Communications, John Wiley and Son, New York, 1965.

61. A. Monroe, Digital Processes for Sampled Data Systems, John Wiley and Son, New York, 1962.

62. E. Eastwood, Radar Ornithology, Methuen, London, 1967.

63. W. L. Flock and J. L. Green, Proc. IEEE, 62, 1974, p. 745.

64. K. Hardy and I. Katz, Proc. IEEE, 57, 1969, p. 468.

65. K. Hardy, D. Atlas and K. Glover, J. Geo. Res., 71, 1966, p. 1537.

66. R. Hajovsky, A Deam and A. Lagrone, IEEE Trans. Anten. Prop., AP-14, 1966, p. 224.

67. K. Glover, K. Hardy, T. Konrad, W. Sullivan and A. Michaels, Science, 154, 1966, p. 967.

68. J. Richter and D. Jensen, Proc. IEEE, 61, 1973, p. 143.

69. C. Metcalf, W. Flint and R. Metcalf, Destructive and Useful Insects, McGraw-Hill Book Co., New York, 1962.

70. J. Richter, Rad. Sci., 4, 1969, p. 1261.

71. J. R. Kerr, P. J. Titterton, A. R. Kraemer, and C. R. Cooke, Proc. IEEE, 58, 1970, p. 1691.

72. V. E. Noble, R. D. Ketchum and D. B. Ross, Proc. IEEE, 57, 1969, p. 594.

73. D. B. Ross, V. J. Cardone and J. W. Conaway, IEEE Trans. Geo. Elect., GE-8, 1970, p. 326.

74. L. H. Tveten and R. D. Hunsucker, Proc. IEEE, 57, 1969, p. 487.

75. J. W. Wright, IEEE Trans. Anten. Propag., AP-16, 1968, p. 217.

76. F. Saiedy and D. T. Hilleary, App. Opt., 6, 1967, p. 911.

77. P. Beckmann, Proc. IEEE, 53, 1965, p. 1012.

78. P. Beckmann, Proc. IEEE, 54, 1966, p. 280.

79. C. E. Prettyman and M. D. Cermak, IEEE Trans. Geo. Sci., GE-7, 1969, p. 235.

80. G. Tober, R. C. Anderson and O. H. Shemdin, App. Opt., 12, 1973, p. 788.

81. J. W. Rouse, Proc. IEEE, 57, 1969, p. 605.

82. A. E. Siegman, App. Opt., 5, 1966, p. 1588.

83. H. T. Yura, App. Opt., 11, 1972, p. 1399.

84. S. J. Halme, B. K. Levitt and R. S. Orr, Quart, Prog. Rep., Res. Lab. of Elect., M.I.T., Cambridge, Mass., 93, 1969, p. 163.

85. E. V. Hoversten, private communication.

86. B. K. Levitt, Quart. Prog. Rep., Res. Lab. of Elect., M.I.T., Cambridge, Mass., 99, 1970, p. 114.

87. B. K. Levitt, "Variable Rate Optical Communication through the Turbulent Atmosphere," Technical Report 483, Res. Lab. of Elect., M.I.T., Cambridge, Mass., 1971.

88. D. E. Barrick, IEEE Trans. Ant. Propag., AP-22, 1974, p. 135.